SPATIALLY FILTERED FEEDBACK FOR MODE CONTROL IN VERTICAL-CAVITY SURFACE-EMITTING LASERS

by

MEI TING CHA

B.Sc., University Putra Malaysia, 2002
M.S., University of Malaya, 2006

A Thesis Submitted in Partial Fulfillment
of the Requirements for the Degree of

MASTER OF APPLIED SCIENCE

in the Department of Electrical and Computer Engineering

© Mei Ting Cha, 2008
University of Victoria

All rights reserved. This thesis may not be reproduced in whole or in part, by photocopy or other means, without the permission of the author.

SUPERVISORY COMMITTEE

SPATIALLY FILTERED FEEDBACK FOR MODE CONTROL IN VERTICAL-CAVITY SURFACE-EMITTING LASERS

by

MEI TING CHA
B.Sc., University Putra Malaysia, 2002
M.S., University Malaya, 2006

Supervisory Committee

Dr. Reuven Gordon, (Department of Electrical and Computer Engineering)
Supervisor

Dr. Thomas E. Darcie, (Department of Electrical and Computer Engineering)
Departmental Member

Dr. Lisa Rosenberg, (Department of Chemistry)
Outside Member

ABSTRACT

SUPERVISORY COMMITTEE

Dr. Reuven Gordon, (Department of Electrical and Computer Engineering)
Supervisor

Dr. Thomas E. Darcie, (Department of Electrical and Computer Engineering)
Departmental Member

Dr. Lisa Rosenberg, (Department of Chemistry)
Outside Member

Transverse mode control of a vertical-cavity surface-emitting laser (VCSEL) is achieved by spatially filtered optical feedback. The spatial filter consisted of a pinhole, either 42 μm or 81 μm, in the 5.8× magnified VCSEL image plane of a confocal lens arrangement. The pinhole was translated to map out the voltage drop across the VCSEL from spatially-selective feedback. For low injection currents, spatially filtered feedback enabled single fundamental mode operation due to higher-order mode suppression by appropriately locating the pinhole. For higher injection currents with five laser modes, spatial selection of feedback enabled control of the relative mode intensities and wavelengths. The maximum increase in mode intensity achieved was 1.8× for the 42 μm pinhole and 2.4× for the 81 μm pinhole. The maximum frequency shift achieved was -2.7 GHz and -7.1 GHz with the 42 μm and the 81 μm pinholes. The spatially-selective optical feedback produced long-lived changes to the VCSEL even after the feedback was blocked – results for two separate trials where the recovery time was 38 minutes are presented (although results varied for different bias and feedback conditions).

TABLE OF CONTENTS

List of Tables

List of Figures

ACKNOWLEDGEMENT

I would like to express my sincere gratitude to my supervisor, Dr. Reuven Gordon for his informative guidance through the entirety of this work. Additional appreciation goes to the members of the supervising committee, Dr. Thomas E. Darcie, Dr. Lisa Rosenberg and Dr. Lukas Chrostowski for their efforts in thoroughly reading this thesis, which resulted in a highly improved final version.

I am grateful to my friends and colleagues in the Optical Systems and Technology Laboratory at the University of Victoria, in particular, Dr. Jinye (James) Zhang, J. Thomas Blakely, Fatima Eftekhari, Min Qiao, Yingying Lu, Pramodha Marthandam, Donna Shannon, Farzaneh Afshinmanesh, Alireza Marandi, Vahid Tavassoli and many others. Many thanks is expressed for their support, assistance, and insightful discussions, and additionally for these established friendships which made this project successful and memorable. Not forgotten also, are my Malaysian friends who would comfort me with news of my home country, bringing unity to my life in Canada.

Finally, my deepest gratitude goes to my parents, sisters and brother for their unconditional love and support.

DEDICATION

This work is dedicated to my friends and family.

CHAPTER 1

INTRODUCTION

1.1 BACKGROUND

Semiconductor lasers, developed in the 1960s, have found vast commercial applications in CD and DVD players, telecommunications, optical storage and medical application. With the advent of commercial optical fiber, such laser diode radiation properties, such as brightness, directivity, narrow spectral width, and coherence made them the best light sources for optical telecommunications. They are unique when compared to other types of lasers, such as gas lasers, and pump solid-state lasers. They are small, they operate with relatively low input power, and they are very efficient and inexpensive.

They also require the merging of two different materials and the laser action occurs in the interface between those two materials. One of the materials has an excess of electrons (*n*-type) and the other material (*p*-type) has a deficit of electrons, or, in another words, an excess of holes (missing electrons). When a forward bias current is placed across this junction, electrons are forced into junction from the *n*-type material and holes are forced into the junction from the *p*-type material. These electrons with a negative charge and the holes with a positive charge are attracted to each other, and when they "collide" they neutralize each other and in the process emit recombination radiation. The electrons in the *n*-type material exist (at normal operating temperatures) at a higher energy (conduction band) than the holes (valence band). This energy difference is designated as the *bandgap* of the material: the amount of energy per photon that is released when the recombination radiative process occurs. Different material combinations have different bandgaps and thus emit different wavelengths of light [1].

Two types of semiconductor laser devices are edge-emitting lasers and surface-emitting lasers. Edge-emitting lasers have the laser beam parallel to the surface of the junction region. Typically the mirrors are produced by using the cleaved surfaces at the ends of

the laser crystal. The surface-emitting lasers have the laser beam emitting in a direction perpendicular to the junction region with multilayer Bragg reflecting mirrors incorporated into the crystal. Each of these laser types will be described later in Chapter 2.

Vertical-cavity surface-emitting lasers (VCSELs) are among the latest developments in the technology of light sources. GaAs-based VCSELs operate mainly in the infrared portions (850 nm) of the spectrum. They have been the dominant technology for optical transmitters to achieve high performance for short-range data links and optical network switches due to low cost, ease of fiber coupling, and straightforward fabrication of large multi-element 2D arrays [1]. Having a size much smaller than conventional lasers, VCSELs have many advantages over the edge-emitting lasers, i.e. they are inexpensive to produce, emit a circular beam, operate in single mode with a low threshold current, have high output power and produce high modulation rates.

External cavity laser diodes are used to improve the spectral properties, i.e., to reduce the linewidth or to tune the wavelength and frequency of the lasers. Figure 1 shows a model of a laser diode with an external cavity. The external reflector can be a mirror or a wavelength-selective grating.

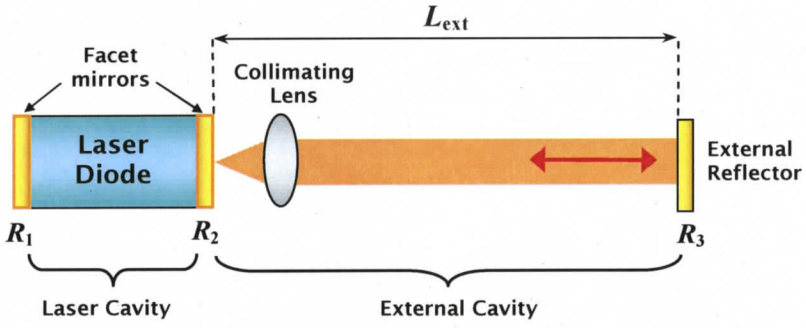

Figure 1 A model of a laser diode with an external cavity. R_1, R_2 and R_3 are the power reflectivities of the mirrors and L_{ext} is the length of external cavity.

VCSEL applications based on the external cavity setup have been proposed and used in diverse applications such as optical communications, optical spectroscopy, optical information processing and optical sensors.

1.2 Motivation

The motivation of the research undertaken here is initiated by an interest in the transverse mode control of VCSELs. Understanding that spatial and spectral properties of the multimode VCSELs, where interplay between the spatial distribution of the carriers and the optical field affects the transverse mode properties of the VCSELs, there exists an opportunity to change the mode properties of a multimode VCSEL by exciting the carriers distribution on part of its local gain region only with optical feedback light.

1.3 Research Objectives

The objectives of this study are as follows:

i) To design and analyse an external feedback optical scheme by means of a spatial filter pinhole to a multimode VCSEL for controlling its transverse modes.

ii) To investigate the design parameters of spatially filtered feedback system, such as the external cavity length, VCSEL's injection current, external mirror alignment, size and location of a spatial filter pinhole in the laser cavity to spatially control the feedback strength in terms of varying the intensity (amplitude) and frequency of the modes.

iii) To study the performance of the system and propose the applications for this design.

1.4 Thesis Outline

The most important goal of the research in this thesis is to develop a scheme to control the transverse modes of VCSELs for frequency tuning applications such as the tuning of high-frequency mode-beating sources and may also enable transverse mode-locking application.

In Chapter 2, the theory related to semiconductor lasers is reviewed. First, the basics of semiconductor laser diodes are reviewed before going deeper into the semiconductor laser rate equations, linewidth enhancement factor, and noise. Secondly, the type of VCSEL used in this thesis is introduced and distinguished from its counterparts, the edge-emitting lasers. The characteristics of VCSELs in terms of its transverse modes, polarization properties and performance issues are also briefly discussed.

In Chapter 3, the literature review on the effects of external optical feedback on lasers is presented. The drawbacks and benefits of external optical feedback on lasers are explained. Previous designs of external optical feedback to control the characteristics of VCSELs as well as the applications of such designs are discussed.

In Chapter 4, a detailed description of the methodology and the equipment used in the experimental setup are given and discussed. The design parameters such as the injection current, pinhole size and the external cavity length are varied in order to investigate the effects of these parameters on the performance and characteristics of the VCSEL under the light feedback condition.

In Chapter 5, the voltage change from spatially selective feedback is mapped out over the image plane of the VCSEL for low and high injection currents are shown in the first section. Next, higher-order mode suppression is demonstrated for low currents and selective mode intensity control is shown for high currents. The frequency shift of different modes by spatial feedback selection is presented. Mode control by changing the alignment of the mirror is shown. Finally, the recovery time of the VCSEL after spatially selective feedback is also discussed in this Chapter.

Chapter 6 draws the conclusion and future work of this study.

CHAPTER 2

SEMICONDUCTOR LASER THEORY

In this chapter, a brief introduction on the properties of semiconductor materials, energy band, p-n junction and the Fermi distribution is given before going into how semiconductor lasers work. Next, the important parameters and rate equations that describe the characteristics of semiconductor lasers will be presented. Then, vertical-cavity surface-emitting lasers (VCSELs) will be introduced and the difference between VCSELs and edge-emitting lasers will be discussed. Finally, the discussion on VCSEL characteristics in terms of its polarization properties, transverse modes, mode patterns and its performance issues will be given.

2.1 OPTICAL EMISSION FROM SEMICONDUCTORS

To gain an understanding of the light-generating mechanicsms within the semiconductor lasers, it is necessary to consider both the fundamental atomic concepts and the device structure. The review of the light-emitting mechanicsm in optical sources, the properties of semiconductor materials and energy band, especially with regard to the *p-n* junction will be presented.

2.1.1 Absorption and emission of radiation

Figure 2 illustrates a two energy state, E_1 and E_2, where an atom is initially in the lower energy state E_1. These discrete energy states for the atom may be considered to correspond to electrons occurring in particular energy levels relative to the nucleus. When a photon with energy $(E_2 - E_1)$ is incident on the atom it may be excited into the higher energy state E_2 through absorption of the photon. This process is sometimes referred to as stimulated absorption. Alternatively, when the atom is initially in the

higher energy state E_2 it can make a transition to the lower energy state E_1 providing the emission of a photon at a frequency (f) corresponding to $E = E_2 - E_1 = hf$, where h is the Planck constant. This emission process can occur in two ways, i.e., by spontaneous emission and stimulated emission as illustrated in Figure 2(b) and (c) respectively.

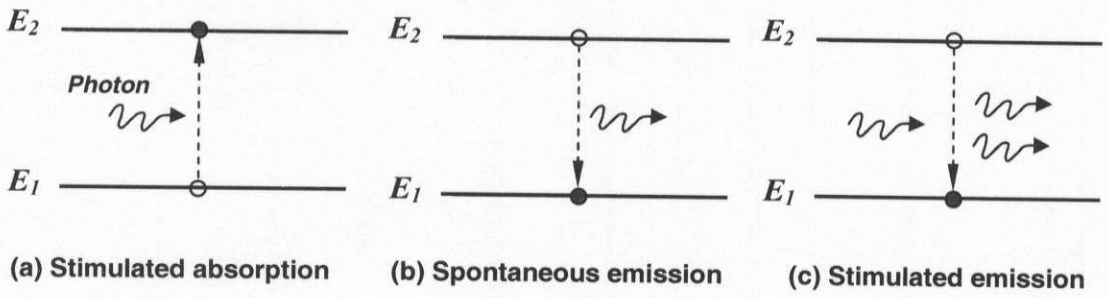

Figure 2 Energy state diagram showing: (a) absorption, (b) spontaneous emission and (c) stimulated emission. The black circle and dot indicate the states of the atom before and after a transition respectively [2].

The spontaneous emission process, in which the atom returns to the lower energy state in an entirely random manner, gives incoherent radiation. This similar emission process in semiconductors provides the basic mechanism for light generation within the light-emitting diodes (LED).

It is the simulated emission process, however, which gives the laser its special properties as an optical source. Firstly, when a photon having an energy equal to the energy difference between the two states ($E_2 - E_1$) interacts with the atom in the upper energy state causing it to return to the lower state with the creation of a second photon. The second photon produced by stimulated emission is generally of an identical energy to the one which caused it and hence the light associated with them is of the same frequency. Secondly, the light associated with the stimulating and stimulated photon is in phase and has the same polarization. Therefore, in contrast to spontaneous emission, coherent radiation is obtained. To its advantage of the coherent radiation, the released energy can add to the wave in a constructive manner, providing amplification. In lasers, this radiation is amplified by mirrors within a resonant cavity. Stimulated emission of lasers is coherent, intense and has a narrow linewidth.

2.1.2 Semiconductor materials and energy band

Many important properties of semiconductors are described by considering electrons in the conduction band (CB) and holes in the valence band (VB). In order to promote electroluminescence, it is necessary to select an appropriate semiconductor material. The most useful materials (such as, GaAs, GaSb, InAs and InSb) for this purpose are *direct bandgap semiconductors* in which electrons and holes on either side of the energy gap have the same value of crystal momentum and thus direct recombination is possible. This process is illustrated in Figure 3(a) with an energy-wavevector (E-k) diagram for a direct bandgap semiconductor. The upper and lower E-k curves correspond to the states in the CB and VB. Note that crystal momentum is related to the wavevector k for an electron in a crystal by $p = \hbar k$, where $\hbar$ is the reduced Planck constant [2]. Hence when electron-hole recombination occurs the momentum of the electron remains virtually constant and the energy released, which corresponds to the bandgap energy E_g.

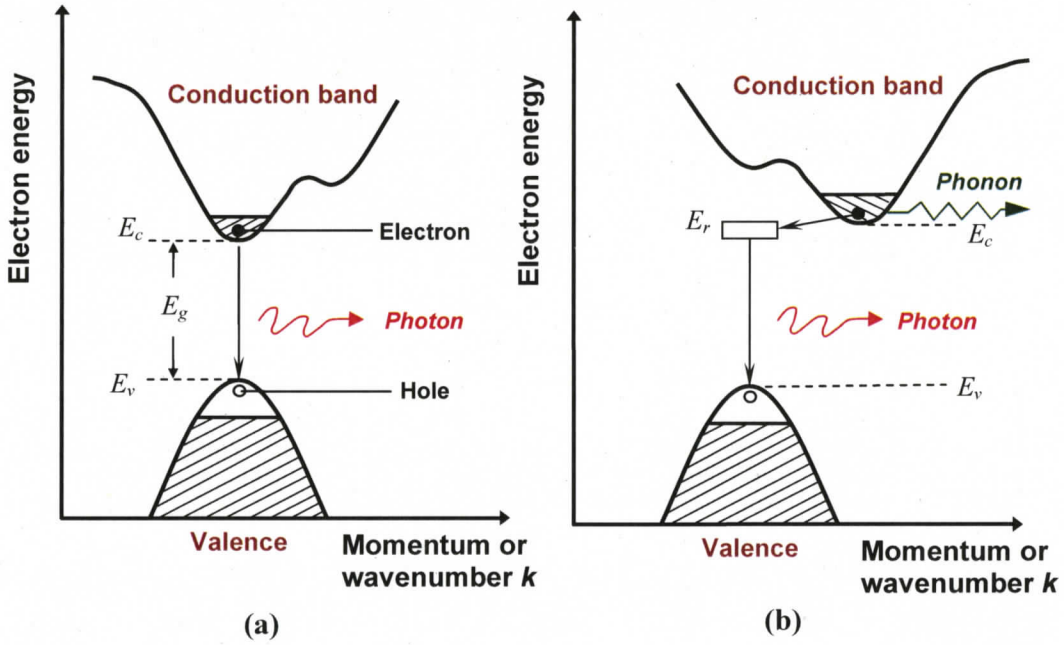

Figure 3 Energy-wavevector diagrams showing the types of transition: (a) direct bandgap semiconductor and (b) indirect bandgap semiconductor. [4]

The electron-hole recombination could be either radiative or non-radiative. Non-radiative recombination may be caused by recombination at traps or defects, surface recombination, or Auger recombination [3]. In non-radiative recombination the energy released is dissipated in the form of lattice vibrations and thus heat. However, in band-to-band radiative recombination the energy is released with the creation of a photon with a frequency where the energy is approximately equal to the bandgap energy E_g, and therefore, $E_g = h\nu = hc/\lambda$, where c is the velocity of light and λ is the optical wavelength.

In the *indirect bandgap semiconductors* (such as Si and Ge), however, the maximum and minimum energies occur at different values of crystal momentum (displaced on the k-axis). For electron-hole recombination to take place, it is essential that the electron losses momentum such that it has a value of momentum corresponding to the maximum energy of the valence band. As illustrated in Figure 3(b), the recombination process in these elemental semiconductors (Si and Ge) occurs via a recombination center at an energy level E_r within the bandgap. These recombination centers may be crystal defects or impurities. The electron first captured by the defect at E_r. The change in the energy and momentum of the electron by this capture process is transferred to the lattice vibrations, i.e., to *phonons*. The captured electron at E_r can quickly fall down into an empty state at the top of the VB and thereby recombine with hole. The conservation of momentum requires the emission or absorption of a third particle, a photon. This three-particle recombination process is relatively slower and less likely than the two-particle process produced by direct bandgap semiconductors. In some indirect bandgap semiconductors, such as GaP, however, the recombination of the electron with a hole at certain recombination centers results in photon emission as shown in Figure 3(b).

2.1.3 The Fermi-Dirac distribution

For a semiconductor in thermal equilibrium the energy level occupation is described by the Fermi-Dirac distribution function. Consequently, the probability $P(E)$ that an electron gains sufficient thermal energy at an absolute temperature T such that it will be found occupying a particular energy level E, is given by the Fermi-Dirac distribution [5]

$$P(E) = \frac{1}{1 + \exp(E - E_F)/k_B T} \tag{2.1}$$

where, k_B is Boltzmann's constant and E_F is known as the Fermi energy or Fermi level.

The Fermi level is a mathematical indication of the probability distribution of carriers within the material and is the energy level between E_c and E_v for which the probability of a state being occupied by an electron is 1/2.

The most useful definition of E_F is in terms of a change in E_F. If V is the potential difference between two points, then

$$\Delta E_F = eV \tag{2.2}$$

where e is the electronic charge (=1.60218 × 10^{-19} Coulomb).

For a semiconductor system in thermal equilibrium, and with no applied voltage, $\Delta E_F = 0$ and E_F must be uniform across the system as shown in Figure 4(a). Quasi-fermi levels are energy levels used to specify the carrier concentration inside a semiconductor under non-equilibrium conditions. For example, when the semiconductor is forward biased, the equilibrium conditions are being disturbed and two energy levels are used, E_{Fn} (the quasi-level for electrons) and E_{Fp} (the quasi-level for holes), which are by definition related to the non-equilibrium carrier concentrations in the same way E_F is related to the equilibrium carrier concentrations.

2.2 Principle of the Laser Diode

The laser is a device that amplifies, or generates, light by means of the stimulated emission of radiation. For a semiconductor to function like a laser, three main conditions should be met, that is, population inversion, stimulated emission and positive feedback.

Consider a heavily doped direct bandgap semiconductor *p-n* junction whose Fermi level E_{Fn} in the *n*-side is in the CB and that E_{Fp} in the *p*-side is in the VB as shown in Figure 4.

Without applied voltage, the Fermi level is continuous across the diode, $E_{Fp} = E_{Fn}$. The depletion region in such a *p-n* junction is very narrow. There is a built-in voltage V_o that gives rise to a potential energy barrier eV_o that prevents electrons in the CB of *n*-side diffusing into the CB of the *p*-side. There is a similar barrier stopping hole diffusion from *p*-side to *n*-side.

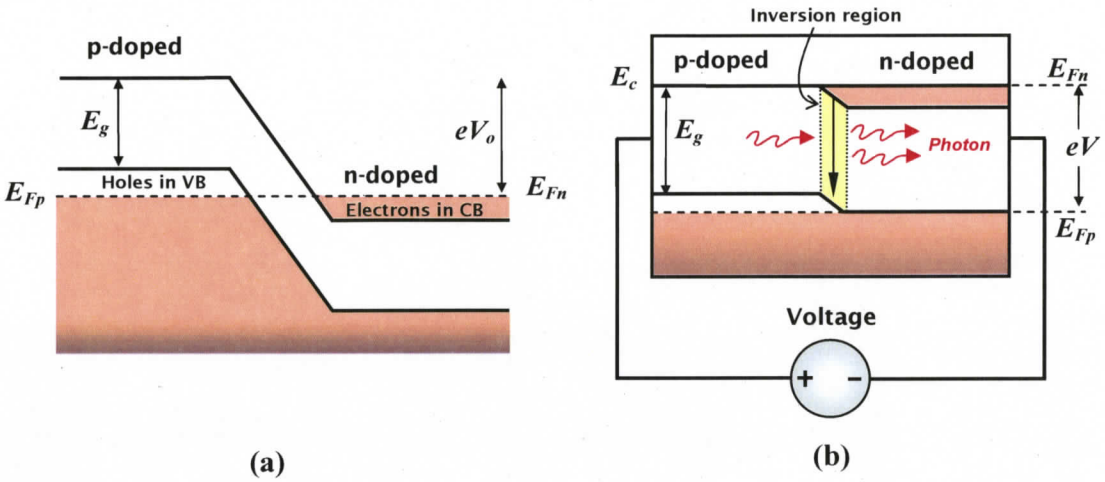

Figure 4 The *p-n* junction: (a) with no applied voltage; (b) with strong forward bias. [4]

When a voltage is applied to a *p-n* junction device, the change in the Fermi level from end-to-end is the electrical work done by the applied voltage as expressed in Equation (2.2). Suppose that this heavily doped *p-n* junction is forward biased by a voltage V greater than the bandgap voltage; $eV > E_g$ as shown in Figure 4(b). The separation between E_{Fn} and E_{Fp} is now the applied potential energy or eV. The applied voltage diminishes the built-in potential barrier to almost zero which means that electrons flow into the inversion region and flow over to the *p*-side to constitute the diode current. There is a similar reduction in the potential barrier for holes from *p* to *n*-side. The final result is that electrons from *n*-side and holes from *p*-side flow into the inversion region or the active region. In other words, there is a *population inversion* between energies near E_c and those near E_v around the junction and the condition for inversion in a semiconductor laser is given by $E_{Fn} - E_{Fp} = eV > E_g$.

2.2.1 Population inversion and stimulated emission

At the basis of the lasing process stands the phenomenon of spontaneous emission, which initializes the stimulated emission of radiation from the population inversion.

When population inversion just starts, we say the diode is at transparency. In the case of diode lasers, the population inversion is achieved by a sufficient number of

electron-hole pairs supplied by an electrically pumped current through the doped sandwich layers. The population inversion layer along the *p-n* junction is called the *active region*. An incoming photon with energy of ($E_c - E_v$) can stimulate an electron to fall down from E_c to E_v. Population inversion is necessary because the greater the number of excited electrons, the greater the number of stimulated photons that can be radiated. The region where there is population inversion and hence more stimulated emission than absorption, has an optical gain because an incoming photon is more likely to cause stimulated emission than being absorbed. The optical gain depends on (E_{Fn} - E_{Fp}) which depends on the applied voltage and hence on the diode current.

To achieve lasing action, sufficient population inversion must be present to overcome all the losses in the cavity. Two main loss mechanisms are: First, many photons are absorbed within the semiconductor material before they can escape to create radiation. Secondly, mirrors do not reflect 100% of the incident photons. In other words, the loss stems mainly from the absorption and transmission of the stimulated photons and to make a laser diode generate light, gain must exceed loss. Loss is a constant for a given diode as shown in Figure 5, but gain can be changed. Increasing gain is done by increasing the forward current. Eventually gain becomes equal to loss, a situation called *threshold condition* and the corresponding forward current is called *threshold current*, I_{th}. At this threshold condition, a semiconductor diode starts to act like a laser as shown in Figure 5 and Figure 9.

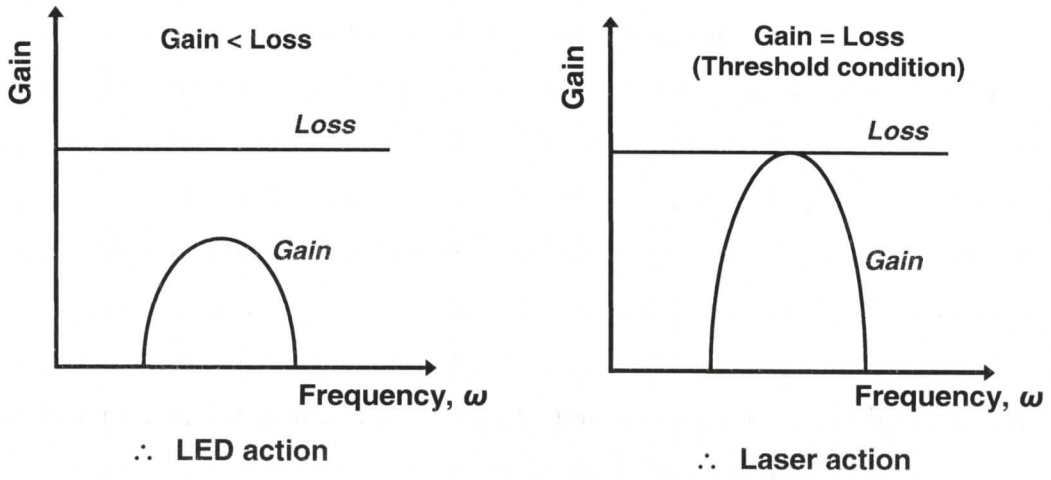

Figure 5 Gain and loss profiles in semiconductor lasers.

When the current exceeds the threshold current, the excess carriers brought in by the current recombine by stimulated emission increasing the intensity of the laser output light. In other words, the gain and carrier density in the cavity at threshold are clamped and further increase in carrier input goes over to the laser output by stimulated recombination. Additional explanation will be given in the next Section on laser rate equations.

2.2.2 Positive feedback

In addition to population inversion, we also need to have an optical cavity to implement a laser oscillation, that is, to build up the intensity of stimulated emission by means of an *optical resonator*. This would provide a continuous coherent radiation as output from the device. To achieve this, two mirrors are designed to provide *positive optical feedback* – *positive* because the feedback adds the output (stimulated photons) to the input (external photons). For example, two photons – one external and one stimulated – are then reflected back and directed to the active layer again. These two photons now work as external radiation and stimulate the emission of two other photons. These four photons are reflected back into the active layer by the mirror and this process continues ad infinitum. These two mirrors, then, constitute a *resonator*.

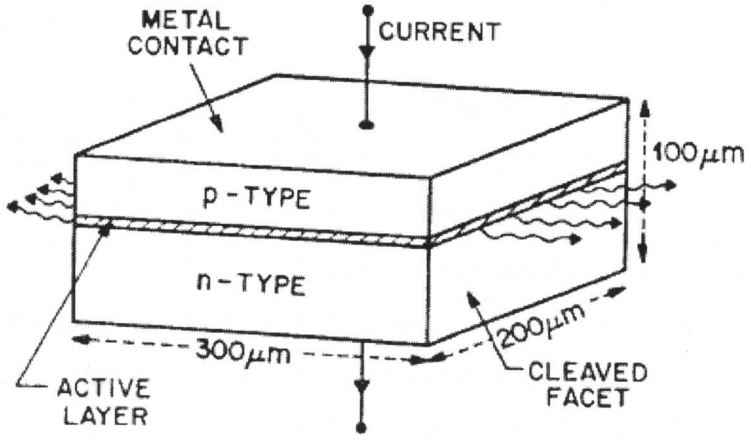

Figure 6 Basic structure of an edge-emitting broad area semiconductor laser. [1]

Figure 6 shows schematically the structure of an edge-emitting laser diode. The ends of the crystal are cleaved to be flat and optically polished to provide reflection and hence form an optical cavity. Photons that are reflected from the cleaved surfaces stimulate more photons of the same frequency and so on. This process builds the intensity of the radiation in the cavity. Therefore, two mirrors and the active medium between them form a laser and this simple structure is also known as a Fabry-Perot resonator as illustrated in Figure 7(a). The wavelength of the radiation that can build up in the cavity is determined by the length L of the cavity because only multiples of the half-wavelength can exists in such an optical cavity, as will be explain below.

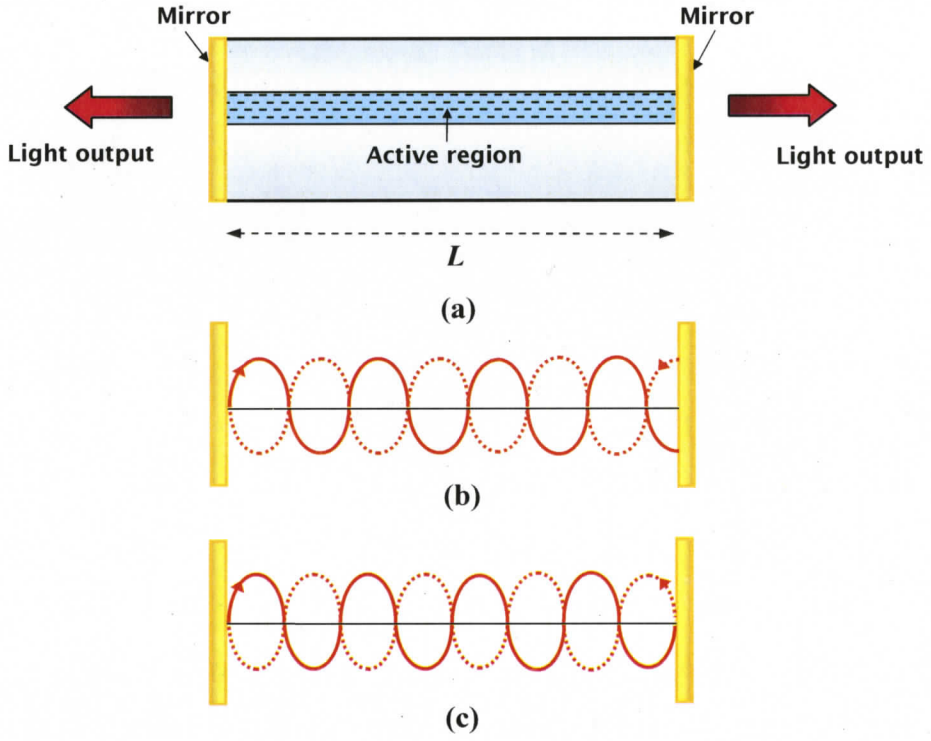

Figure 7 (a) A Fabry-Perot laser diode, (b) Fabry-Perot resonator with arbitrary wave, and (c) Fabry-Perot resonator with standing wave

As Figure 7(b) shows, an arbitrary wave travels from left-hand mirror to the right-hand mirror, this wave is reflected at the right mirror with the dashed-line showing the reflected wave; hence, the wave experiences a 180^{o} phase shift because reflection causes a phase shift of 180^{o} when the incident wave traveling in the medium of lesser index of

refraction (with greater speed) is reflected off a medium of higher index of refraction [6]. Since there is a break in its travel path, the resonator does not support this wavelength. In the next diagram, Figure 7(c), after the wave experiences 180^{o} phase shift and it continues to propagate. Thus, the second wave yields a stable pattern called a *standing wave*.

A resonator can support only a wave with a certain wavelength, the wave that forms a standing-wave pattern as illustrated in Figure 7(b). This physical requirement can be written as [1]

$$2L/\lambda = N \tag{2.3}$$

where L is the distance between mirrors and N is an integer.

What is important to discern here is that this resonator may support many wavelengths that satisfy Equation (2.3): $2L/N$, $2L/(N \pm 1)$, $2L/(N \pm 2)$, $2L/(N \pm 3)$, and so forth. Wavelengths selected by a resonator are called *longitudinal modes*. These modes are composed of an EM field whose electric-field (**E**) and magnetic-field (**H**) vectors are perpendicular to the direction of propagation – the centerline of a resonator. They are distinguished only by their frequency or by the integer N mentioned above. When the length of a resonator increases or decreases, the laser switches from one longitudinal mode to another. This is called *mode hop*.

Although the resonator can support an infinite number of waves whose wavelengths satisfy Equation (2.3), the active medium provides gain within only a small range of wavelengths. Therefore, only several resonant wavelengths that fall within the gain curve might be radiated as illustrated in Figure 8.

Eventually, only those resonant wavelengths that are within the gain-over-loss curve will actually be radiated. Waves with λ_N, $\lambda_{N\pm1}$, $\lambda_{N\pm2}$ and $\lambda_{N\pm3}$ might be radiated, but only waves with λ_N, $\lambda_{N\pm1}$ and $\lambda_{N\pm2}$ will be actual laser output. The depicted shaded modes, $\lambda_{N\pm3}$, are not generated. The spacing between two adjacent longitudinal modes can also be obtained as follows:

$$\lambda_N - \lambda_{N+1} \approx 2L/N^2 = \lambda^2/2L \tag{2.4}$$

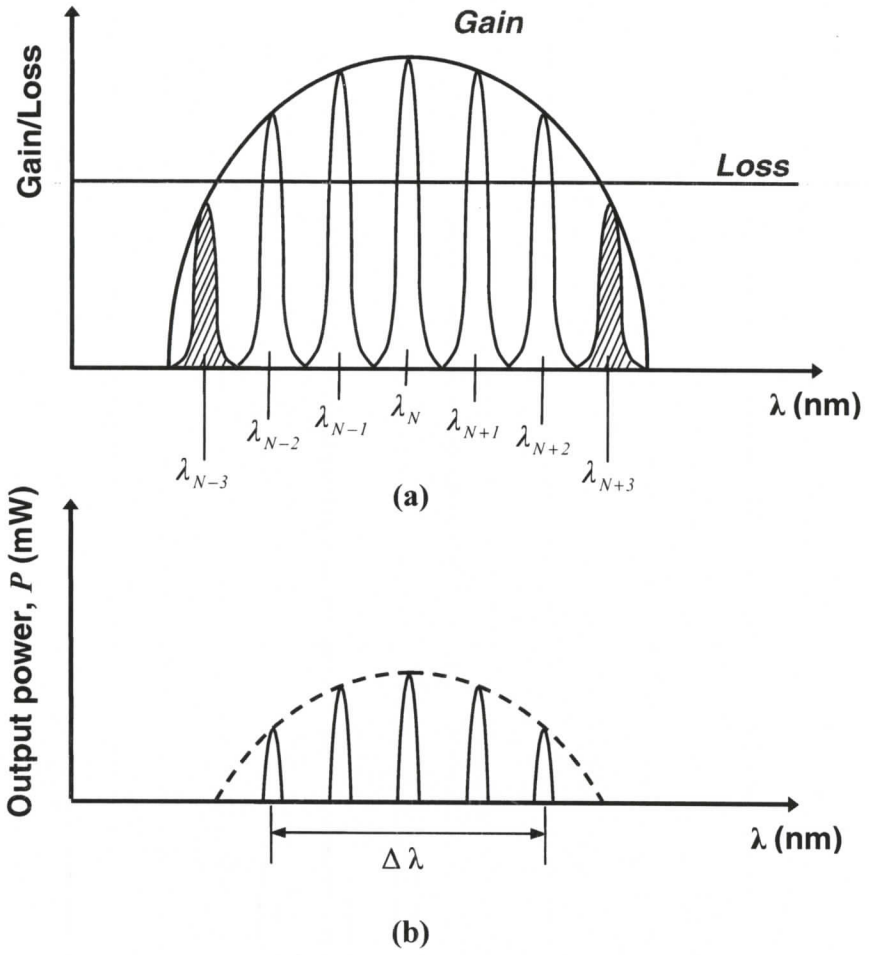

Figure 8 (a) Gain-loss curve and possible longitudinal modes; (b) actual multimode radiation

The coherence length of a laser is distance from a coherent source to a point at which the electromagnetic wave can maintain its coherency, i.e., the standing wave pattern. This means that for any temporal separation, all points within the coherence length of the laser are predictable in terms of their phase. In practice, the coherent wave can exist only over a finite time duration Δt that correspond to a coherence length expressed as [2]

$$\ell_c = c\Delta t = \frac{\lambda^2}{\Delta\lambda} \tag{2.5}$$

2.2.3 Lasing effect and input-output characteristics

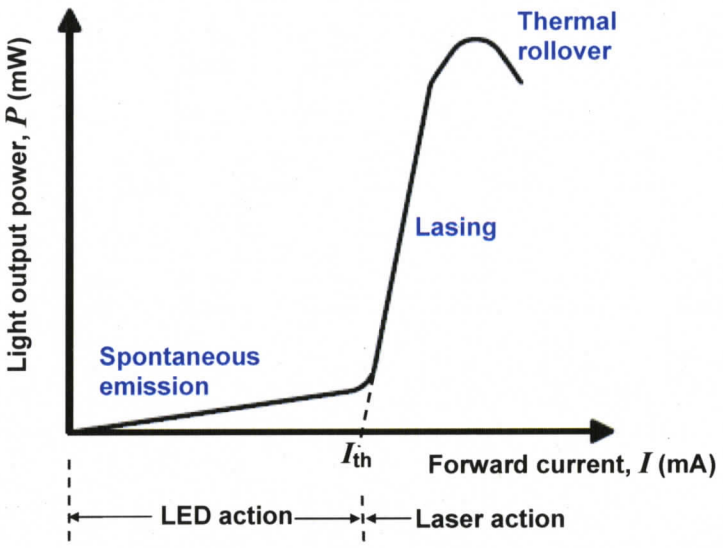

Figure 9 *P-I* diagram of a semiconductor laser showing three different regions: spontaneous emission, lasing and damped by heating (rollover)

Figure 9 demonstrates the graph of output light power (P) versus input forward current (I), P-I characteristics and is sometimes also referred to as an "L-I graph", where "L" stands for "luminescence". When a small current is applied, a number of electrons are excited and the diode radiates like a light-emitting diode (LED).

When the current density becomes sufficient enough to create population inversion and the threshold condition is reached (where gain equals loss), the diode starts to work like a laser. After the threshold current, I_{th}, has been exceeded, increasing output power requires much less current to flow than before it was passed. In other words, the slope, $\Delta P/\Delta I$, becomes much steeper than that for an LED. The slope, $\Delta P/\Delta I$ in watts/amp above threshold, can be used to calculate the differential quantum efficiency, η_d, which is defined as the number of photons out per electron in from a measured P-I characteristic.

The differential quantum efficiency equation is given by [7]

$$\eta_d = \left(\frac{e}{h\nu}\right)\frac{dP_0}{dI} \tag{2.6}$$

where, $[dP_0/dI]$ can be found by measuring the slope and then multiplying this number by $[e/h\nu]$ in Coulombs/Joule.

Continual increase in the current will cause 'rollover' behaviour due to current heating in the cavity which exists from the current leakage paths that "turn-on" at higher current. The excessive heating of the gain materials will lead to laser performance degradation. Further discussion on the temperature dependence of laser diodes will be presented in Section 2.4.4.

2.2.4 Derivative analysis

The voltage vs. current (*V-I*) curve shows the voltage drop across the laser and is often used in derivative characterization techniques that is acquired during electrical characterization of the laser diode. In addition to the *V-I* curve, it is common to plot the *I dV/dI* vs. *I* curve (expressed in volts) and this derivative curve is a very important tool for diode laser manufacturer. Analysis of *I dV/dI* data allows equivalent circuit models for the specific diode laser under test to be created [7, 8]. These models will show series and shunt, linear and nonlinear, resistive circuit elements. From this data, junction ideality factor, contact resistance, leakage currents, and threshold can be calculated.

In fact, this method of characterization permits threshold calculation without the time-consuming (and expensive) inconvenience of having to position the die in front of a detector (for *P-I* curve plotting). Thus, in production applications where a bare laser die must be characterized before mounting and packaging, the derivative analysis method has proven to be extremely convenient.

The diode *V-I* is described by [7]

$$I = I_o\left[\exp\left(\frac{eV_d}{n_d k_B T}\right) - 1\right] \tag{2.7}$$

where I_o is the saturation current, e is the electron charge, n_d is the diode ideality factor, k_B is the Boltzmann's constant and T is the temperature.

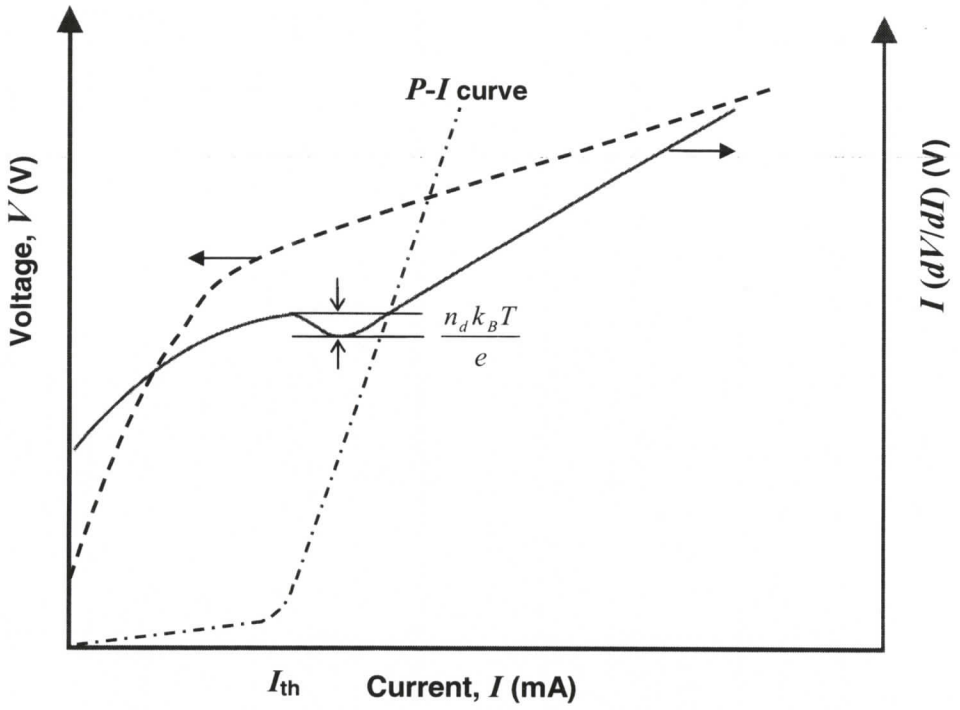

Figure 10 Plots of terminal voltage, V, and $I\,dV/dI$ vs. current I for a laser diode. The *P-I* curve is overlaid here to show the threshold current.

As illustrated in Figure 10, voltage across the junction clamps at threshold with the carrier density, a kink in the curve occurs at that point. The equation of total laser diode current at threshold and further increase in current onwards with consideration that the terminal voltage of diode is expressed as $V = V_d + IR$ where V_d represents the voltage across an ideal diode and R is the parasitic resistance in series with an ideal diode. Therefore, by rearranging Equation (2.7) we get:

$$I = I_o\left[\exp\left(\frac{e(V - IR}{n_d k_B T}\right) - 1\right]$$

$$V = \frac{eIR + \left(n_d k_B T \times ln\frac{I_o + I}{I_o}\right)}{e}$$

Taking derivative of the equation above and solving for $\frac{dV}{dI}$ with assumption that I is much greater than I_o but below threshold yield

$$\frac{dV}{dI} = R + \frac{n_d k_B T}{e(I + I_o)}$$

$$I\frac{dV}{dI} = IR + I\frac{n_d k_B T}{e(I + I_o)}$$

Below threshold, we obtain $I\frac{dV}{dI} = IR + \frac{n_d k_B T}{e}$ for $I \gg I_o$, while above threshold V_d is constant, so $I\frac{dV}{dI} = IR$. The kink at the threshold current results in this, $\frac{d^2V}{dI^2} = 0$. The equation $I\frac{dV}{dI} = IR + \frac{n_d k_B T}{e}$ is in slope-intercept form ($y = mx + c$) and the magnitude of this kink is $n_d k_B T/e$ as shown in Figure 10. The slope above and below threshold should be R.

2.3 Semiconductor Laser Rate Equations – A Deeper Look

The dynamics of diode lasers can be adequately described by the complex optical field and the number of electron-hole pairs in the active layer. The temporal behaviour of the optical field and the number of electron-hole pairs is governed by a set of coupled rate equations.

2.3.1 Carrier dynamics

Consider a laser diode under forward bias as in Figure 4(b). The current carries the electrons into the active region providing the generation term (G_{gen}), and various radiative and non-radiative recombination process plus carrier leakage (due to thermionic emission or by lateral diffusion if no lateral confinement exists) providing the recombination terms (R_{rec}).

Assuming charge neutrality (electron density equals the hole density) in the active region, we can simplify the dynamics analysis of the electron-hole population by tracking only the electron density n. In general form, the carrier-density rate equation is [7, 9]

$$\frac{\partial n}{\partial t} = G_{gen} - R_{rec}$$

$$= D(\nabla^2 n) + \frac{J}{ed} - R(n) \qquad (2.8)$$

where n is the carrier-density in the active medium. The first term on the right-hand side of (2.8) accounts for carrier diffusion (D the diffusion coefficient). The second term accounts for the rate of carrier generation (J the current density, e the elementary charge, and d the depth of the active layer) as a result of the pump-current. The last term accounts for the carrier loss due to electron-hole recombination processes, both radiative and non-radiative.

Due to the small dimension of the active layer compared to the diffusion length, the first diffusion term can be neglected and $\partial n/\partial t$ can be replaced by dn/dt (n is spatially independent). The last term can be split into four parts as [9]

$$R(n) = An + Bn^2 + Cn^3 + R_{st}N_{ph}, \qquad (2.9)$$

where An accounts for non-radiative recombination at defects, Bn^2 accounts for spontaneous radiative recombination, and Cn^3 is due to Auger recombination processes. The last term is due to stimulated recombination that leads to coherent light emission. N_{ph} is the intracavity photon density and R_{st} is the net rate of stimulated emission given as [9]

$$R_{st} = (c/\mu_g)g(n) = v_g g(n), \qquad (2.10)$$

with c being the speed of light, $g(n)$ the optical gain, and μ_g the group index of the dispersive semiconductor material given by [9]

$$\mu_g = \mu + \nu(\partial\mu/\partial\nu), \qquad (2.11)$$

where μ is the refractive index of the active medium and ν is the lasing frequency. In Equation (2.10), $v_g = c/\mu_g$ is the group velocity. The carrier lifetime τ_n can be given by [9]

$$\tau_n^{-1} = A + Bn + Cn^2. \qquad (2.12)$$

Equation (2.8) can then be rewritten as

$$\frac{dn}{dt} = \frac{J}{ed} - \frac{n}{\tau_n} - v_g g(n) N_{ph} . \tag{2.13}$$

The gain $g(n)$ can be approximated by [9, 10]

$$g(n) = a(n - n_0) = \frac{\partial g}{\partial n}(n - n_0) , \tag{2.14}$$

where $a = \partial g / \partial n$ is the gain coefficient and n_0 is the carrier density at transparency. By introducing the differential gain $\xi = v_g a$, along with Equation (2.14), Equation (2.13) becomes

$$\frac{dn}{dt} = \frac{J}{ed} - \frac{n}{\tau_n} - \xi(n - n_0) N_{ph} . \tag{2.15}$$

As the current increases and provides more pumping, N_{ph} increases (helped by the optical cavity), and eventually the stimulated term dominates the spontaneous term (as in Figure 9). The threshold electron concentration n_{th} and threshold current I_{th} refers to that condition when the stimulated emission just overcomes the spontaneous emission and total loss mechanism. When current exceeds threshold current, the output light power P_o is proportional to N_{ph} and the output optical power increases sharply with the current (Figure 11) so we can just take $N_{ph} = 0$ when $I = I_{th}$.

Initially, when the current is increased slightly above the threshold current, the carrier density and gain increase to values above their threshold levels (for on the order of a nanosecond), and the photon density increases. However, the stimulated recombination term R_{st} also increases, reducing the carrier density and gain until a new steady-state dynamic balance occurs. In other words, stimulated recombination term in Equation (2.15) uses up all excess carriers brought in by the pump current. Under steady state conditions above threshold, the carrier density n in the active region remains at n_{th}, though the rates of carrier injection and stimulated recombination have increased. Thus,

after threshold condition, n clamps ($dn/dt = 0$) causing the gain to clamp also as shown in Figure 11.

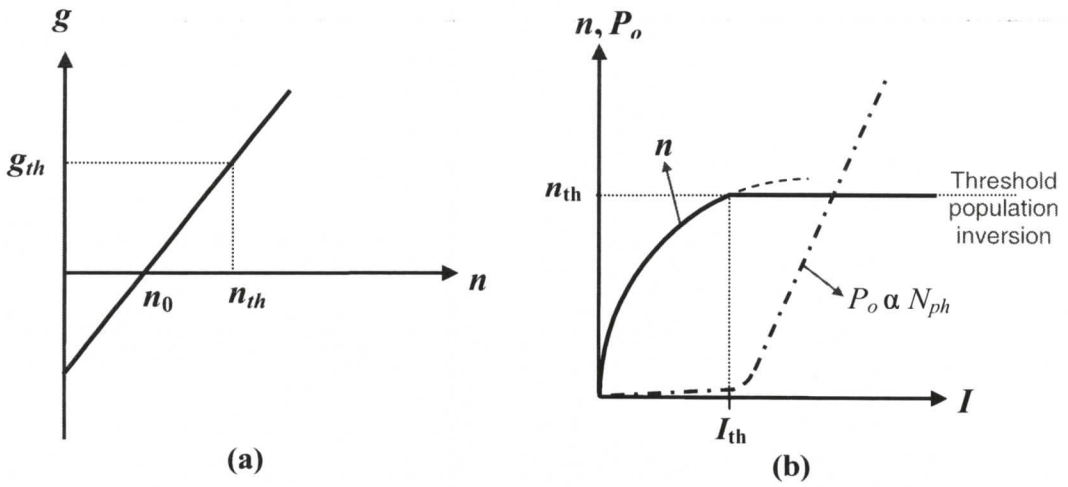

Figure 11 (a) Gain g vs. carrier density n, and (b) carrier density n and coherent radiation output P_o vs. current I. [7]

2.3.2 Field dynamics

Starting from the Maxwell wave equation, it can be shown that the electric field in the cavity for a single mode case satisfies the following equation [9]

$$\frac{dE}{dt} = \frac{i\overline{\mu}}{\mu_g}(\omega - \Omega)E + \frac{i\omega}{\mu_g}\left(\Gamma\Delta\mu_p + \frac{i\overline{\alpha}}{2k_0}\right)E, \tag{2.16}$$

where $\overline{\mu}$ is the mode index, Ω is the cavity-resonance frequency, Γ is the confinement factor [1, 9, 10], $\Delta\mu_p$ is the carrier-induced index change, $k_0 = \omega/c$, and $\overline{\alpha}$ is the mode-absorption coefficient given by [9]

$$\overline{\alpha} = -\Gamma g + \frac{1}{v_g \tau_p}, \tag{2.17}$$

with τ_p being the photon lifetime given as [9]

$$\tau_p = \frac{1}{v_g(\alpha_m + \alpha_{\text{int}})}, \tag{2.18}$$

where α_m is the mirror loss coefficient and α_{int} is the internal loss coefficient.

Expressing $E = A\exp(-i\phi)$ in (2.16), we get

$$\text{Left-hand side} = \frac{dE}{dt} = \frac{dA\exp(-i\phi)}{dt} = A\frac{d\exp(-i\phi)}{dt} + \exp(-i\phi)\frac{dA}{dt}$$

$$= A\frac{d\exp(-i\phi)}{d\phi}\frac{d\phi}{dt} + \exp(-i\phi)\frac{dA}{dt}$$

$$= \left[-iA\frac{d\phi}{dt} + \frac{dA}{dt}\right]\exp(-i\phi), \tag{2.19}$$

Right-hand side

$$= \left\{i\left[\frac{\overline{\mu}}{\mu_g}(\omega-\Omega) + \frac{\omega}{\mu_g}\Gamma\Delta\mu_p\right]A - \frac{\omega}{\mu_g}\frac{-\Gamma g + (1/v_g\tau_p)}{2\omega/c}A\right\}\exp(-i\phi). \tag{2.20}$$

Equating the real and imaginary parts of (2.19) and (2.20), we find the amplitude and phase equations as [9]

$$\frac{dA}{dt} = \left[\frac{1}{2}\Gamma v_g g - \frac{1}{\tau_p}\right]A, \tag{2.21}$$

$$\frac{d\phi}{dt} = -\frac{\overline{\mu}}{\mu_g}(\omega-\Omega) - \frac{\omega}{\mu_g}\Gamma\Delta\mu_p. \tag{2.22}$$

Another useful form of the field equation is obtained as follows. Assume small bandwidth, i.e., let $\omega - \Omega \approx 0$ [9].

$$\Delta\mu_p = -\frac{\beta_c\Delta g}{2k_0} = -\frac{c\beta_c\Delta g}{2\omega}, \tag{2.23}$$

where the β_c parameter is the ratio of the real to imaginary part of the pump-induced susceptibility [9, 10] and is called the *linewidth enhancement factor*.

The imaginary part of dE/dt in (2.16) can now be approximated as

$$\text{Im}\left(\frac{dE}{dt}\right) = -\frac{\omega\Gamma}{\mu_g}\frac{c\beta_c\Delta g}{2\omega}E = \frac{1}{2}\beta_c\Gamma v_g\Delta g E = \frac{1}{2}\beta_c\left(\Gamma v_g g - \frac{1}{\tau_p}\right)E, \tag{2.24}$$

where we have defined $G \equiv \Gamma v_g g$ and used $\Delta G = \Gamma v_g \Delta g = G - \tau_p^{-1}$ [9].

While the real part of dE/dt in Equation (2.16) can be calculated as

$$\mathrm{Re}\left(\frac{dE}{dt}\right)=-\frac{\omega\overline{\alpha}}{2\mu_g k_0}E=\frac{1}{2}v_g\left(\Gamma g-\frac{1}{v_g\tau_p}\right)E=\frac{1}{2}\left(\Gamma v_g g-\frac{1}{\tau_p}\right)E. \tag{2.25}$$

Combining (2.24) and (2.25), we get

$$\frac{dE}{dt}=\frac{1}{2}(1+i\beta_c)\left[\Gamma\xi(n-n_0)-\frac{1}{\tau_p}\right]E, \tag{2.26}$$

where we have used the fact that $v_g g=v_g a(n-n_0)=\xi(n-n_0)$.

For the case of external optical feedback to a laser, the normalized field dynamics rate equation based on Lang-Kobayashi [11] becomes

$$\frac{dE}{dt}=\frac{1}{2}(1+i\beta_c)\Gamma\xi\Delta N(t)E(t)+\gamma E(t-\tau)e^{-i\omega_o\tau}, \tag{2.27}$$

This model is illustrated in Figure 1 whereby the external optical feedback was provided from an external mirror with power reflectivity $R_3 = r_3^2$ and is positioned at a distance $L_{ext} = c\tau/2$ from the right facet (R_2), where τ is the round-trip time in the external cavity.

The optical feedback is accounted for by two parameters: the delay time τ, and the feedback-rate γ which is defined for a symmetric cavity and is given by [10]

$$\gamma=\frac{1-r^2}{\tau_{in}}\frac{r_3}{r}, \tag{2.28}$$

where τ_{in} is the round-trip time of the field in the laser chip, r is the reflectivity of the diode facet, and r_3 is the reflectivity of the external mirror.

The first parameter τ has two roles in the feedback term; (1) in the delayed amplitude $E(t-\tau)$ and (2) the phase factor, $\exp(-i\omega_o\tau)$, where ω_o is the angular frequency of the solitary laser. In Chapter 3, by varying external cavity length and optical feedback level, the five regimes of qualitatively different behaviour of laser will be discussed.

2.3.3 Spectral linewidth and linewidth enhancement factor

Here, the two parameters: *spectral width* and *linewidth*, of a laser will be distinguished first. The spectral width ($\Delta\lambda$) of the radiation from a multimode laser is essentially determined by its gain curve because this diode radiates many modes (lines) inscribed in the gain curve as illustrated in Figure 8. The spectral width of such a laser diode is measured as the full width at half maximum (FWHM) of the pulse power. While, for single mode laser diodes, the spectral width of light radiated is the linewidth because they radiate only one mode, or line.

The shape of a radiated line is governed by the Lorentzian function and its FWHM width is determined by the following equation [3]:

$$\Delta f = \frac{R_{sp}(1+\beta_c^{\,2})}{N_{rad}} \tag{2.29}$$

where, R_{sp} is the rate of spontaneous emission, β_c is the linewidth enhancement factor, and N_{rad} is the number of photons radiated inside the laser cavity. N_{rad} can be related to the output power, P, and we can express linewidth in terms of output power P and other parameters of a laser diode [3]:

$$\Delta f = \frac{R_{sp}(1+\beta_c^{\,2})}{P} M \tag{2.30}$$

where, $M = (E_p v\alpha_{tr}/8\pi)$ and $E_p = h_\omega = hc/\lambda$ (photon's energy), while $v\alpha_{tr}$ is the rate at which photons escape from a laser resonator. Here, $v = c/\mu_p$ is the group velocity of light within the active region, whose refractive index is μ_p. Transmission loss, α_{tr} has been discussed briefly in Section 2.2.1.

It is customary to measure linewidths of some laser diodes with very narrow linewidths in Hertz (Hz) rather than in nanometer (nm). The relationship between $\Delta\lambda$ and Δf follows from the fundamental formula $\lambda f = c$. So we can easily obtain

$$\Delta f \cong -\left(\frac{c}{\lambda^2}\right)\Delta\lambda \tag{2.31}$$

From Equation (2.30), there are three important parameters that determine the linewidth of a laser diode. First, the linewidth is inversely proportional to output power,

P, and this equation relationship holds for the low-power devices (up to 10 mW) and tends to saturate when power increases significantly. Secondly, linewidth is proportional to the rate of spontaneous emission, R_{sp}. Spontaneous transitions occur between different energy levels and this results in the emission of different wavelengths. This emission contributes to output-stimulated light and spreads the linewidth.

The third important parameter is the linewidth enhancement factor, β_c, (or more commonly denoted by 'α' in some texts), which accounts for the coupling inside the laser cavity of the EM wave amplitude with its phase. Another way to understand the physics of this phenomena is to examine the following equation rearranged from Equation (2.23) [3, 12]:

$$\beta_c = -2k_0\left(\frac{\Delta\mu_p}{\Delta g}\right) \tag{2.32}$$

where $k_0 = 2\pi/\lambda_0$ is the wave number, λ_0 is the wavelength in free-space, $\Delta\mu_p = \partial\mu/\partial n$ is the rate of change of refractive index, μ, as a function of the density of the injected carriers, n, and Δg is the differential gain. The linewidth enhancement factor varies from about 1.5 to 10 [12].

The refractive index of an active medium, μ, is a function of the charge carriers' density; this derivative changes with differential gain. Equation (2.32) also shows the linewidth enhancement factor depends on lasing wavelength.

2.3.4 Laser noise

Light radiated by a laser diode fluctuates in its intensity, frequency and phase even when biasing current is ideally constant. These fluctuations, caused mostly by spontaneous emission, are random in nature. They are called *laser noise*.

Phase fluctuations

Also, known as *chirp* – result in broadening of a linewidth of radiated light. Chirp that exists in lasers during modulation causes a change in light intensity leading to a change in frequency of the light. In short, chirp is the deviation of laser frequency from its

radiation-center frequency. The physical mechanism of a chirp is that a change in carrier population – and hence, gain – causes a change in the refractive index of an active region. This phase fluctuation during modulation due to the change in the refractive index is associated with the change in the absorption coefficient and thus, results in spectral broadening in semiconductor lasers [3].

Intensity fluctuations

The intensity noise of laser diodes is usually measured as *relative intensity noise* (RIN), given by [13]:

$$\mathrm{RIN}(1/\mathrm{Hz}) = \frac{\langle P_N^2 \rangle}{\langle P^2 \rangle BW} \tag{2.33}$$

where $\sqrt{\langle P_N^2 \rangle}$ is the average noise power, $\langle P \rangle$ is the average output power and BW is the bandwidth. Since measurement of a laser diode's RIN requires a receiver and a link between them, BW here is the bandwidth of the receiver and the link.

Two major mechanisms produce RIN in laser diodes. The first, as mentioned above, is the spontaneous emission that is amplified within laser cavity. The second is back-reflection, which can occur at any components at a fiber link (connectors, splices, and even the fiber itself). Light reflected back into a laser diode is amplified by the active region and is added to the main stream, resulting in intensity fluctuation. Several research studies on the effect of feedback on the RIN of lasers will be presented in Section 3.1.2.

2.4 Vertical-Cavity Surface-Emitting Lasers

The first vertical-cavity surface-emitting laser, namely, VCSEL, was invented almost 30 years ago by Soda, Iga and co-workers [14] and was first demonstrated in 1989 [15] in room-temperature operated at low threshold current owing to the advances in epitaxial technologies where semiconductor distributed Bragg reflectors (DBRs) with extremely

high reflectivity could be made. Since then, VCSELs have been manufactured drastically and played an important role as transmitter sources in many applications.

VCSELs are essentially made by sandwiching a light emitting layer, (i.e., a thin semiconductor of enhanced optical gain by quantum wells made within this active region) between two highly reflective mirrors of distributed Bragg reflectors (DBRs) as illustrated in Figure 12(a). The Bragg reflectors are made of stacks of layers with alternate high and low refractive-index material as shown in Figure 12(a). Each of these layers is $\lambda/4$ thick and is made from GaAs ($n = 3.6$) and AlAs ($n = 2.9$). These layers works like highly reflective mirrors. By spacing multiple high-to-low index interfaces a distance $\lambda/2$ apart, the reflectivity of each interface adds constructively to produce mirrors with a maximum reflectance of > 99% [16]. Since the space within a resonator is called the cavity, the words 'vertical-cavity' mean that the structure providing laser feedback is arranged in the vertical direction. The words 'surface-emitting' mean, in this context, that the laser's beam is emitted perpendicular to the wafer as shown by the block arrow in the figure below.

The gain-guiding mechanism can be realized by forming a circular metal contact close to the active layer. The carrier concentration provided by the injection current defines the gain region to confine the transverse mode. As shown in Figure 12(b), the implanted region is defined selectively to control the flow of the injection current into the active layer. Implantation of ions into the top distributed Bragg reflectors (DBR) mirror can be used to provide the nonconductive material around the laser cavity. This is done by bombarding ion species (H^+, O^+, N^+, F^+) on the crystal vacancies to create damage for free carriers' compensation leading to regions of high resistivity. As a result, the injected current concentrates into the active medium as depicted by the solid arrow lines in the laser substrate in Figure 12(b).

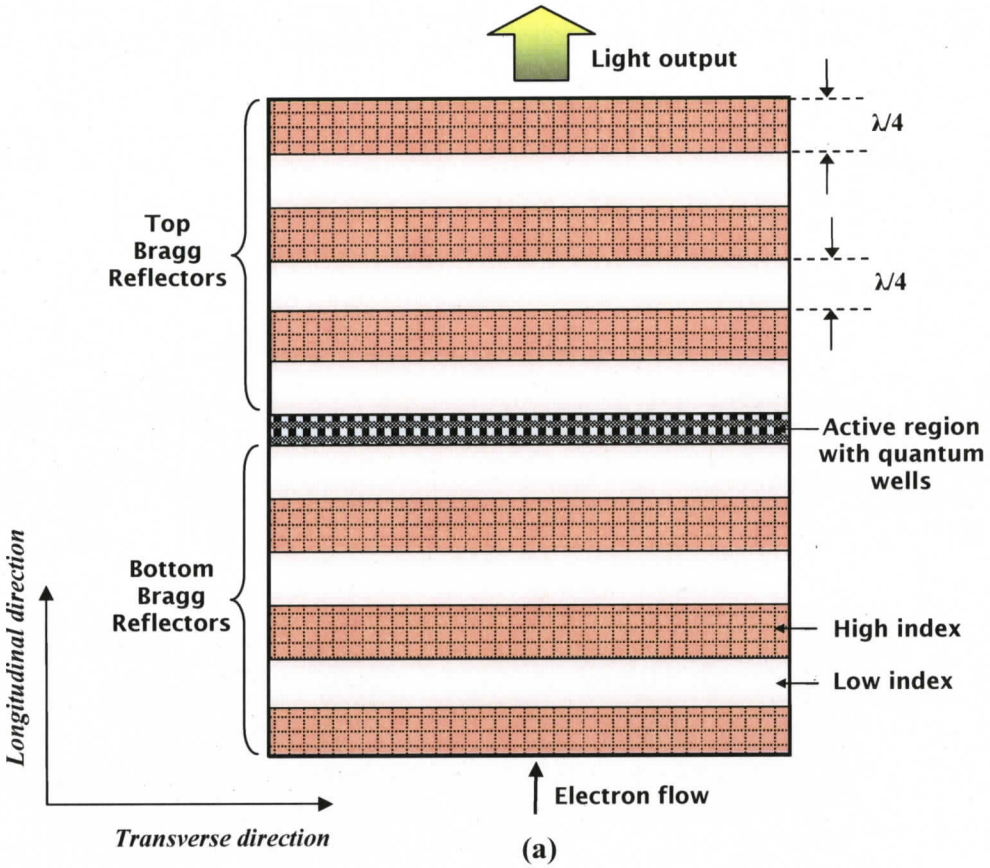

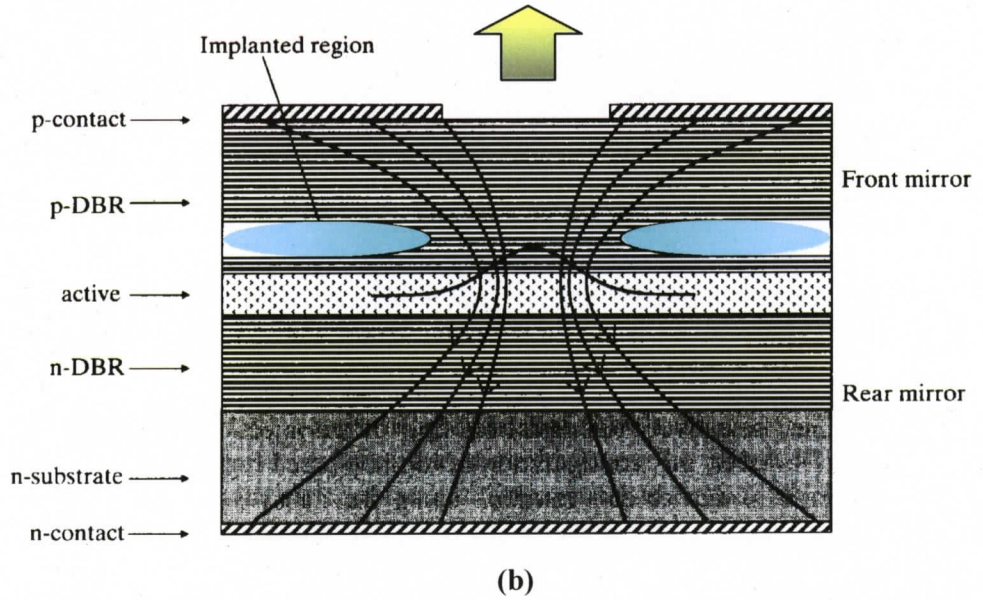

Figure 12 Vertical-cavity surface-emitting laser, VCSEL: (a) principle of operation and (b) schematic diagram [17]

2.4.1 VCSELs versus edge-emitting lasers

A VCSEL is generally smaller than an edge-emitting laser, both in wafer area and in active region volume, and one can fit many VCSELs on a two-inch wafer. Several significant advantages of VCSEL diodes over edge-emitting diodes are [18]:

- As the size of the resonant cavity is very small (on the order of 2 μm), this results in huge spacing between two adjacent longitudinal modes as can be calculated from Equation (2.5). For operating wavelength of a VCSEL, say $\lambda = 850$ nm and cavity length, $L = 2$ μm, the longitudinal mode spacing is computed to be 180.625 nm. The spectral width of a gain curve is only a few nanometers; consequently, not more than one mode can be within the gain curve. Thus, a VCSEL diode operates in a *single longitudinal mode*.
- The small size of a VCSEL's resonant cavity leads to its key advantage: *low power consumption* and *high-speed modulation* with low driving current. The first advantage results from the high quantum efficiency of the device. High current density is reached with low current value of the small active area. The second advantage stems from its high relaxation frequency. The highest modulation speed reached for GaInAs VCSELs was reported at 25 Gb/s [18].
- VCSEL diodes have very small dimensions: A typical resonant cavity and diameter of the active region are about 1 to 20 μm, and the thickness of the active layer is about 0.025 μm [19]. This allows for manufacturers to fabricate many diodes on one substrate, thereby making *one- and two-dimensional array* of laser diodes, for multi-channel systems.
- A VCSEL diode radiates a *circular output beam* vertically, parallel to the epitaxial growth direction in contrast to that radiated by edge-emitting lasers, thus enables easy and efficient coupling to a fiber. Red arrows in Figure 13 show light emission from the structure of the lasers.
- The fabrication technology for VCSELs is very similar to that for electronic chips, a fact that gives them the enormous range of advantages that chips have, such as *low cost* and *small packaging capability* (due to its planar configuration

that simplifies fabrication process and packaging), *on-wafer wavelength control* [20, 21], and *wafer level testing* for low-cost manufacturing (due to the geometry of VCSELs).

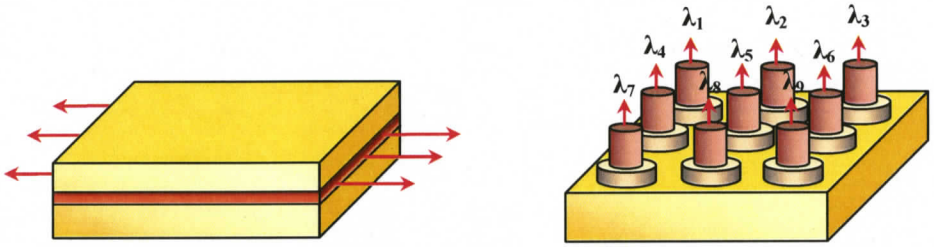

Figure 13 Illustration for (a) edge-emitting laser and (b) two-dimensional array of vertical-cavity surface-emitting lasers (VCSELs)

Although VCSELs have many advantages over the edge-emitting lasers, they have their disadvantages as well. The performance issues of VCSELs will be discussed in Section 2.4.4.

2.4.2 Transverse modes of VCSELs

In the earlier Section 2.2.2, we have discussed the longitudinal modes of a laser diode. However, the longitudinal modes are not the only patterns of an EM field that a laser diode can support. EM waves whose **E** and **H** vectors are slightly tilted with respect to the resonator centerline can also exist because not all practical lasers cavities have flat reflectors at the ends. A better way of visualizing modes is to realize that a mode off-axis self-replicating rays propagating along different paths within the laser-diode cavity and form various radiation patterns. These patterns are called transverse modes. Transverse modes represent amplitude distributions of the EM field that can replicate itself after one round trip in directions transverse to the propagation of the laser beam within the resonator. The greater the transverse size, the more of these off-axis modes can exist. Note that transverse modes can also be described as spatial modes, whereas longitudinal modes are associated with frequencies.

Transverse modes depend on the optical cavity dimensions, reflector sizes and other size limiting apertures that may be present in the cavity. The modes either have Cartesian

(rectangular) or polar (circular) symmetry about the cavity axis. The transverse mode patterns can be numerically obtained from solving the Fresnel-Kirchhoff integral equation in the rectangular (x-y) or cylindrical coordinates [2].

For x-y symmetry solutions, the distribution of electric field on the mirrors are described as the products of Hermite polynomials and the Gaussian distribution function of [2]:

$$U_{pq}(x,y) = H_p\left(\frac{\sqrt{2}x}{w}\right)H_q\left(\frac{\sqrt{2}y}{w}\right)e^{-(x^2+y^2)/w^2} \tag{2.34}$$

where p and q are integers that designate the order of the Hermite polynomials. Thus, every set of (p, q) represents a specific stable distribution of wave amplitude at one of the mirrors. For instance, $U_{00}(x,y) = \mathrm{TEM}_{00}$, $U_{01}(x,y) = \mathrm{TEM}_{01}$ and $U_{11}(x,y) = \mathrm{TEM}_{11}$. It is also possible to solve the Fresnel-Kirchoff integral equation using cylindrical coordinates; however they lead to a complex set of Laguerre-Gaussian solutions, which are not as simply described as the Hermite-Gaussian solutions and thus are not presented here [2].

As a general rule for all lasers, if there are no radially nonsymmetric losses within the cavity, the laser beam that develops within the cavity will have circular symmetry and the evolving modes will have circularly shaped patterns [2]. Generally, most lasers will develop modes that follow the Hermite-Gaussian pattern due to a slight astigmatism within the cavity because the symmetry of most optical resonators is restricted by polarizing elements.

Images of several mode distributions for various types of lasers are shown in the Figure 14 below as they might be observed if a laser beam were projected onto a screen. Figure 14(a) depicts Laguerre-Gaussian modes having circular symmetry; Figure 14(b) shows Hermite-Gaussian modes with x-y symmetry. These mode patterns occur in the directions transverse to the direction of travel of the laser beam. The lowest order mode TEM_{00} has an intensity distribution that is radially symmetric about the cavity axis and has a Gaussian intensity distribution across the beam cross section everywhere inside and outside the cavity. All parts of the propagating wavefront of TEM_{00} mode are in phase and it also has the lowest divergence angle. This is not so, however, with higher order

modes (TEM_{10}, TEM_{11}, etc.) where phase reversals produce the various mode patterns. Thus greatest degree of coherence, together with the highest level of spectral purity, may be obtained from a laser which operates in only the TEM_{00} mode. These properties render mode TEM_{00} highly desirable and many single-mode laser designs optimize on TEM_{00} while suppressing other modes.

It was proven experimentally that the VCSEL transverse mode behaviour is very similar to that of edge-emitting lasers and complete families of both Laguerre-Gaussian and Hermite-Gaussian optical modes have been shown to exist in VCSELs using spectroscopically and polarization resolved near field emission [22-24]. VCSELs emit single longitudinal mode, however the modal behaviour depends strongly on the transverse dimension of the device and on the confinement mechanism. For small VCSELs with transverse dimension, typically less than 5 μm, only fundamental transverse mode is supported by the small cavity. In larger VCSELs of transverse dimension more than 5 μm, single-mode is possible only over a limited range of bias currents slightly above threshold [19, 22]. With a relatively large cavity diameter, VCSEL emission consists of a single longitudinal mode, but with possibly multiple transverse optical modes.

The transverse modes of VCSELs are nearly all TEM modes, because the laser's transverse dimension is typically significantly larger than its effective cavity length [22]. The number of transverse modes grows when gain increases. Since the current carrier distribution determines the gain profile, gain can be increased by increasing forward current and/or by increasing the dimension of an active layer. Chang-Hasnain *et al.* [22, 23] have reported a 5 μm square-aperture VCSEL emits only the fundamental TEM_{00} mode, whereas a 15 μm square-aperture VCSEL starts to lase in the fundamental TEM_{00} mode and at higher currents, the higher-order modes, TEM_{01*} and TEM_{10} successively appear but only dominates for a small range of drive currents. At even higher current, the laser emits both TEM_{00} and TEM_{11}. On the other hand, a 20 μm square-aperture laser supports transverse modes up to TEM_{22}. These modes patterns are presented in Figure 15 for comparison with the mode patterns shown in Figure 14 for all types of lasers. Notice that the VCSEL mode patterns have both Laguerre-Gaussian and Hermite-Gaussian solutions.

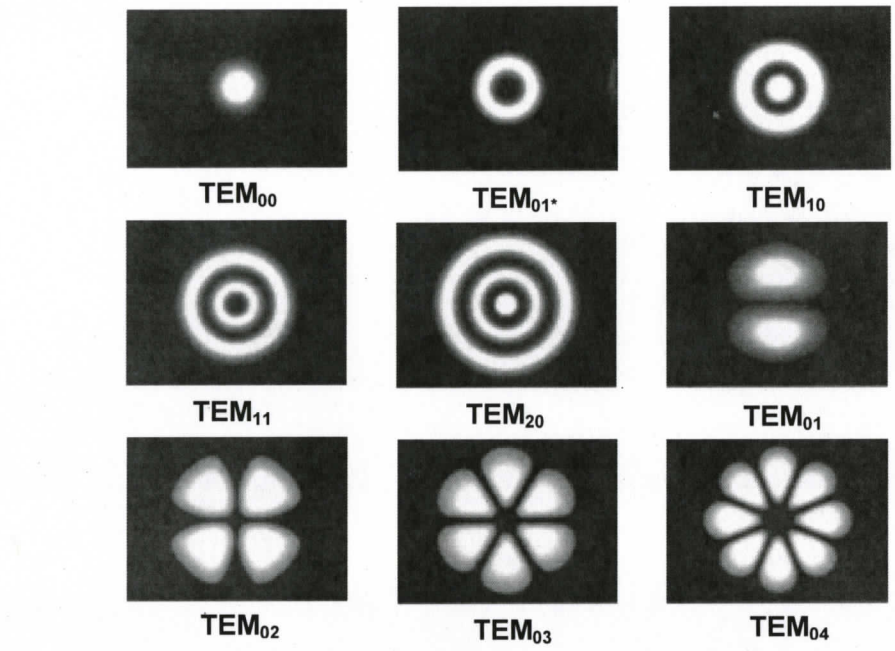

(a)

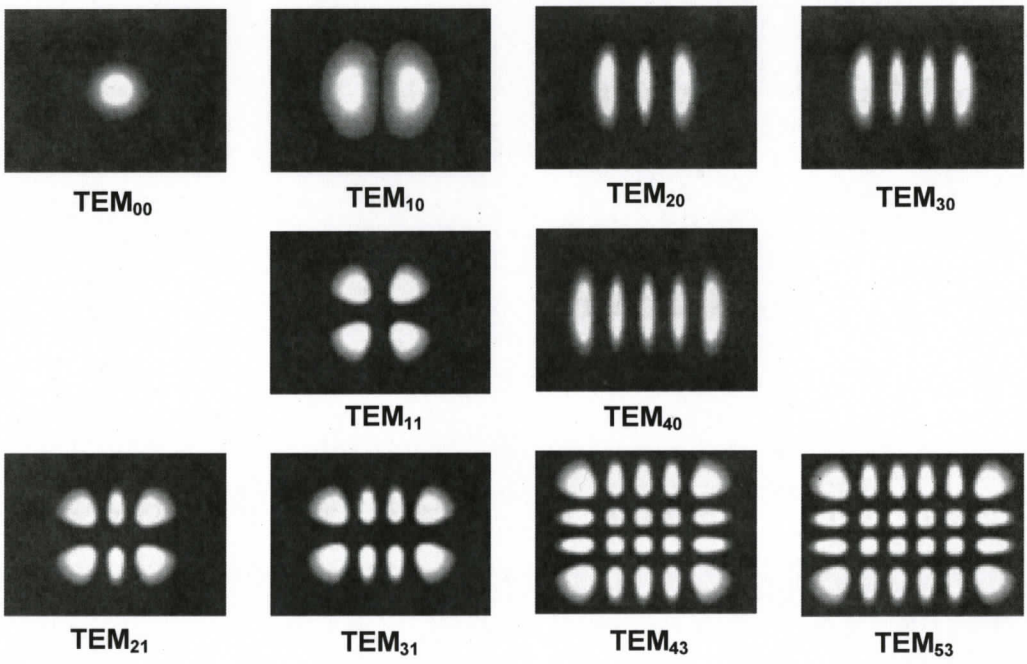

(b)

Figure 14 Mode patterns for various transverse laser modes: pure modes in (a) circular symmetry and (b) *x*-*y* symmetry [2]

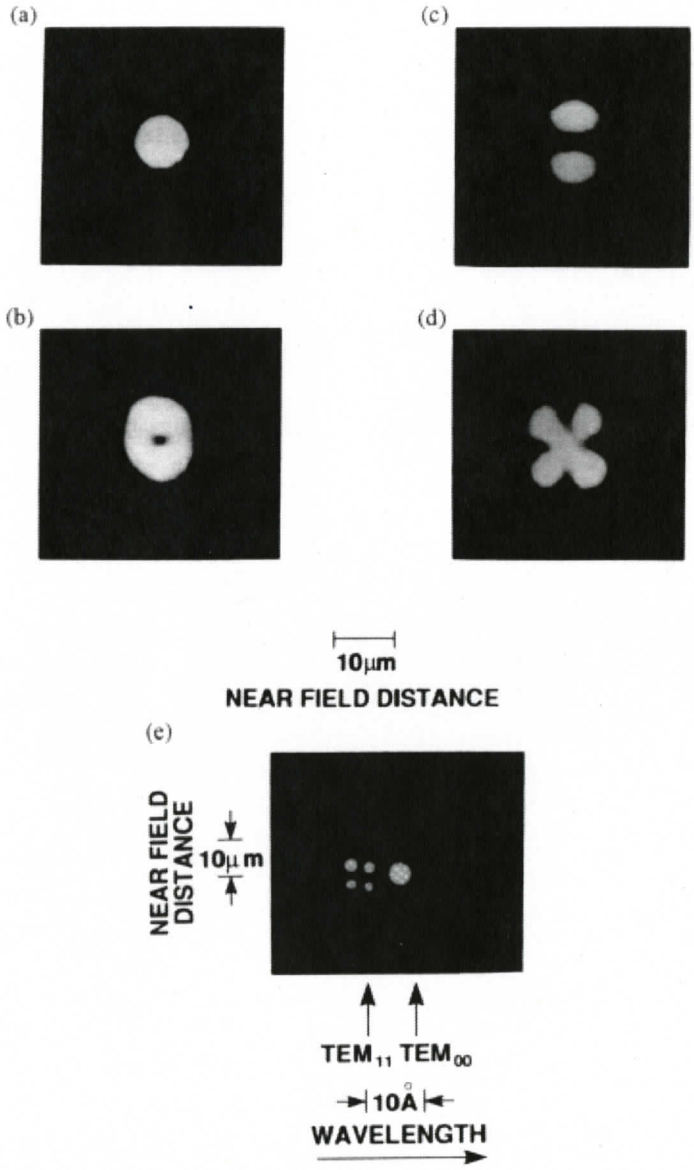

Figure 15 The CW near-field patterns of a 15 square-aperture VCSEL emitting (a) fundamental TEM_{00} at current near threshold, (b) TEM_{01^*}, (c) TEM_{10} at higher current, (d) both TEM_{00} and TEM_{11} at even higher currents. The mode pattern in (d) is spectrally resolved to show the near-field image in (e), where the TEM_{00} and TEM_{11} modes are clearly separated due to their wavelength differences. [22, 23]

It is worth mentioning that transverse mode characteristics of VCSELs were also analyzed by the cylindrical dielectric waveguide theory in [17] because it was justified that VCSELs with cylindrical geometry have transverse confinement structures similar to that of the optical fibre. Linearly-polarized (LP) modes were proposed to replace the complete set of transverse-modes in a weakly guiding cylindrical waveguide. Here, LP modes are treated as transverse modes because the longitudinal components of LP modes are very small. Figure 16 depicts **E** field distribution of the LP_{01} and LP_{11} modes.

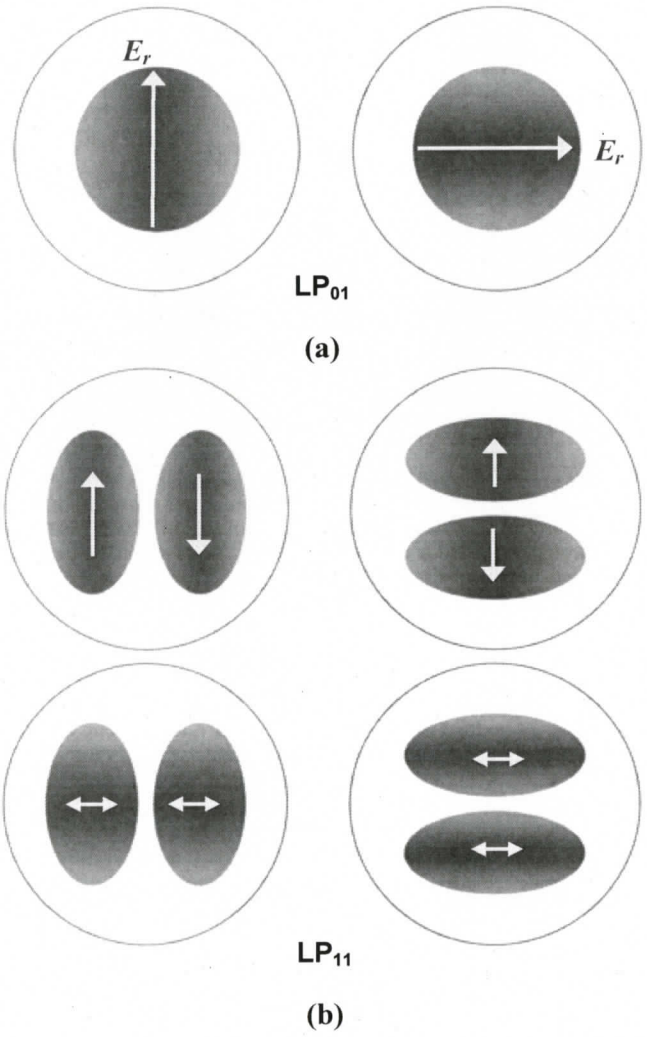

Figure 16 Field distribution of the (a) LP_{01} mode, and (b) LP_{11} mode (both modes have two polarization states) [17]

2.4.3 Polarization properties of VCSELs

It has been shown experimentally that the unintentional anisotropy introduced during the fabrication of VCSELs causes them to have two orthogonal linearly-polarized (LP) states in the fundamental transverse mode [23]. As a result, two LP modes with slightly different wavelengths and consequently with slight different gains are supported by the VCSEL cavity [25]. Polarization switching occurs between the two orthogonal x- and y-LP modes as the injection current increases [26]. The switching originated from the current heating with increasing injection current that redshifts the spectral alignment of the gain maxima in relation to the cavity resonances for the two polarization [27].

2.4.4 Performance issues of implanted VCSELs

Ion-implanted VCSELs have advantages of planar device geometry with enhanced heat sink and excellent reliability. Their performance drawbacks include a lack of inherent optical confinement to support lasing modes, which can lead to varying thresholds and modulation limitations [16, 17].

Although the configuration of the ion-implanted region in Figure 12(a) defines an electrical current path into the optical cavity (active layer), there are several problems, i.e., it has no control on the diffusion of carrier concentration along the transverse direction of the active layer. Implanted VCSELs require the creation of a 'thermal lens' at the centre of the cavity which is thermally induced refractive index gradient that will support the lasing optical mode. The formation of the 'thermal lens' will determine how various transverse modes arise during VCSEL operation. As discussed in the previous section, a VCSEL typically exhibit multiple transverse optical modes. Near threshold current, VCSEL emits the fundamental Gaussian mode initially and followed sequentially by higher order transverse optical modes with increasing injection current. Even though thermal lensing tends to promote the fundamental Gaussian mode, higher-order transverse modes can be excited in the influence of spatial hole burning (SHB) [28-30] of carrier concentration, which is an undesired characteristic of VCSELs. SHB is excited by stimulated emission of carrier concentration inside the active layer, and the shape of SHB follows the profile of the transverse fields. For high power operation, SHB

depresses the gain in the centre of the device which allows it to rise at the edges, thus forming the appearance of the higher-order transverse mode LP_{11}, doughnut mode [28]. As a result, the wallplug efficiency (electrical to optical conversion) of VCSELs is reduced and the corresponding threshold current is increased. The self-focusing [29] effect narrows the beamwidth of the transverse modes so that the stability operation of the fundamental mode is further reduced .

Threshold currents of VCSELs under pulsed and continuous-wave (CW) operation can increase significantly if the carriers are injected into the active region faster than the formation of the thermal lens due to greater diffraction loss in the cavity [31, 32]. Therefore, the relatively long time required to form a thermal lens (~ 1μsec) will cause an obvious switching turn-on delays of the VCSEL output under pulsed operation.

The other problem is the electrical resistivity of the DBRs, which increases the heat generation inside the laser cavity. As temperature increases, both the cavity resonance and laser gain shift to longer wavelengths in consequence of the refractive index and bandgap temperature dependence. The laser gain spectrum shifts to longer wavelengths faster than the cavity resonance, leading to spectral misalignment between the cavity resonance and peak gain resulting in performance degradation of the laser [33]. Threshold current is also a function of laser substrate temperature [34]. Minimum threshold was found to occur approximately at the temperature where the cavity resonance overlaps the peak laser gain.

In addition, the spectral misalignment between the cavity resonance and laser gain can impact other optical properties, include the high power operation [31] and the emission polarization of the VCSEL [35]. As shown in Figure 9, the 'rollover' behaviour of the VCSEL output occurs due to the increase of cavity temperature and the thermally induced misalignment of the cavity resonance and laser gain during laser operation. As discussed in Section 2.4.3, VCSELs exhibit unique polarization properties where its lasing emission is distributed between two orthogonal transverse electric (TE) polarization states [23, 35]. The dominant polarization state has been found to vary depending upon the relative spectral alignment between the polarization cavity resonance and the laser gain profile induced from wafer non-uniformity [35] or cavity temperature [34].

The resulting variation in the thickness of the optical cavity significantly changes the cavity resonance wavelength. Therefore, usually during the epitaxial growth of VCSEL, cavity resonance is often intentionally designed to be at a slightly longer wavelength relative to the peak laser gain at room temperature, so that at higher operating temperature, i.e., at higher injection currents, the peak laser gain shifts into alignment with the cavity resonance for optimum VCSEL performance [36].

A recent innovation to improve the electrical and optical confinement was achieved in oxide-confined VCSELs which incorporated buried oxide apertures [18]. With the buried selectively oxidized design, the DBR mirrors can be fully make use of by utilizing the entire top mirror to conduct current into the active region. This will avoid the current crowding effects from the ion-implantation damage in implanted VCSELs. Also, positioning the current apertures immediately adjacent to the optical cavity minimizes lateral current spreading outside of the laser cavity, which is prevalent among implanted VCSELs. With improved electrical confinement, oxide-confined VCSELs produce reduced threshold voltage and reduced threshold current as compared with implanted VCSELs [37]. Moreover, the stronger index-guiding in oxide-confined VCSELs contributes to the reduced threshold because of the reduced diffraction loss since formation of a thermal lens is not required. Consequently, the reduced threshold current and voltage reduces parasitic current heating [32]. The strong optical confinement of oxide-confined VCSEL influences the optical characteristics such as transverse modes and output beam stability. As reported in [32], during single-mode operation, the oxide-confined VCSEL maintains a constant pointing direction and beam divergence, which only increases slightly during multimode operation. On the other hand, implanted VCSEL's beam divergence and pointing direction varies with increasing current.

2.5 SUMMARY

The principle of operation and the important parameters of a semiconductor laser were presented in the earlier section of this Chapter. A semiconductor laser is essentially a resonant cavity consisting of two mirrors with a photon-generating active material between. The material has a thin layer of the so-called active region sandwiched between a *p*-typed layer and an *n*-typed layer on top and bottom. When the *p-n* junction is forward biased, electron-hole pairs are injected into the active layer where they recombine to produce light. Cleaved facets at the two sides of the *p-n* junctions act as partially reflecting mirrors; thereby forms an optical cavity.

Since this thesis work was done using a vertical-cavity surface-emitting laser, a comprehensive theory on the differences between VCSELs and conventional edge-emitting lasers, the VCSEL's important characteristics such as its transverse mode patterns, polarization properties and its performance issues was given.

In the next chapter, the background review as well as the previous works on the effects of external optical feedback to semiconductor lasers and in particular, feedback effects on VCSELs, will be presented and discussed.

CHAPTER 3

LITERATURE REVIEW: EXTERNAL OPTICAL FEEDBACK ON SEMICONDUCTOR LASERS

In this chapter, the effects and benefits of external optical feedback on lasers will be described. The various applications that utilize the feedback control of VCSEL characteristics will be presented. In this work, we are concerned with the transverse mode control of VCSELs through external optical feedback. Therefore, the background review on the previous works related to transverse mode control of VCSELs will be discussed.

3.1 EFFECTS OF OPTICAL FEEDBACK ON LASERS

The effects of external optical feedback on semiconductor lasers have been studied in detail both theoretically and experimentally since the early 1980s [11, 38-42]. Back-reflection to lasers is common in fibre-to-laser coupling [43-45] and from external optical components [46]. External feedback to lasers is known to change their behaviour. Depending upon the strength, polarization, delay time and phase, feedback can cause altered characteristics, such as, linewidth change [39, 44, 45, 47-52], intensity noise [53-56], polarization switching [57, 58], polarization mode-hopping [59], and power instabilities [60-62].

3.1.1 Linewidth change

When feedback is provided to a semiconductor laser, a change in the laser's linewidth, either narrowing or broadening, depending on the strength and phase of the feedback were reported. It has been realized that with small amounts of feedback and proper phase

matching, significant linewidth reduction can be achieved [63]. When feedback strength is increase further, the linewidth broadens until a certain point, coherence collapse occurs, where the spectral peak unexpectedly broadens dramatically and the coherence length of the laser emission drops significantly. When feedback is provided to a semiconductor laser, a change in the laser's linewidth, either narrowing or broadening, depending on the strength and phase of the feedback were reported. It has been realized that with small amounts of feedback and proper phase matching, significant linewidth reduction can be achieved [63].

When feedback strength is increase further, the linewidth broadens until a certain point, coherence collapse occurs, where the spectral peak unexpectedly broadens dramatically and the coherence length of the laser emission drops significantly. Coherence collapse happens because coherence mismatch exists between the feedback light and the output light when feedback light re-enters the laser's cavity, due to the longer round-trip time taken by the feedback light to return to the laser's cavity. The earlier work [12] has proven theoretically that at relatively high feedback levels, the noise from increasing phase fluctuation resulting from diminishing coherence, is more pronounced than the noise from the quantum fluctuations from spontaneous emission, thus, resulting in coherence collapse. This phenomenon was observed and reported both in edge-emitting lasers [47, 64] and VCSELs [50].

Single-mode semiconductor lasers provided with various levels of feedback strength have been classified into five distinguished regimes of feedback effect [42, 52, 65]. The five regimes of feedback effects are summarized in the following and illustrated in Figure 17:

- Regime I: With very weak feedback, the linewidth can be narrowed or broadened depending on the feedback phase.
- Regime II: As feedback is increased at out of phase, mode-hopping occurs due to splitting of emission mode from substantial linewidth broadening. Further increase in feedback will lock the laser to a single narrow maximum linewidth operation.
- Regime III: Laser operates on a single narrow maximum linewidth with higher feedback strength than regime II when mode-hopping is suppressed. Starting

here, the spectral characteristic of the laser does not depend on the distance of the reflector.

- Regime IV: This regime represents the 'coherence collapse' regime where the linewidth of the laser shows drastic reduction with a relatively strong optical feedback.
- Regime V: Laser operates on a single narrow linewidth for all phases of feedback at this strong optical feedback regime, also known as the stable operation regime.

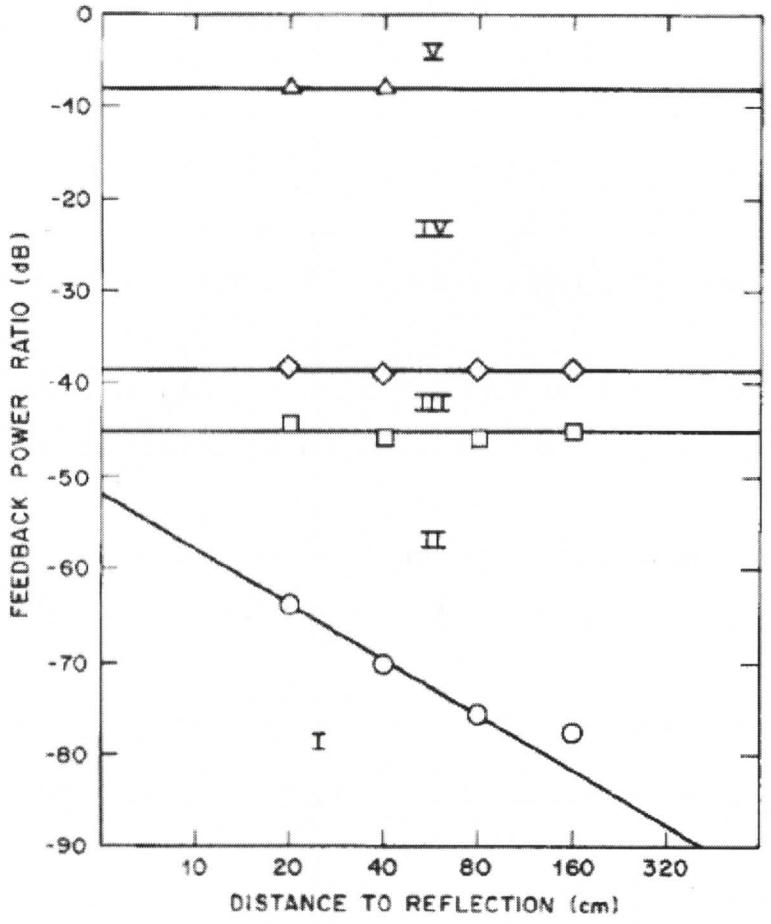

Figure 17 Five regimes of feedback effects, namely, I, II, III, IV and V, experimentally investigated on a 1.5-μm distributed feedback laser with various feedback strength as a function of external cavity length. Regime I and V denote very low and high feedback, respectively. [65]

In the following figure, the feedback power ratio is defined as:

$$FB = 10\log\left(\frac{\text{reflected power}}{\text{emitted power}}\right) \quad \text{[dB]} \tag{3.1}$$

where, the reflected power corresponds to the power re-entering the laser.

Although the classification of the feedback regimes was based on the edge-emitting laser, Chung and Lee [52] have shown that the VCSEL spectral characteristics effects subjected to optical feedback demonstrated well-defined regimes of feedback as that of the conventional edge-emitters .

The VCSEL used in this thesis was operating at the border of regimes IV and V, i.e., between -3 dB and -11 dB with 81 μm and 42 μm pinholes as the spatial filter in the laser's external cavity. The linewidth of the VCSEL was stable and narrow as presented in Chapter 5 because intentional good coupling to the laser was ensured. There was no coherence collapse phenomenon observed although the VCSEL was operating at regime IV. This could be explained by the high feedback levels of -11 dB being right at the borderline close to the strongest feedback regime V.

3.1.2 Relative intensity noise

Since the relative intensity noise (RIN) and linewidth are strongly related as discussed in Section 2.3.4, the external feedback to lasers also affects the RIN of lasers. Kallimani *et al.* [54] have shown a thorough study on the effects of various levels of feedback on the noise characteristics of semiconductor lasers. For weak (regime I) to moderate feedback levels (regimes III), the RIN is low, whereas in the coherence collapse regime (regime IV), the RIN increases significantly [54]. Finally, RIN reduces drastically in the strong feedback regime (regime V) with laser maintaining in the single-mode operation. Ho *et al.* [53] had shown comparable trend of RIN when the experiment was performed on a VCSEL as a function of their optical feedback strength. Later, another work investigated numerically the RIN characteristics of VCSEL's under feedback conditions with a more complete model that includes the spatial dependences of both the optical field and the carrier density [55]. The spatial effects are essential in characterizing a VCSEL,

especially for the case of multimode operation where spatial hole burning plays a role in the intermodal coupling that can influence the laser's performance.

3.1.3 Polarization switching

Recent research work in lasers, especially VCSELs, subject to optical feedback has largely focused on the polarization dynamics of a single-transverse mode [59, 66, 67]. It was mentioned in the previous Chapter that the free-running VCSELs undergo polarization switching between two nearly degenerate LP modes when changing the injection current. In general, polarization switching in VCSELs happens through a region of polarization mode-hopping or a region of hysteresis [25]. Here, in the case of optical feedback, the existence of these modes has a major consequence. Sciamanna et al. [59] have demonstrated anticorrelated hopping between the two LP modes induced by optical feedback. Besnard *et al.* have reported that the optical feedback induces polarization switching even when the solitary VCSEL is emitting light with a stable polarization [58]. This phenomena is perceived as a drawback as it reduces the length of the fiber link that uses a VCSEL as the transmitter due to the polarization and chromatic dispersion [67]. The effects of optical feedback on the polarization bistability in VCSELs were studied and reported by Hong et al. [68].

3.1.4 Power instabilities

A form of unstable dynamics in semiconductor lasers exposed to moderate amount of optical feedback is low-frequency fluctuations (LFF). Abrupt power dropouts occurred near the free-running laser threshold leading to a turnoff of the laser followed by gradual recovery of the light emission, which is again followed by a dropout [69]. As reported by Pan *et al.* [70], LFF was reported to take place everywhere along the boundary between regimes IV and V of Figure 17. Later, Hong *et al.* [61] observed experimentally that the regularity of power dropouts increase with the increase of the external cavity length. When external cavity length is close to the VCSEL coherence length, coexistence of LFF and stable emission is observed.

3.2 The Benefits of Optical Feedback on Lasers

Feedback on lasers has been well-known not only for reducing the threshold of the lasers [38, 49], but also for controlling laser emission, in particular, transverse modes [71-76], linewidths [44, 48, 49, 51, 52], wavelength [20, 74, 77] and polarization states [59, 78, 79]. Some other research groups have also shown hysteresis phenomena in microcavity lasers by providing external optical feedback [80-83].

Single-mode operation is desired for high-speed fiber-optic connections and a wide variety of other applications requiring a high quality single wavelength source, in particular, single-transverse-mode and stable polarization state emission. Providing external optical feedback using an external mirror or a grating can be used to select a distinct longitudinal mode, to attain significant linewidth narrowing or to tune the emission frequency of a laser. Improved single-mode emission has been achieved through the use of hybrid reflector structures employing spatial filtering [84], spatially and frequency-selective fiber bragg reflector [85] and in devices which employ a passive antiguiding structure [86].

There have been many studies on the polarization control and stability analysis of lasers subject to external optical feedback [56, 66, 67, 79, 87]. An important study area on the feedback effects of VCSELs in terms of its polarization dynamics was on the polarization self-modulation to VCSELs with polarization-rotated optical feedback [88-91]. The recent experimental work by Gavrielides et al. [88] showed the optical feedback with polarization state that is orthogonal to the laser's natural operating mode via Faraday rotator, was able to force the laser to switch between the dominant polarization mode and the orthogonal mode. As described by Li et al. [92], the polarization emission states of VCSELs follow the feedback polarization state by enhancing the mode that has the same polarization direction as the feedback, while suppressing the other mode. As proven by Hong et al. [79], polarization switching can be eliminated by providing polarization-selective feedback because polarization stability is achieved by ensuring that the injected light is of the same polarization as the dominant lasing mode. Other similar work on polarization self-modulation of VCSELs employing a quarter wave plate was used within the external cavity to switch the VCSEL's

polarization emission direction yielding polarization modulation of 9 GHz [90]. Polarization self-modulation of VCSELs has a myriad of useful applications, especially in the production of optical pulses at multi-GHz repetition rates without the need for high-speed electronics.

3.3 Various Applications of VCSELs based on Optical Feedback

Studies have shown that the effects of feedback on VCSELs are similar to those of the edge-emitters [52, 93]. Initially, the VCSEL was believed to have immunity to external optical feedback due to the high reflectivity of its facet mirrors (>99%) [94]. Because of the short internal cavity of VCSELs, the highly reflective feature of the mirrors is required for extending the lifetime of photons within the VCSEL's cavity. However, the feedback light that managed to enter the cavity will likely to stay in the VCSEL's cavity for a while, thus, is able to change the characteristics of the laser. Thus, regardless of the huge structural difference between VCSELs and the edge-emitters, VCSELs have the same feedback sensitivity as the edge-emitters. VCSEL applications based on optical feedback have been proposed and used in diverse applications such as optical communications, optical spectroscopy, optical information processing and optical sensors.

3.3.1 Optical microscopy

Scanning near-field optical microscopy (SNOM) makes use of the voltage change that occurs across the VCSEL when feedback is provided to map out the two-dimensional (2-D) image of a sample. Feedback-induced voltage change of VCSEL was proposed for 2-D image probing by Hashizume et al. [95] and they demonstrated 2-D imaging of a glass plate with gold mesh pattern by moving a metallic probe around the VCSEL output aperture with a constant distance of less than 1 μm. Later, Heinis et al. [96, 97] extended Hashizume's work and proposed an integrated SNOM microscope with a feedback-induced VCSEL as the detection principle.

Multimode VCSELs are desirable transmitter sources for short-haul fiber-optic data communication links [98, 99]. Imaging of spatial and spectral properties of multimode VCSELs has been investigated by several research groups [23, 100-103]. Near-field scanning optical microscopy [104, 105] was used to map out the spatial and spectral characteristics of the transverse modes of a multimode VCSEL [103]. A later work used spatial-spectral mode images to calculate the refractive index distribution within an oxide-confined multimode VCSEL [106].

3.3.2 Optical disk readout

Study on the use of lasers in optical disk readout is initiated by Lau et al [107]. They performed the experiment with an edge-emitting laser which acts as an integrated source detector combination. Although edge-emitting lasers can achieve reasonable results, it requires precise optical lens design for maximum allowable information density on the optical disk. Hudgings et al. [108] then proposed using a VCSEL in the integrated optical disk readout head. Using a VCSEL over an edge-emitting laser as an optical pickup head has several major advantages. VCSEL has circular beam output, single longitudinal mode emission and surface-normal geometry that allows for high density data storage on the optical disk, intermodal noise elimination and increase in information bandwidth due to the potential parallel readout of the 2-D array construction in the optical disk device.

3.3.3 Optical information processing

Some experimental works [109-111] have demonstrated bistability effect on VCSELs which showed that a hysteresis loop existed in the light output versus current (L-I) curve switching from a non-lasing ('off') state to a lasing ('on') state at the threshold current with increasing current. For decreasing current from above threshold to below threshold the switching drops from lasing ('on') state to non-lasing ('off') state with the 'on' stage lasted a little longer resulting in a 'window' of bistable operation. The variation in the amount of hysteresis was also reported from device to device and mostly observed at threshold or at mode hops between transverse lasing modes. Understanding this

phenomenon, Naumenko et al. [83] proposed a scheme of VCSEL coupled to an external cavity with a diffraction grating as a frequency-selective element for control the VCSEL to favour the possibility of bi- or multi-stability between different emission states. Bistability between the stable non-lasing state and stable high amplitude external cavity modes was observed. This bistability leads to abrupt switch-on at threshold to a high amplitude state in this setup. Description and analysis of the transition scenarios presented in [83] includes the possibility of switching events between external cavity modes and the resulting hysteresis in amplitude and frequency. This scheme was proposed for all-optical photonic switching devices.

Similar setup of a broad area VCSELs with frequency-selective feedback from a grating [112] was used where bistability can be used to excite spatially localized emission states known as spatial solitons or cavity solitons. These solitons [80, 82] viewed as light dots or 'bits' are created by shining light pulses in the optical cavity of the broad area VCSEL. The light pulses shined into the laser's cavity can be reflected from a grating coupled with pinhole [112] or injected by a secondary tunable laser source [80, 81]. Manipulation of cavity solitons (CSs) are of intense interest because of their ability to be written and erased in any desired location on the laser cavity. A good analogy is drawn by Spinelli and Lugiato [82, 113] between the transverse plane (orthogonal to the propagation direction of the beam) of a laser and a blackboard. Light spots or CSs, can be written or erased from the blackboard provided they are not too close together and are not too close to the boundary. Cavity solitons are believed to have to potential for future all-optically and massively parallel information processing schemes.

3.4 Previous Work on Transverse Mode Control of VCSELs

Among semiconductor lasers, vertical-cavity surface-emitting lasers (VCSELs) have a short optical cavity with a single longitudinal mode and a small number of transverse modes lasing. VCSELs often operate in multi-transverse modes in orthogonal polarizations. The onset of higher order transverse modes degrades the beam quality and the coherence of the laser. The oscillations of higher transverse modes lead to complex

dynamical behaviour of the lasers. Therefore, many researchers have sought methods to control their modal behaviour and polarization. Recent works have attempted to use optical feedback to control the mode properties of multimode VCSELs and to enable ideal single-transverse-mode operation.

Marino et al. [76] showed control of transverse modes and polarization modes of a VCSEL through frequency-selective feedback in the Littman configuration. Single fundamental mode operation was maintained over a large range of injection current ($\sim 2.5I_{th}$) and polarization control of the fundamental mode was achieved in the frequency-selective feedback setup. Other previous schemes employing polarized, spatially filtered feedback with a millimeter-size pinhole in an external cavity multimode VCSEL have demonstrated stable single-mode operation [73, 74] and wavelength tunability [74]. More recently, higher-order transverse mode suppression has been demonstrated using preferential alignment of the external feedback mirror [75].

In this work, we demonstrate mode control by means of a micron-size, spatial filter pinhole in the image plane of the VCSEL prior to the external feedback mirror. This method allows for fundamental single transverse operation at low injection currents. At higher injection currents, spatial selection can be used to increase the feedback to some modes while reducing the feedback to others, which alters the intensity and wavelength of the different modes.

3.5 SUMMARY

External optical feedback on semiconductor lasers is known to change the linewidth, intensity noise, polarization switching, polarization mode-hopping and power instabilites of the lasers. The description of these effects was discussed in the beginning of this chapter.

As mentioned earlier, external feedback can be beneficial for lasers in terms of reducing the threshold, controlling the transverse mode, polarization states, wavelength tenability and linewidth. Thus, VCSELs based on feedback scheme are use in various applications such as optical microscopy, optical disk readout and optical information processing.

In this thesis work, the transverse mode control of VCSELs was the objective. The previous schemes that have taken the advantage of external optical feedback to control the transverse modes of VCSELs were reviewed. The difference between this work and the previous works was drawn out in the last section of this chapter. The next chapter will discuss the methodology of our study of the proposed spatially filtered feedback system.

CHAPTER 4

EXPERIMENTAL TECHNIQUES

In this chapter, the methodology used in this research and the approach taken to achieve the objectives are described. A detailed description of the experimental equipment used is given. The motivation in this work is to control the transverse modes of a VCSEL through spatially filtered optical feedback. Also, the methods, precautionary steps and recommendations for setting up the experiments are discussed in the final section of this chapter.

4.1 THE SPATIALLY SELECTIVE FEEDBACK OF VCSEL SYSTEM

Previous works have described the spatial and spectral properties of multimode VCSELs [23, 100-103]. The multi-transverse-mode characteristics in VCSELs originate from the interplay between the spatial distribution of the carriers and the optical field, also known as the spatial hole burning (SHB) effect [29, 30, 114, 115]. Numerical [116, 117] and experimental [103] analysis has shown that spatial competition between modes occurs in the optical field because some modes share the same local optical gain.

Consequently, there exists an opportunity to control the transverse modes of VCSELs by providing optical feedback through spatial selection on the image plane of the VCSEL. This is done by moving a micron-size pinhole around the transverse direction of the VCSEL's image plane within the laser's external cavity, thus is named spatially optical feedback selection. Previous works used spatially filtered method with milimeter-sized pinhole for single-mode operation. There was no other published work that uses the same method of controlling the transverse modes of VCSELs as this work to date.

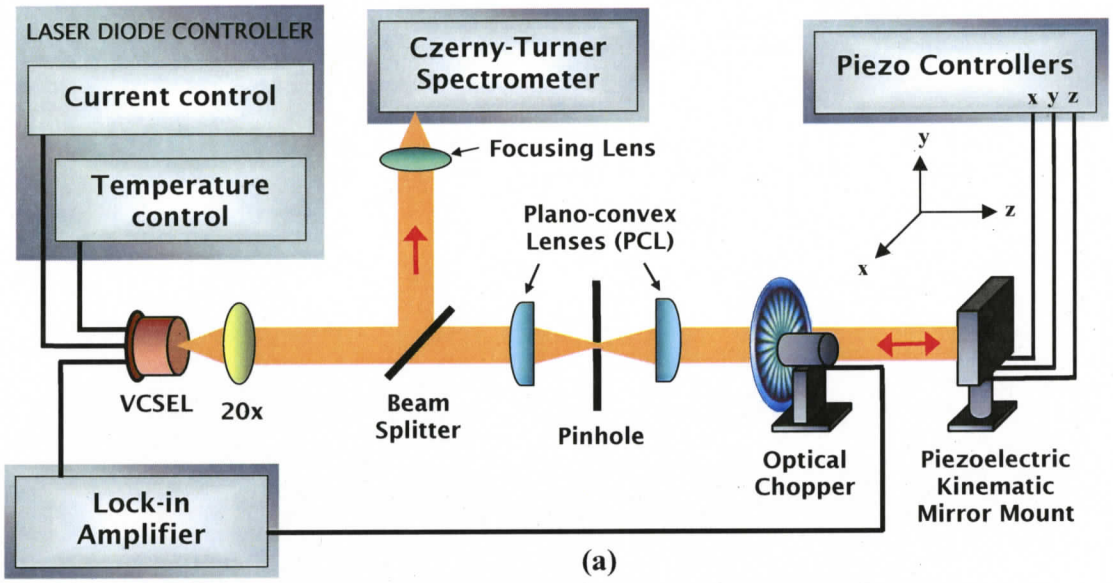

(a)

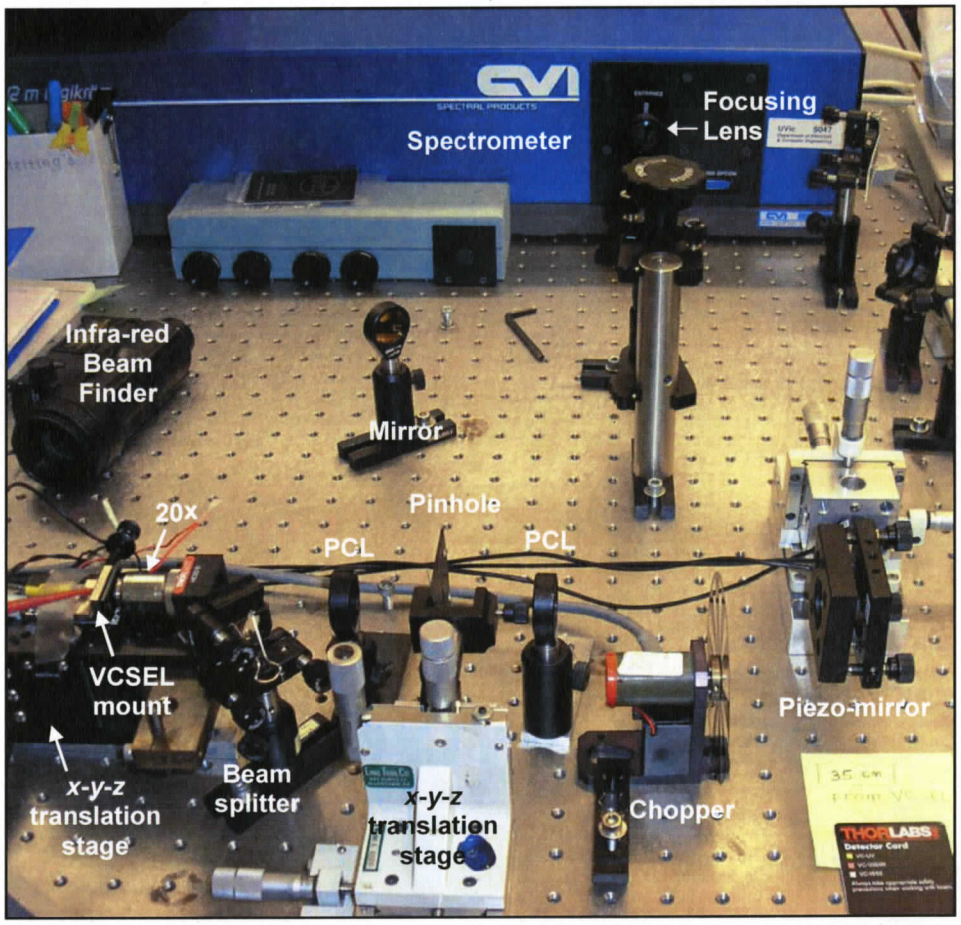

(b)

Figure 18 Experimental setup: (a) schematic diagram and (b) at the Optical Systems and Technology Laboratory, University of Victoria.

Figure 18 shows the experimental setup with spatially filtered optical feedback, which is defined by the plano-convex lenses, pinhole, and mirror. The optical chopper with lock-in amplifier combination was added to map feedback efficiency with high-precision. In the following sections, the main components used in the experiment are discussed.

4.1.1 The vertical-cavity surface-emitting laser

The VCSEL used in this experiment is a commercially available proton-implanted, multimode VCSEL (Finisar's Advanced Optical Components HFE4080-321) designed to emit 850 nm. The schematic structure of the VCSEL shown in Figure 19(a) consists of the top Bragg reflector (p-mirror stack), the bottom Bragg reflector (n-mirror stacks) and the active region. The active region contains three GaAs quantum wells surrounded by $Al_{0.25}Ga_{0.75}As$ spacers to form a single wavelength cavity. The p-mirror comprise of 20.5 periods of alternating layers of $AlAs/Al_{0.15}Ga_{0.85}As$, while the n-mirror comprise of 22.5 periods of $AlAs/Al_{0.15}Ga_{0.85}As$. The VCSEL has a 15 μm diameter window of metal ring contact for coupling light out and a 20 μm inner diameter of proton-implanted active region for current confinement. The VCSEL used in this experiment was also used in other published work [45, 103].

The output emission of the VCSEL used in this experiment is typically multi-transverse mode and a single longitudinal mode verified from the spectra taken by the spectrometer. The fundamental mode (denoted by 'Mode 0' in this thesis) was found to be at 855.55 nm wavelength at near threshold operating current. The expected coherence length of the VCSEL is calculated to be 0.86 mm from Equation (2.5).

A laser diode controller (Newport Model 6000) was used to control the injection current and to maintain the operational temperature at 20°C. The threshold current (I_{th}) of the free-running VCSEL was 3.5 mA. Table 1 shows the output functions of the VCSEL's pins that are schematically labelled in Figure 19(b). The pinouts were connected to the laser diode controller pinouts based on the following table, for example, Pin 1 was connected to laser cathode pinout, LD(-), of the laser diode controller. Figure 19(c) shows the VCSEL was mounted on an *x*-*y*-*z* stage with a 20× microscope objective for collimation. Further elaboration on the light collimation method of VCSEL will be discussed in Section 4.2.

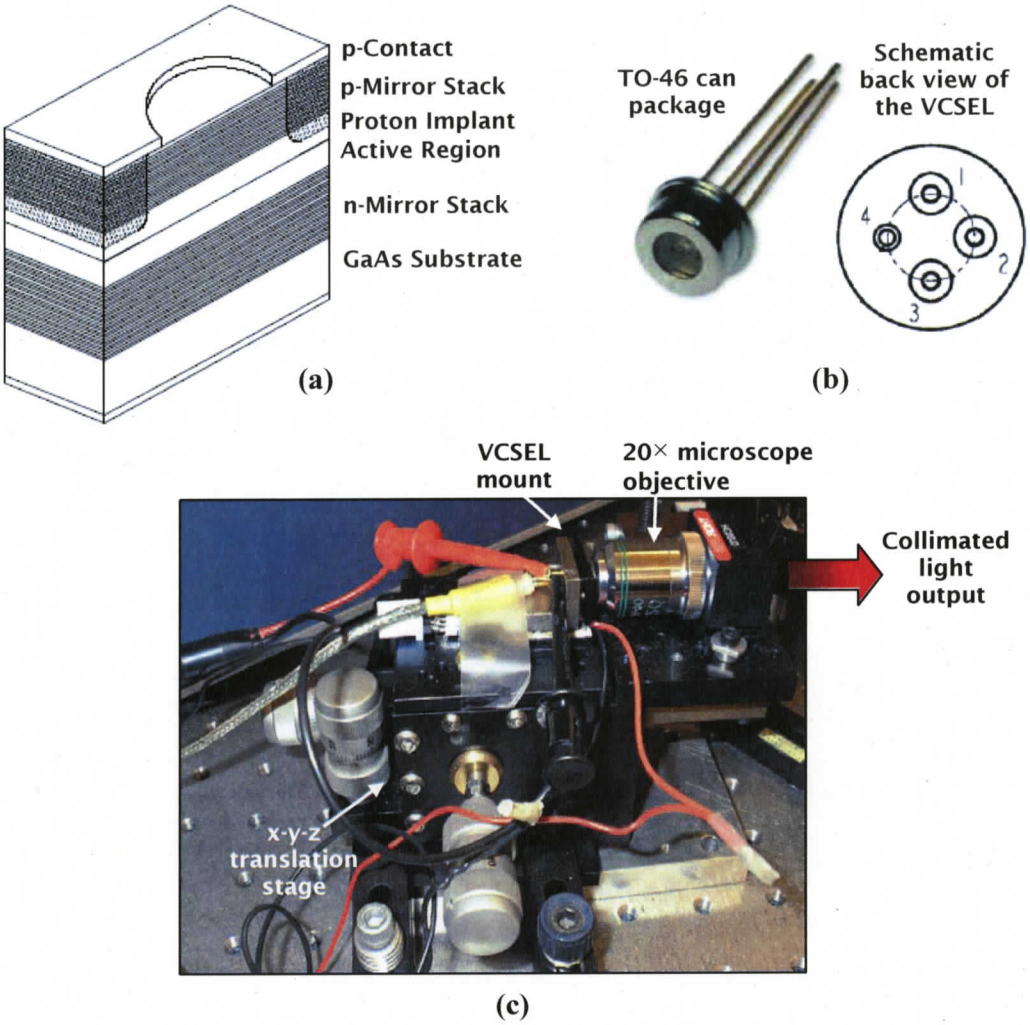

Figure 19 Finisar Advanced Optical Components VCSEL (HFE4080-321): (a) schematic diagram [118], (b) the actual VCSEL package used in the experiment, and (c) VCSEL light collimation setup [119]

Table 1 Pinouts of VCSEL HFE4080-321

Pin number	Function
1	Laser cathode output, LD(-)
2	Laser anode output, LD(+)
3	Photodiode anode output, PD(-)
4	Ground (case)

4.1.2 Spatial filter

Figure 20 shows the principle of operation of a spatial filter in this work. A spatial filter, consisting of two identical plano-convex lenses and either a 42 μm or a 81 μm pinhole, was used in this experiment. The focal length of both plano-convex lenses was 50 mm. Notice the rounded sides of the lenses facing the collimated light. The pinhole location was translated in the transverse (*x*- and *y*-axes) image plane of the VCSEL with an *x*-*y*-*z* translation stage. There was a 5.8× magnification of the VCSEL image at the image plane of the spatial filter, thus the VCSEL's image on beam spot was 87 μm. The pinholes used in this work were smaller than the VCSEL's image size because only the modes on part of the laser's local active region were provided feedback for mode control. Pinholes smaller than 42 μm, for example 30 μm and 20 μm were used. However, the feedback light intensity was too weak to change the behaviour of the VCSEL. Also, the pinhole was used to map out the voltage drop across the VCSEL through spatially-filtered feedback and these feedback-induced voltage drop maps are presented in Chapter 5.

Magnification factor

The magnification factor at the image plane is given by

$$M_{\text{image plane}} = \frac{f_2}{f_1} \tag{4.1}$$

where, f_1 is the focal length of the microscope objective and f_2 is the focal length of the spatial filter lenses as illustrated in Figure 20. The magnification factor at the object plane, $M_{\text{object plane}}$ is the inverse of Equation (4.1).

The size of the VCSEL's image projected on itself after going through the 42 μm and 81 μm pinhole aperture in the external cavity is given by magnification factor multiplied by pinhole aperture diameter. The following table shows the calculation for the VCSEL's image size based on the magnification factor at the object plane, pinhole sizes and microscope objectives.

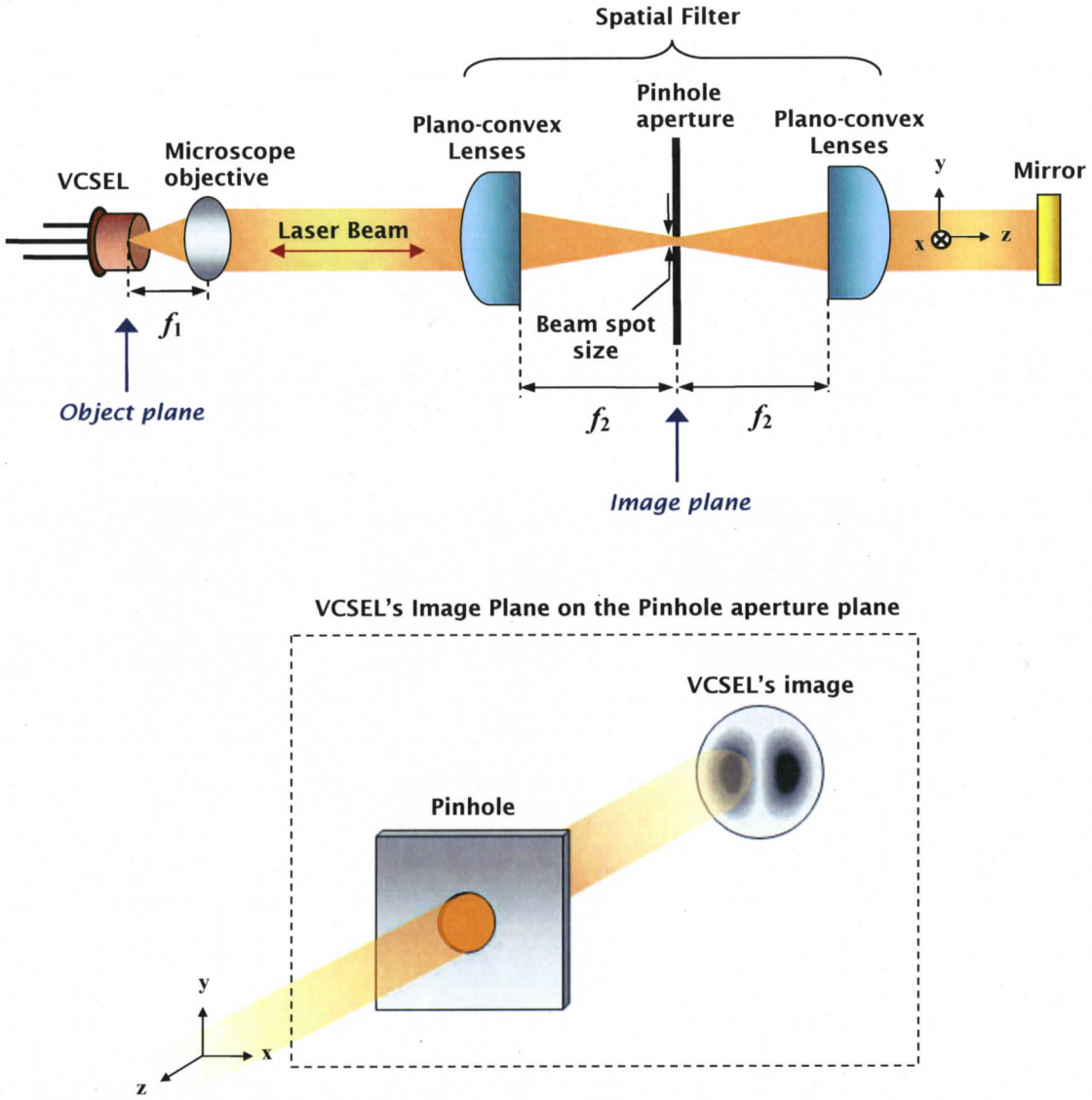

Figure 20 Principle of spatially filtered optical feedback

Table 2 VCSEL's image size on the object plane through different pinhole sizes and microscope objectives

Microscope objective	Numerical aperture (NA)	Focal length, f_1(mm)	Focal length, f_2(mm)	Magnification of image on object plane ($M_{\text{object plane}}$)	VCSEL's image size on object plane through the pinhole aperture diameter	
					81 μm	42 μm
20×	0.4	8.6	50	0.172	13.9 μm	7.22 μm
40×	0.65	4.5		0.09	7.29 μm	3.78 μm

Spatial resolution

The Fraunhofer diffraction pattern from a circular pinhole aperture forms an image of the VCSEL light output that looks like an airy disk. The diameter of the focused spot is the minimum limit of diffraction when image is projected back on the VCSEL's aperture and is given by [120]

$$(\Delta\ell)_{\text{diff}} = \frac{1.22 f_1 \lambda}{\text{D}} = \frac{1.22\lambda}{\text{NA}} \tag{4.2}$$

where, f_1 is the focal length of the microscope objective, λ is the wavelength of the VCSEL, D is the diameter of laser beam on the microscope objective and NA is the numerical aperture of the microscope objective. An assumption is drawn when the numerical aperture is used in the equation above. Laser beam is assumed to hit the entire diameter of the microscope objective lens. In practice, the laser beam does not utilize the whole diameter of the objective lens; therefore the spatial resolution should be slightly higher. Therefore, the calculated diffraction-limited spot size on the VCSEL's aperture based on the Equation (4.2) above were 1.6 μm and 2.6 μm when 40× and 20× microscope objectives were used.

Equation (4.2) shows that the size of the finest details that can be resolved is proportional to λ/NA. Using a lens with higher NA (40× objective) will be able to visualize finer details than a lens with lower NA (20× objective) because higher NA lenses have more light-gathering power. Thus, the spatial resolution is finer (improved) using a 40× microscope objective with a higher numerical aperture and the VCSEL

image size through 42 μm pinhole aperture projected on its object plane is 3.78 μm which is quite close to the diffraction limit.

4.1.3 Czerny-Turner imaging spectrometer

Some light is split at the beam splitter and transmitted to a 0.5 m Czerny-Turner imaging spectrometer (CVI Digikrom DKSP480). Figure 21 shows the schematic diagram of a typical Czerny-Turner monochromator.

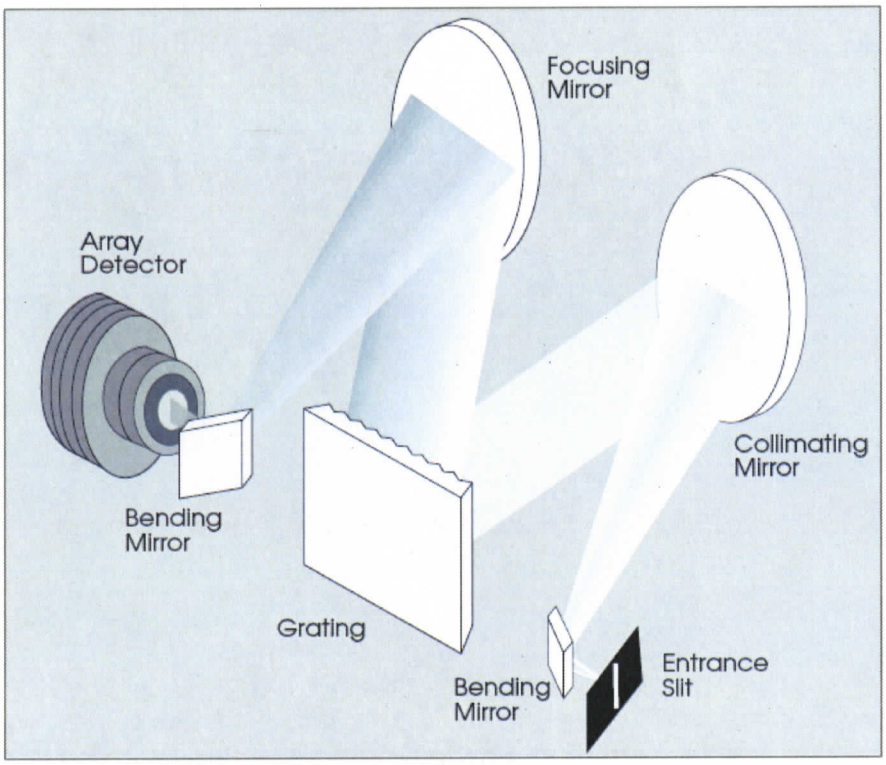

Figure 21 Schematic diagram of a Czerny-Turner monochromator [121]

As illustrated in Figure 21, the collimated light from the beam splitter is focused on the entrance slit of the spectrometer and directed by the first bending mirror, to the parabolic collimating mirror. The focused beam is collimated and directed to the grating, which diffracts and reflects the radiation. The diffraction grating serves as a wavelength diffraction element.

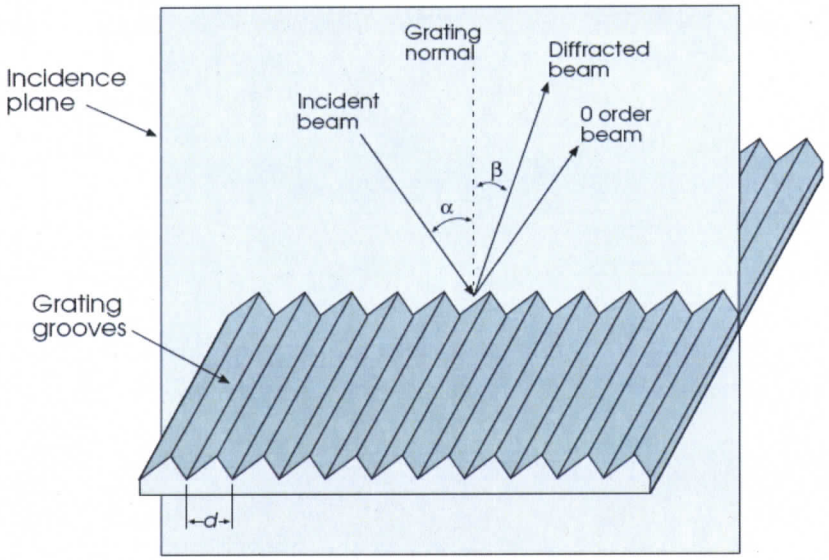

Figure 22 A reflective diffraction grating in the spectrometer [121]

The grating equation, for both transmission and reflection is given by [120]

$$m\lambda = d(\sin\alpha - \sin\beta) \tag{4.3}$$

where, α is the incident angle, β is the diffracted angle, d is the groove spacing and m is an integer ($= \pm 1, \pm 2, \pm 3, \ldots$). The values of m specify the order of the various principal maxima.

By the rotation of the grating, a particular wavelength of the light determined is directed to the focusing mirror, which reforms the image (of the slit) and focuses the light onto the array detector via the second bending mirror. The array detector is a thermoelectrically (TE) cooled Silicon CCD camera (ST-6) that has an array of detectors (known as pixels) and is mounted along the focal plane of the focusing lens. The array is cooled for noise reduction and long-term stable operation. The array detector elements see a signal that is proportional to the amount of the entrance-slit image that falls on the element. The wavelength scanning is accomplished by electric read-out means of a multi-channel detector.

The parameter settings for the spectrometer are listed in Table 3. The fundamental mode was found to be at 855.55 nm when VCSEL was operated near its threshold current. TE cooler CCD was set at 0° Celsius. The definition for resolution of a spectrometer is the full-width-at-half-maximum (FWHM) measured for a single

monochromatic spectral line. In practice, the resolution depends upon the resolving power of the grating, slit width setting, effective system focal length and other parameters.

Table 3 Parameters for the Spectrometer

no.	**Parameter**	**Unit**
1	Wavelength	855.55 nm
2	Temperature	0° Celsius
3	Scan rate	100 nm/min
4	Grating	1200 grooves/mm
5	Effective system focal length	480 mm
6	CCD binning setup	1 × 2
7	CCD resolution mode	750 × 121
8	CCD pixel size	11.5 × 54 μm

The spectral resolution of a spectrometer is a measure of its ability to separate two close wavelength lines and is dependent on the resolving power of the grating, which is given by the Raleigh criteria as [120]

$$\Re \equiv \frac{\lambda}{(\Delta\lambda)_{\min}} \tag{4.4}$$

where $(\Delta\lambda)_{\min}$ is the least resolvable wavelength difference, or limit of resolution, λ is the mean wavelength. The resolving power can also be expressed as the product of the diffraction order m and N, the number of grooves being illuminated by the incident radiation $\lambda/(\Delta\lambda)_{\min} = mN$, or [120]

$$\Re = \frac{Nd(\sin\alpha - \sin\beta)}{\lambda} \tag{4.5}$$

The width of the spectrometer's entrance slit also plays a significant role in determining the spectrometer's resolution and bandpass/bandwidth (FWHM). The entrance and exit slits are set at the same width. The light intensity passing through is a function of the overlap of the entrance slit image with the exit slit. The image of the entrance slit will sweep across the exit slit by rotating the grating for a wavelength scan.

The resolution of the spectrometer as a function of slit width and CCD pixel size is given by

$$\text{Resolution} = \text{Resolution factor} \times \text{Pixel resolution} \times \frac{\text{Slit width}}{\text{Pixel size}}$$

$$= \text{Resolution factor} \times \frac{\text{Bandwidth}}{\text{Pixel number}} \times \frac{\text{Slit width}}{\text{Pixel size}} \qquad (4.6)$$

where resolution factor is 1.8 for DKSP480, bandwidth is the spectrometer's wavelength window range (= 13 nm), pixel number is 750, pixel resolution is 0.018 nm/pixel and pixel size is 11.5 μm. With 1200 grooves per millimetre grating and smallest slit width of 10 μm, the maximum resolution of the spectrometer was 0.03 nm [121].

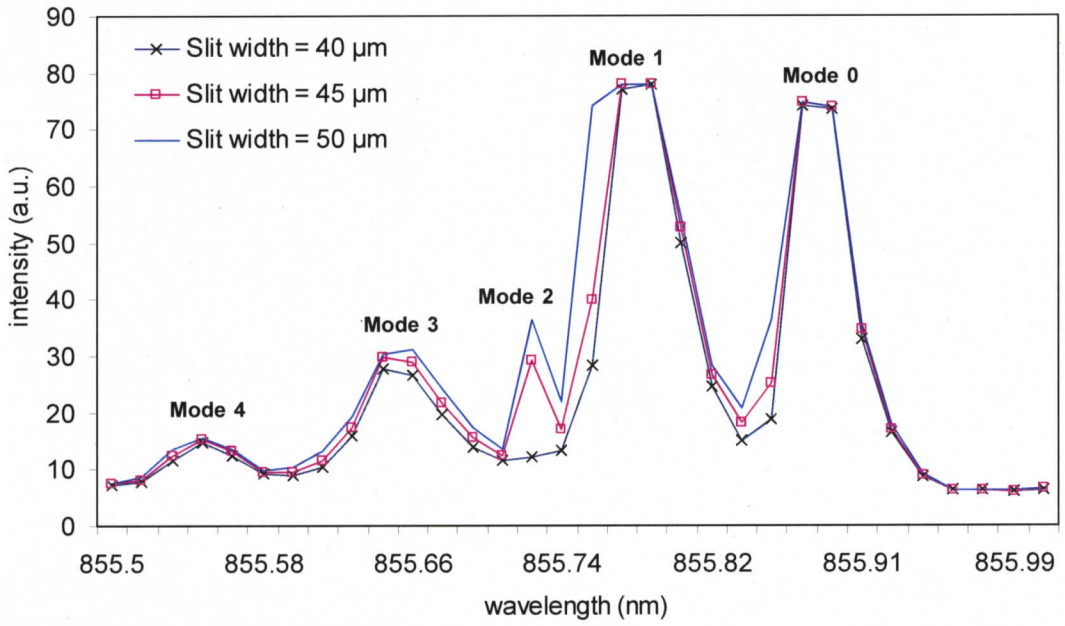

Figure 23 Graph of intensity vs. wavelength at 8.5 mA for slitwidth comparison

Also note that if the slit width is a lot smaller than the laser beam, some modes will be lost in the spectrum because the modes are spatially dependent. The entrance slit width of the spectrometer should be calibrated first before taking any data. The plot above shows the effect of slit width on the spectra for a free-running VCSEL at 8.5 mA. As shown in Figure 23, slit width of 40 μm has only 4 modes (peaks), however, at slit width

of 45 μm, there were 5 modes. This means that if the slit width is not calibrated, we will lose some modes due to narrow slit width and the larger the slit width, the wider the linewidth of each mode. It was found that slit width of 45 μm is the optimum value for capturing the light emission of the VCSEL at injection currents of 4.2 mA, 4.45 mA and 8.5 mA. These are the currents for measurements taken, analyzed and presented in this thesis.

4.1.4 Lock-in amplifier and optical chopper

The feedback-induced voltage change across the terminals of lasers has been discussed in Chapter 3. Presented here is the method of the voltage drop detection when feedback is in effect on the VCSELs. The lock-in amplifier and optical chopper combination is a common method of detecting changes in the voltage drop across the laser [38, 97]. In this experiment, the combination was used to detect changes in VCSEL's voltage drop as a function of the pinhole position. The schematic setup diagram is shown in Figure 24.

In a lock-in amplifier system, whether analogue or digital, a concept of phase sensitive detection is required that converts AC signals to DC output for the detection system. Therefore, the special rectifier, namely, the phase-sensitive detector (PSD) (also known as the demodulator), which performs the conversion, forms the heart of the instrument [122]. In a light measurement system, the chopper causes the signal to be modulated and the reference waveform is an output coherent with the chopping action (in this case, 100 Hz) [123]. A BNC connector was connected between the reference ports of optical chopper control unit (Scitec Instruments) and lock-in amplifier (Stanford Research Systems SRS 510). Thus, the frequency of the bandpass filter in the lock-in amplifier is locked onto the chopper's frequency.

The input ac signal to be analyzed by the lock-in amplifier is the modulated feedback light detected by the photodetector from within the VCSEL and this signal output was detected as the voltage change across the VCSEL's LD(+) and LD(-) pins where the pin 1 and 2 of the VCSEL were labelled in Figure 19(b). The VCSEL's pins were connected to the signal input of lock-in amplifier by means of the electrical connectors (BNC connector with spring clips). Setting the required parameters by the lock-in amplifier as

listed in Table 4, the output voltage drop across the terminals of the VCSEL were shown on the display of the lock-in amplifier.

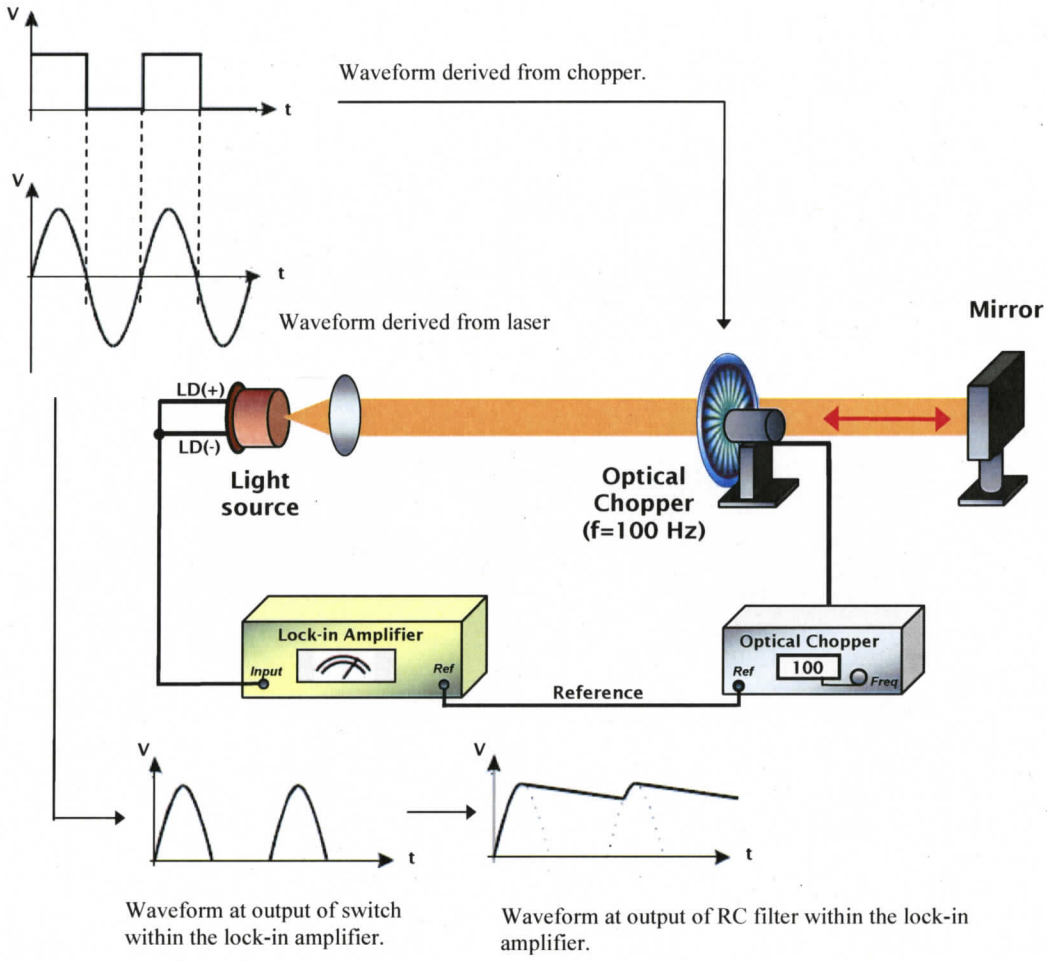

Figure 24 Schematic diagram for lock-in amplifier and optical chopper setup in the spatially filtered feedback system

The laser diode controller can also be used to measure the voltage drop (denoted as V_f) on the laser but it can only measure as low as 1 mV. In this experiment, switching between feedback and non-feedback V_f values were shown on the laser diode controller display. When the smaller pinhole (42 μm) was used, there was no switching of the feedback and non-feedback V_f values shown on the laser diode controller. However,

changes on the VCSEL's spectra were observed when feedback was provided. Thus, the lock-in amplifier and optical chopper combination has been employed as a high precision voltmeter for detecting weak feedback light in this system. With this combination, voltage changes in the range of between hundreds and tens of micro-Volts were detected in this feedback system. In fact, the lock-in amplifier used can measure as low as 100 nV. The parameter settings for the lock-in amplifier are listed in Table 4.

Table 4 Parameters for the Lock-in Amplifier

no.	**Parameter**	**Unit**
1	Signal input	A
2	Signal filter	Bandpass
3	Sensitivity	1 mV
4	Dynamic reserve	low
5	Display	X
6	Expand	X1
7	Rel (relative reading)	off
8	Offset	off
9	Time constant	Pre-filter =100 msec Post-filter = none
10	Reference	*f*, square wave, Hz
11	Phase shift	0°

4.1.5 Three-axis piezo controllers

For nano-positioning of the feedback mirror, a piezoelectric kinematic mirror mount that was connected to the three-axis piezo controller (Thorlabs MDT693A [124]) as shown in Figure 25 was employed. Piezoelectric actuation is a method of generating mechanical movement by generating an electric charge (or voltage) on certain materials. The material used in Thorlabs piezoelectric kinematic mount is the AE0505D08F piezoelectric stack manufactured by NEC Corporation of Japan. From the specification sheet of this material [125], it is reported that a displacement of 6.1 μm is achieved with

applied drive voltage of 100 Volts. The maximum drive voltage of 150 Volts will yield a displacement of 9.1 μm. Thus, the displacement of 60 nm/V can be achieved because it is an almost linear relationship between the displacement and the applied voltage.

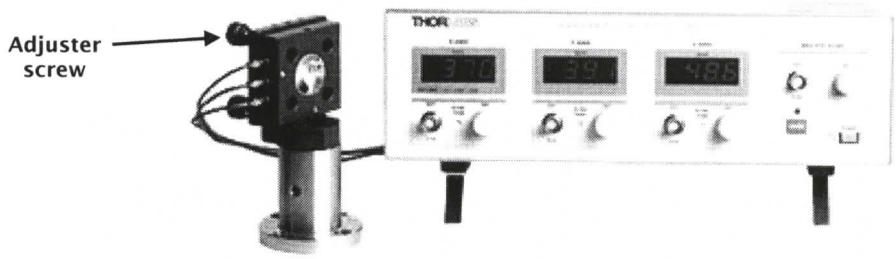

Figure 25 A complete system of piezoelectric kinematic mount and three-axis piezo controller [126]

There are three adjuster screws on the kinematic mount for coarse positioning. The piezoelectric stacks are mounted in the front plate directly under the tips of the three adjuster screws. Therefore, with the three-axis (*x*-*y*-*z*) piezo controller for supplying the driving voltage to the piezoelectric stack, nano-positioning of both the angle (one adjuster at a time) and translation (all three adjusters simultaneously) can be done. By varying the alignment of the mirror, we are able to change the phase and the length of the external cavity. The results on the mirror alignment variations are presented in the next Chapter.

4.2 METHODOLOGY AND RECOMMENDATIONS

Figure 26 shows the step-by-step procedure to set up the experiment.

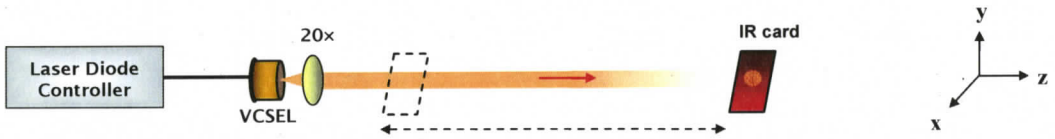

(a) IR card was moved back and forth on the beam path to check for almost perfect collimation.

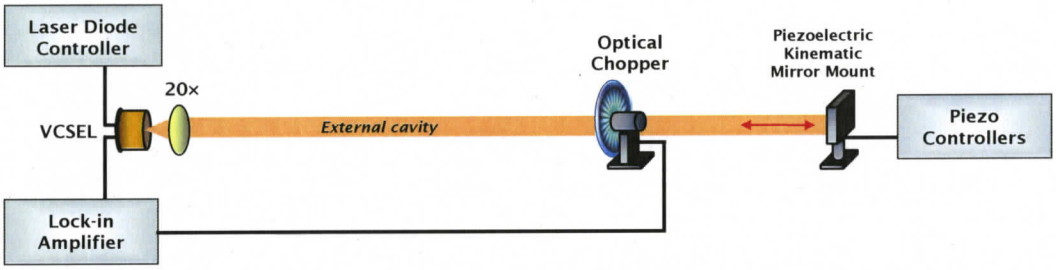

(b) Mirror was placed on the main collimated light path to provide feedback to the laser. Lock-in amplifier and optical chopper combination act as a high-precision voltmeter for feedback efficiency measurement.

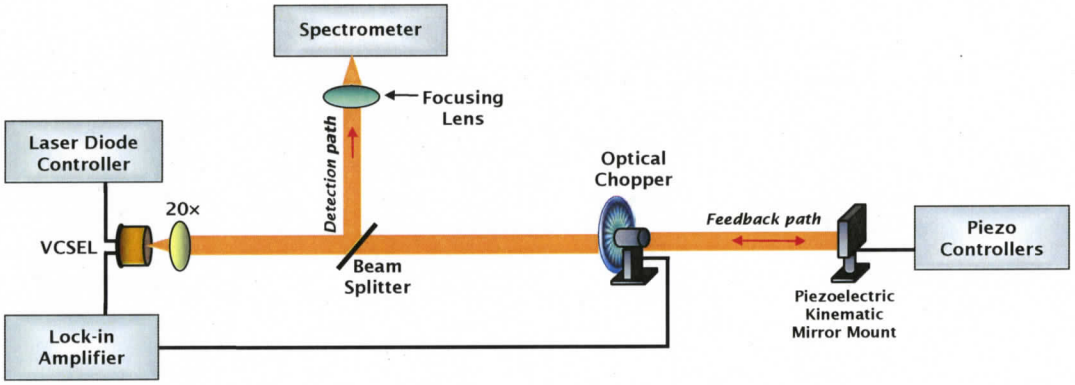

(c) A beam splitter was used to split some light to the spectrometer.

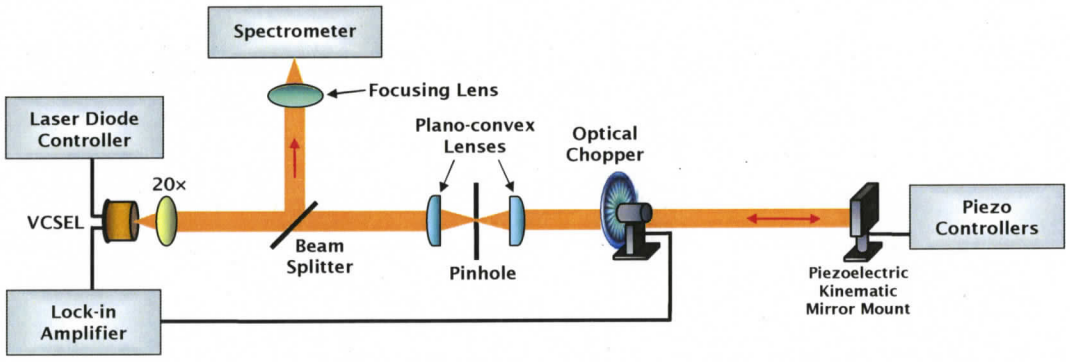

(d) Spatial filter consists of two plano-convex lenses and a pinhole, was used as a spatial optical feedback selection on the VCSEL.

Figure 26 Methodology to setup the spatially filtered feedback system

The first step was to collimate the light emission from VCSEL before the rest of the components were placed in as shown in Figure 26(a). The laser output was collimated with a 20× microscope objective (of numerical aperture, NA = 0.40 and focal length, f = 8.6 mm). Laser was mounted on an x-y-z micro-positioning stage and a 20× microscope objective was placed at its focal length of 8.6 mm away from the VCSEL for laser beam collimation as shown in Figure 19(c). To ensure that the microscope objective was placed at approximately 8.6 mm distance away from VCSEL, the x-y-z micro-positioning stage where the laser was mounted on, was carefully adjusted so that the VCSEL's beam was the same size at a point near and far from the 20× lens using an infrared (IR) viewing card. The Thorlabs IR viewing cards have a special sensor area which is made of slow-fading phosphor that is active in the 800-1700 nm range and is typically used for locating non-visible IR beam. The phosphor must be charged with room light before use. The collimated light path was also ensured to be emitted parallel to the holes on the optical table and of the same height from the optical table.

After the light is collimated, a gold mirror was placed at a distance from the VCSEL, thus forming an external cavity as depicted in Figure 26(b). The distance between the mirror and the VCSEL was adjustable between 28 cm and 50 cm (set at 35 cm for this study). The mirror was mounted on a piezoelectric kinematic mirror mount, so that micro- and nano- positioning of the piezo-mirror can be done to align the feedback light to coincide with the output light of the VCSEL. The trick here was to place a thin piece of tissue paper in the light path and with the aid of the IR beam finder (see Figure 18), both transmitted and reflected beams can be seen on the paper. By adjusting the alignment of the mirror, the reflected beam can be made to coincide with the transmitted beam. At first, coarse feedback alignment (micro-positioning) was done using the knobs on the mount before adjusting the nano-positioning via the piezo controllers. When feedback was provided to the laser, voltage drop across the terminals of the laser was obtained [38] and this was shown on the laser diode controller as well as the lock-in amplifier display.

Then, a beam splitter was placed after the collimating lens to split some of the light in the cavity to the spectrometer for spectral analysis as shown in Figure 26(c), thus forming

the detection and feedback paths. This position is suitable to measure both cases when laser is solitary and when feedback is provided.

The last step is to place a spatial filter in the setup. In the feedback path, a spatial filter, consisting of two identical plano-convex lenses and a pinhole, was positioned after the beam splitter. Two plano-convex lenses were placed in the external cavity first and the feedback light was again checked to be aligned with the emitted light. After that, a pinhole was placed in between the lenses. The pinhole was held by a clamp that was attached to an x-y-z translation stage. Since the size of the pinhole is in microns, it is not easy to shine light through the hole if the pinhole was placed right in between the lenses. The trick to speed up the process is to start at some distance away from the middle point between the lenses (beam waist). This was found to be easier and faster to get the light through the pinhole. Once the light had been detected with an IR card on the other side of the pinhole, the pinhole was slowly translated in the z-direction to the middle point between the lenses while making sure that the beam was still detected on the IR card. It was found that the light intensity of the beam shown on the IR card behind the pinhole seen from the VCSEL was brighter when the pinhole position is in the middle of the lenses. We want to pass as much light as possible through the pinhole, so that higher feedback light intensity will be reflected back to the laser. The feedback position on the VCSEL was adjusted through the transverse (x- and y-axis) pinhole locations inside the laser cavity. This was verified with the voltage drop measurement shown on the lock-in amplifier.

The most challenging aspect of this experiment was proper alignment of the feedback beam so that maximum optical feedback to the laser was achieved. Several points and recommendations should be noted for this experiment. Firstly, even when feedback is aligned, it is not uncommon for the feedback light to randomly become misaligned while taking data. Therefore, when data are taken, the voltage drop value shown on the lock-in amplifier has to be ensured to be the same. Preferably all measurements for a particular experiment are suggested to be taken in one run for higher precision. The precision of the results are affected by the nonlinearity nature of VCSELs as discussed in Section 2.4.4 and also by other external factors causing the experimental setup to be

disturbed. Before taking any measurements, on the next day for example, the feedback has to be ensured to be at its maximum.

Secondly, the cleanliness of the optical components especially, the mirror, lenses and beam splitter, is vital. Fingerprints and dust particles tend to stay on the optical components. Cleaning up the components requires a lot of effort and has to be done professionally with the right chemicals. Therefore, gloves must be worn when setting up the experiment. The optical components placed on the optical table must be left in the upright position to minimize dust collection on these components.

Lastly, an anti-static wrist strap should be worn at all times when handling VCSELs, for instance, mounting a VCSEL on the laser mount or connecting the clips to a VCSEL's terminals, so that the device will not be damaged due to static discharge.

4.3 SUMMARY

In this chapter, we have delineated the methodology used in this research. By varying the design parameters, such as the injection current, pinhole aperture size, and mirror alignment, the system performance is analyzed. In this study, the system performance measurement is characterized by the change of laser's spectrum when laser is solitary and when feedback is provided. An in-depth understanding on the spatially selective feedback system of VCSEL is given. The following Chapter will present the VCSEL feedback-induced of voltage drop maps and spectrum results for mode control at both low and high injection currents. Further discussion on the experimental results will also be provided.

CHAPTER 5

RESULTS AND DISCUSSION

The experimental tests on the spatially filtered optical feedback for mode control of a VCSEL were carried out and the results are presented in this chapter. In the first section, the voltage change from spatially selective feedback is mapped out over the image plane of the VCSEL for low and high injection currents. In the second section, higher-order mode suppression is demonstrated for low currents and selective mode intensity control is shown for high currents. In the third section, we measure the frequency shift of different modes by spatial feedback selection. Next, in an external cavity VCSEL setup without spatial filtering, mode control can be achieved by varying the external cavity length of the laser through mirror alignment or translation. Finally, the recovery time of the VCSEL is measured after spatially selective feedback.

5.1 FEEDBACK-INDUCED VOLTAGE DROP

Figure 27 and Figure 28 show a map of the voltage drop across the VCSEL as a function of spatial filter position in the image plane. This image can be interpreted as a representation of how various feedback positions affect the threshold current of the laser modes, where a larger voltage drop corresponds to a larger decrease in threshold current [38]. Note that the x-axis and y-axis of Figure 27 and Figure 28 are position values acquired from the x-y-z translation stage. The extent of the images in Figure 27 and Figure 28 is approximately 70-100 μm, which corresponds to 12-17 μm on the VCSEL (when accounting for the magnification) – this is in reasonable agreement with the known aperture size of the VCSEL of 15 μm.

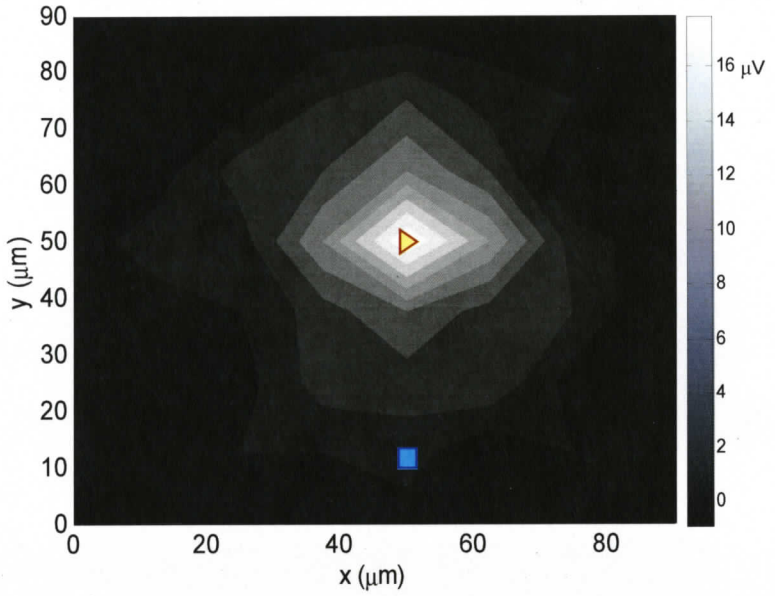

(a)

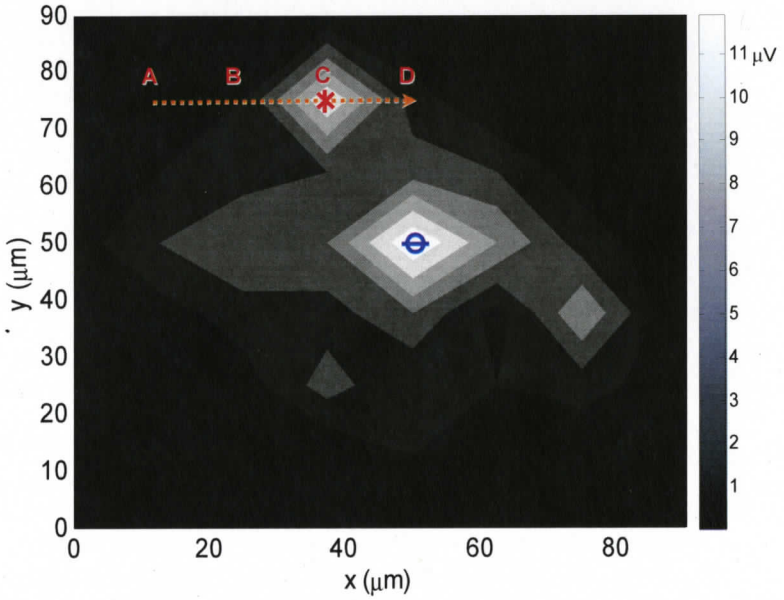

(b)

Figure 27 VCSEL feedback-induced voltage profile mapping at injection currents of (a) 4.20 mA and (b) 4.45 mA, measured with a 42 μm pinhole. The symbols in the diagrams will be discussed later in Section 5.2.

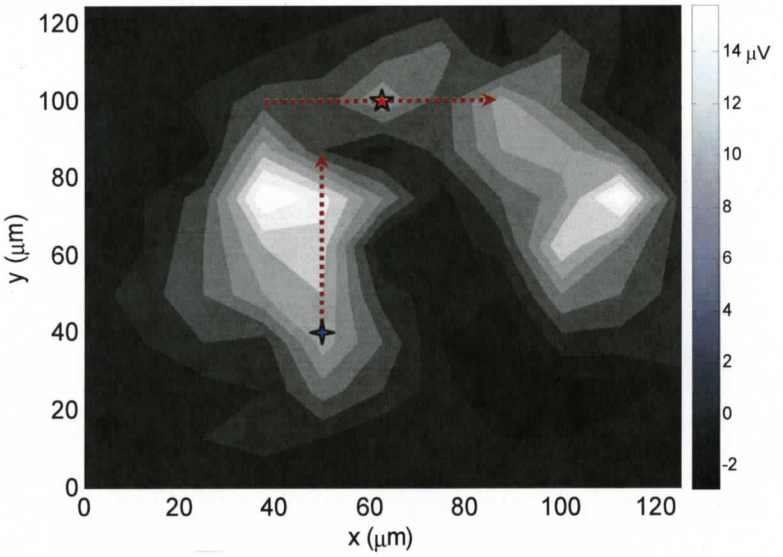

(a)

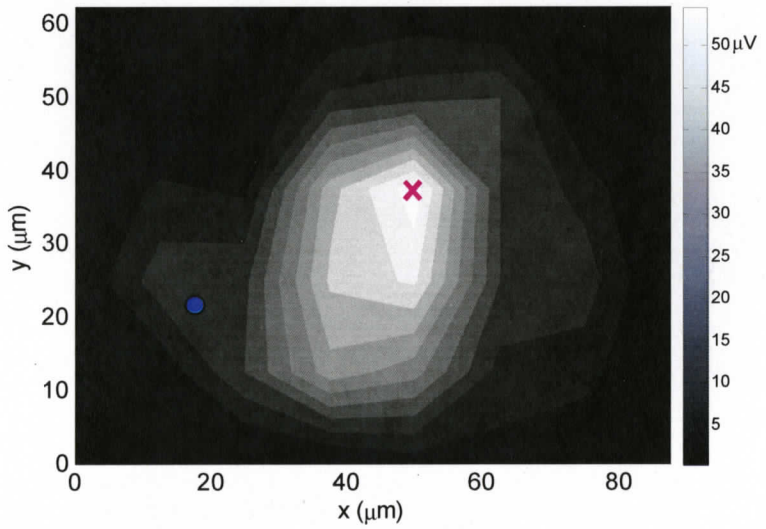

(b)

Figure 28 VCSEL feedback-induced voltage mapping at injection current of 8.5 mA measured with (a) 42 μm pinhole and (b) 81 μm pinhole. The symbols in the diagrams will be discussed later in Section 5.2.

Figure 27(a) and (b) show the VCSEL feedback-induced voltage profile mapping at two different low injections currents of 4.20 mA and 4.45 mA. The feedback voltage drops were shown on the lock-in amplifier by measuring with a 42 μm pinhole at various pinhole locations indicated by *x*- and *y*-axis positioning. As the injection current increases, the numbers of peaks and the non-uniform intensity distribution on the topography representation of the VCSEL feedback-induced voltage profile increase.

Figure 28(a) and (b) show the VCSEL feedback-induced voltage profile mapping measured with two different pinhole sizes, i.e., 42 μm and 81 μm, at a higher fixed injection current of 8.5 mA. The bigger pinhole is similar in size as the aperture diameter of the VCSEL at the image plane (when accounting for magnification), whereas the smaller pinhole is about half the size of the VCSEL's aperture diameter at the image plane. These two figures show that the mapping of the VCSEL's feedback-induced voltage profile varies with aperture diameter and a diameter smaller than the VCSEL image is required to show finer features, such as the three distinct maxima shown in Figure 28(a).

For long external cavities (>15 cm), the behavior of VCSELs has been found to be independent of the phase of reflection [62]. Considering this phase-insensitive behavior, the optical feedback is expected to increase the photons in the cavity, which will reduce the number of carriers by stimulated emission. As a result, the carrier density will drop, which is marked by a corresponding drop in the difference between the quasi-Fermi-levels of the diode. For a fixed current, the voltage drop across the VCSEL will then decrease with the quasi-Fermi-level separation. Therefore, the voltage drop observed in Figure 27 and Figure 28 is expected from the spatially selective feedback for a fixed current.

Since the transverse modes of a VCSEL are position dependent, providing preferential feedback at a single position on the laser's gain region will supply spatial feedback to specific modes. For certain positions, a small voltage increase was observed. This may be the result of mode-competition effects [116, 117], or VCSEL anisotropy influencing the preferred mode orientation [100].

A comparison of small and large pinholes to map the VCSEL feedback-induced voltage profile was investigated. The VCSEL image on the pinhole plane was around 87

μm, after magnification of 5.8× with respect to the actual size of the VCSEL's aperture output. The results in Figure 28 showed that mapping the VCSEL feedback-induced voltage profile using an 81 μm pinhole, about the same size as the VCSEL image at the pinhole transverse plane, yield higher feedback strength but lost the mode profile structure of the VCSEL. Therefore, it was found that the pinhole size should be smaller than the VCSEL image to provide good spatial selection.

5.2 Spectral Selection

For low and high injection current operation, the spectral characteristics of the VCSEL were examined at every pinhole position in the image plane.

Figure 29(a) shows the VCSEL spectra without feedback and with feedback at two different positions as marked in Figure 27(b). Figure 29(b) shows the suppression of the higher order transverse mode for low current operation. The VCSEL was operated at 4.45 mA (I_o=1.3I_{th}) injection current in the two-mode regime where mode 0 represents the fundamental mode and mode 1 represents the first-order mode. The various positions of the pinhole (A, B, C, D) are shown in Figure 27(b). It is clear from this figure that appropriate placement of the pinhole can result in higher-order mode suppression. Several experimental runs were attempted with different pinhole locations, pinhole sizes and lens configurations and the highest current single mode operation found was 4.55 mA, which is 1.3× the threshold current.

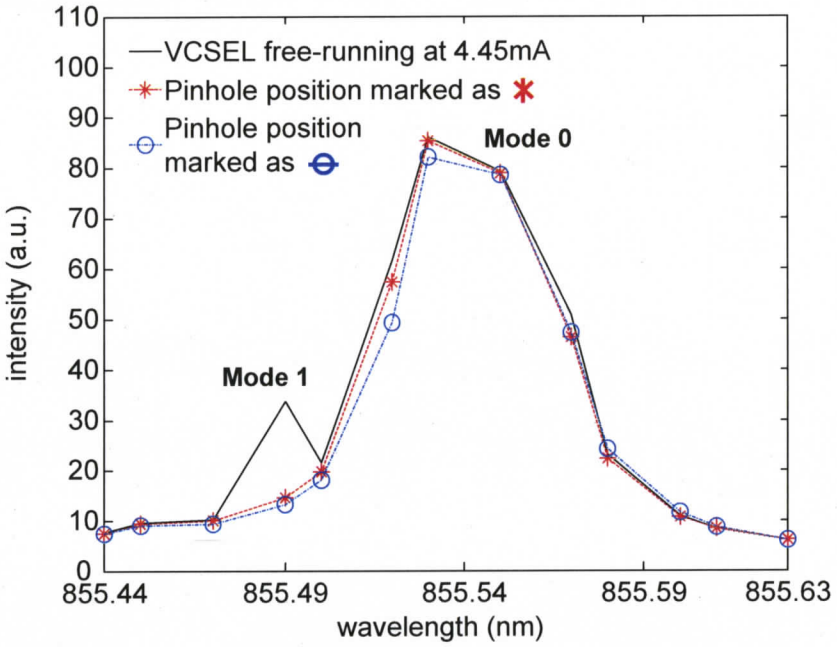

(a)

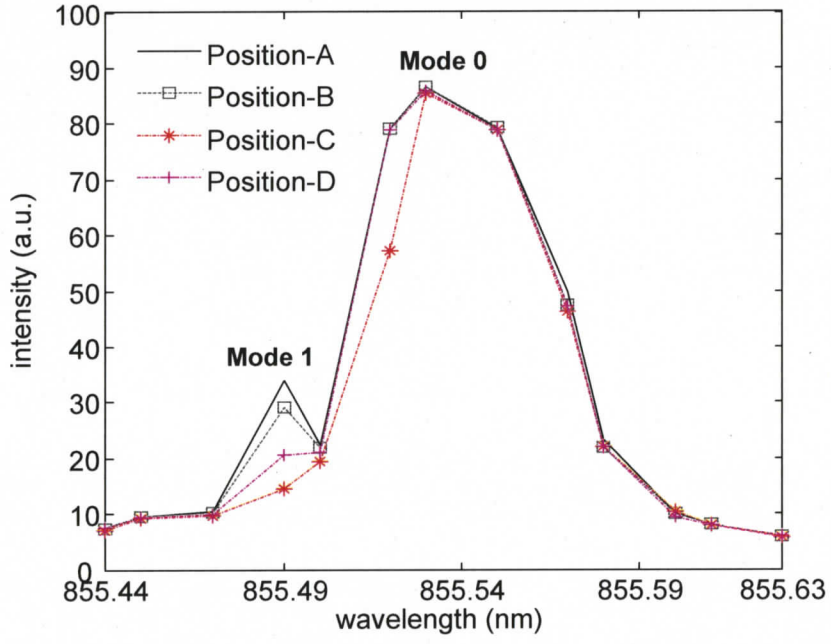

(b)

Figure 29 Spectra of VCSEL showed (a) higher-order mode suppression occurred at the two maximum feedback strength, and (b) higher-order mode suppression at 4.45 mA injection current as the pinhole was translated from position-A to position-D in Figure 27. Mode 0 and mode 1 were 855.53 nm and 855.49 nm, respectively.

Figure 30 shows the optical spectrum with five-mode operation at a higher current of 8.5 mA for the free-running VCSEL, and the maximum spectrum change when feedback is provided at the 'star' and 'cross' shown in Figure 28(b). At the pinhole location marked 'star', the spectral intensity of mode 3 showed a 1.8× increase, whereas the spectral intensity of mode 2 and 4 was reduced. For pinhole location marked 'cross', spectral intensity of mode 2 showed 1.5× increase with a slight intensity decrease in modes 3 and 4 modes as compared to the free-running VCSEL. The two pinhole locations that show the maximum feedback voltage drop at coordinates (x =37.5 μm, y = 75 μm) and (x = 112.5 μm, y = 75 μm) have the same spectra as the free-running VCSEL without feedback.

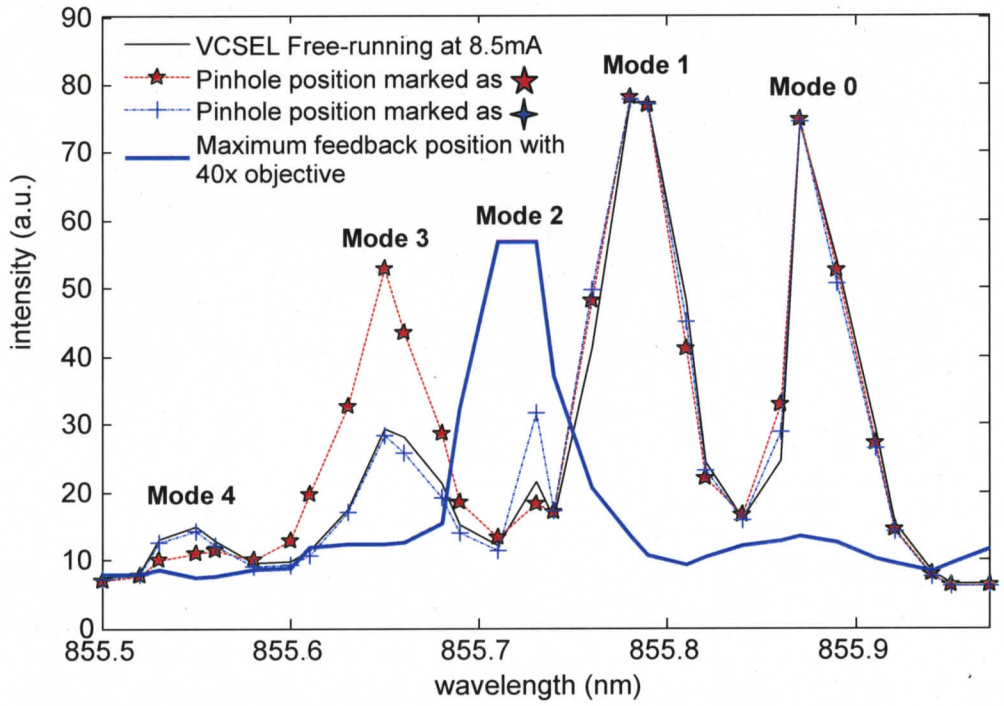

Figure 30 VCSEL spectra taken at 8.5 mA, where 'star' and 'cross' are positions marked in Figure 28(a). The mode 0, mode 1, mode 2, mode 3 and mode 4 peak wavelengths were 855.87 nm, 855.78 nm, 855.73 nm, 855.65 nm and 855.55 nm, respectively

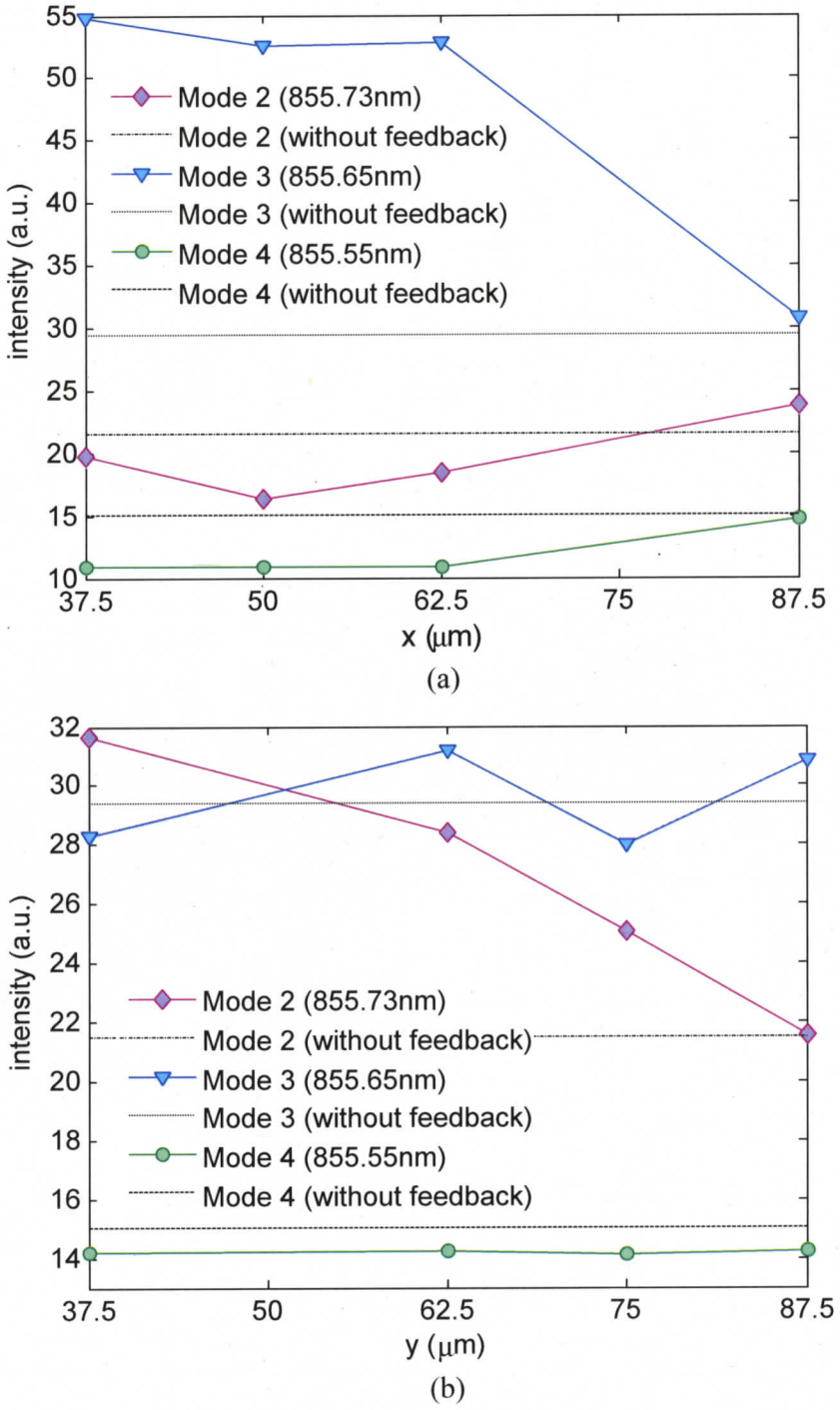

Figure 31 Intensity changes of the mode 2, 3 and 4 as the pinhole was translated across (a) the *x*-axis from 37.5 to 87.5 μm while holding the *y*-axis fixed at 100 μm, and (b) the *y*-axis from 37.5 to 87.5 μm while holding the *x*-axis fixed at 50 μm

Figure 31 illustrates the spectral intensity changes of modes 2, 3 and 4 as the 42-μm pinhole was translated along the *x*- and *y*-axis of the feedback voltage drop map as represented with the arrow signs in Figure 28(a). From Figure 31(a) and (b), mode 3 showed higher sensitivity to *x*-axis translation than other modes, while mode 2 showed higher sensitivity than other modes to *y*-axis translation.

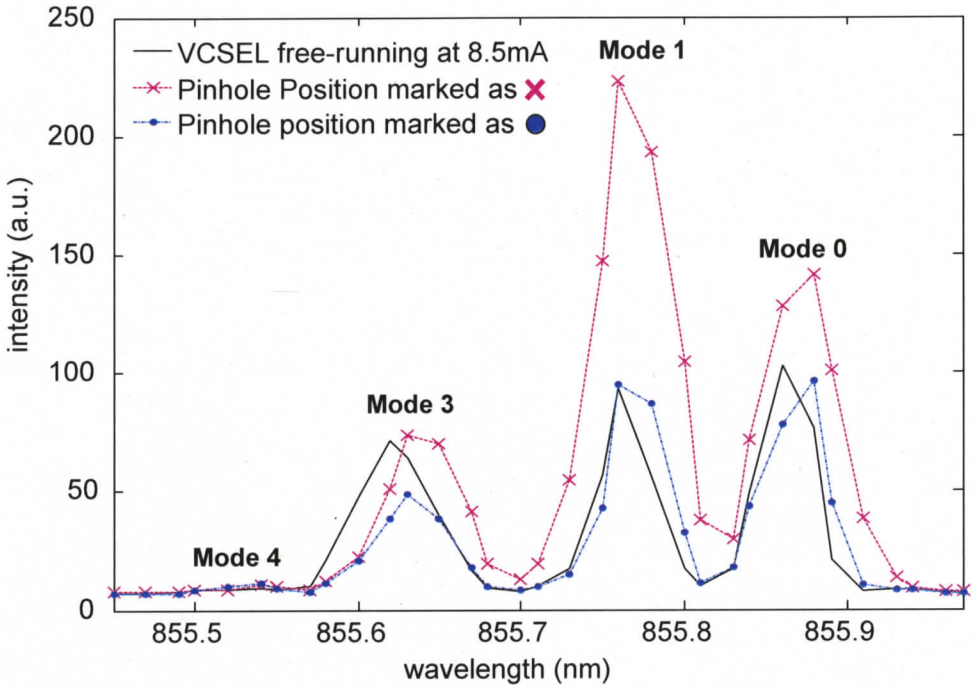

Figure 32 VCSEL spectra taken at 8.5 mA, where '✖' and '●' are positions marked in Figure 28(b). The mode 0, mode 1, mode 3 and mode 4 peak wavelengths were 855.88 nm, 855.76 nm, 855.63 nm and 855.54 nm, respectively.

There exists a dependence of the modes on the pinhole size. Modes 0 and 1 have no changes with 42 μm pinhole feedback with the respective translations; therefore they are not shown in Figure 31. We have observed, however, that only modes 0 and 1 showed enhancements when feedback is provided with an 81 μm pinhole at the maximum voltage-change feedback point marked by '✖' in Figure 28(b). The modes labelled in Figure 32 correspond to the modes labelled in Figure 30. Mode 0 and 1 showed an enhancement of 1.8× and 2.4× respectively as compared to the free-running VCSEL spectral intensity. Notice that there is no Mode 2 in Figure 32. This is because the experiment was carried out with a larger pinhole (81 μm) and smaller spectrometer's

slitwidth (10 μm) at a different time (4 months apart). Using a smaller slitwidth, 10 μm, instead of 45 μm, we will lose mode 2 in the VCSEL spectrum as explained in Section 4.1.3 and illustrated in Figure 23. We repeated the experiments with a pinhole size of 10 μm, which showed little change in the optical spectrum with feedback. This is the result of the limited resolution of the optical setup. The 20× microscope objective, with a NA of 0.4, had a diffraction limited spot size of 2.6 μm on the object plane (of the VCSEL's active region). Therefore, even the 42 μm pinhole was close to the diffraction limit of 15 μm when projected to the image plane (of the aperture). To extend the spatial selection, but still operate away from the diffraction limit, we repeated our experiments with a 40× microscope objective, with a NA of 0.65 and a diffraction-limited spot size of 1.6 μm. With this microscope objective, the maximum voltage drop was 13 μV for a current of 8.5 mA, which is similar to the 18 μV maximum voltage drop seen for the 20× objective. With the 40× microscope objective, it was possible to see greater side-mode suppression at 8.5 mA, as shown with the darker solid line in Figure 30, even though this was still multimode operation.

When feedback was applied to the VCSEL in the two-mode regime (mode 0 and 1), the VCSEL was able to return to single fundamental mode operation, due to the threshold reduction of the fundamental mode from increased feedback. As a result, the higher-order modes were suppressed by mode-competition. However, at high currents when laser operates in five-mode regime, optical feedback is not strong enough to preserve the single-mode behaviour of VCSEL and therefore, preferential selection of modes was observed by providing feedback on the selected positions where the modes exist in the active region. At higher currents, the VCSEL emits in multiple transverse modes [22, 23] due to carrier spatial hole burning [28-30, 114].

It can be seen from Figure 31 that when feedback was provided at a particular position in the active region, several modes' intensities changed. With x-axis translation, mode 3 has higher sensitivity compared to other modes, whereas, with y-axis translation, mode 2 has higher sensitivity. This is an observation for spatial competition between those modes as some modes share the same local optical gain. Numerical [116, 117] and experimental [103] analysis have shown that modes that are spatially overlapped have

strong competition while modes that are spatially separated can coexist by sharing the available gain.

The multimode behavior of VCSELs involves optical, carrier and thermal effects in multiple spatial dimensions and in time. So far, there have been many theoretical investigations of this topic (e.g. [30], [117]). While some have considered the effect of optical feedback (e.g. [60], [127]), spatially selective optical feedback is a topic which requires further study, as alluded to in past theoretical works [127]. (Those past works considered uniform coupling into the different modes for simplicity). Such investigations, however, would represent a significant theoretical contribution, and are therefore beyond the scope of this experimental work. It is worthwhile, however, to consider some physical principles that allow for single mode operation, and to consider limits of single mode operation using this method.

Single mode operation is allowed at low bias currents because: (1) one of the modes has lower optical loss, and/or (2) one of the modes is preferentially pumped by non-uniform current injection, and therefore has higher gain. Spatially selective feedback influences the former, by effectively reducing the optical losses of a single mode by feeding light back into the cavity, (which is a reasonable description for the large external cavity considered here where short-range phase-effects can be neglected). The preferred mode pins the local carrier density, so that the carrier density increases only in the non-lasing mode regions, until those other modes reach threshold. This is the physical principle of single mode selection that was observed in the experiment.

As noted in previous works [60], [127] carrier diffusion is an important parameter in multimode behaviour. If carrier diffusion is fast, the carrier density will be uniform throughout the active region and there will be single mode lasing. Only the mode with the lowest optical losses will have sufficient gain to lase and it will pin the gain of the other modes below threshold. Spatially selective optical feedback favours single mode selection in this case, because it allows for selectively reducing the losses of a single mode. Therefore, VCSELs where the carrier diffusion is large will be more effective for single mode selection, provided that the feedback strength is sufficient to overcome optical losses.

A good indicator for the strength of optical feedback is the voltage drop measured across the cavity, as shown in Figure 27 and Figure 28. Here, the optical feedback is only to one part of the cavity, so this corresponds to a threshold reduction of predominantly one mode that is situated at that location. Considering that the maximum voltage drop we could achieve was of the order of 10 μV, this is a measure of how effectively a single mode is favoured above other modes that are spatially separated. While effective lumped-element circuits may be considered to model the distributed electrical characteristics across the active region [128], past investigations have suggested that more comprehensive analyses are required for proton-implanted VCSELs [8].

The derivative analysis of I (dV/dI) vs. I [7] for the diode was performed and the data is presented in Figure 33. The kink occurred at the diode's threshold current of 3.5 mA. From Section 2.2.4, the magnitude of the kink is $n_d k_B T/e$ and is found to be 20 mV from Figure 33.

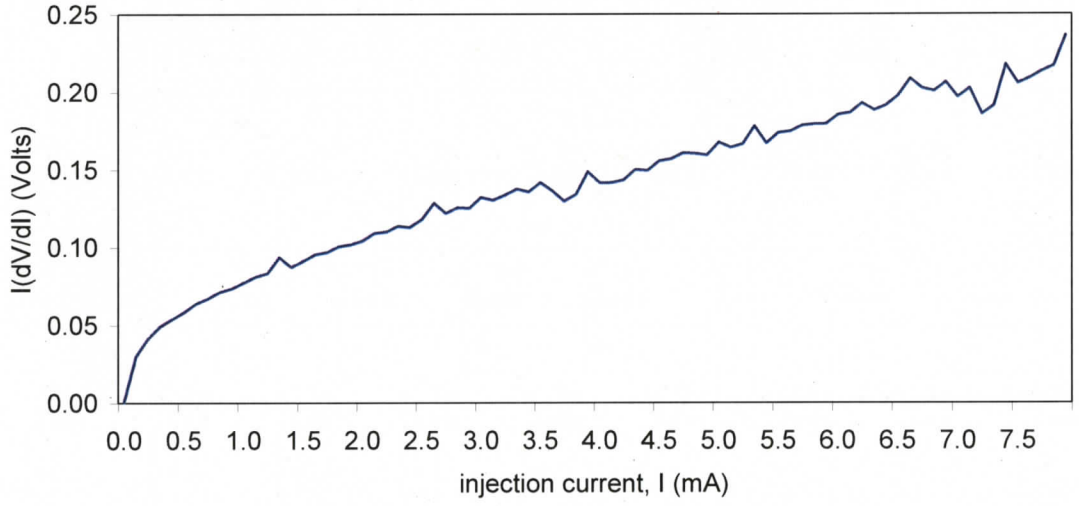

Figure 33 Derivative *I dV/dI* vs. *I* characterization for HFE4080-321 diode laser.

The calculated ideality factor, n_d, was close to 0.8 from the kink at threshold of 3.5 mA, which has been found in other works on proton-implanted VCSELs due to imperfect carrier pinning across the active region [8]. Again this suggests that carrier diffusion was not sufficient to maintain a constant carrier density across the active region.

5.3 Frequency Shift

The frequency shift was calculated from the centroid of the spectra shown in Figure 30. The equation to convert wavelength shift to frequency shift is given in Section 2.3.3, Equation (2.31). Figure 34 presents the frequency shift of modes 2, 3 and 4 on the translation of the 42-μm pinhole along the *x*- and *y*-axes, as represented with the arrows in Figure 28(a). Mode 4 showed the most frequency shift as compared to modes 2 and 3 in the *x*-axis translation, while mode 3 showed the most frequency shift in the *y*-axis translation. For comparison, the free-running frequency is shown with a dashed line (zero corresponds to no frequency shift).

With an 81 μm pinhole measurements at the same injection current as the results above, there was a large -7.13 GHz frequency shift in Mode 3 at the maximum feedback point (marked by '✖'), whereas at the beam-edge position (marked by '●') yield a frequency shift of -3.96 GHz.

It was found that the fundamental mode shifts by -140 GHz between 4.45 mA and 8.5 mA, and there is a corresponding increase in the voltage of 0.126 V. Comparing this with the feedback-induced voltage changes of 0.014 mV in the linear regime, we would expect a much smaller frequency shift (~15 MHz) than observed. This underestimate may be explained by the counteracting effect of current heating: an increase in temperature increases the refractive index, whereas an increase in the carrier density decreases the refractive index. The thermal effects are expected to be much larger for the situation of increasing the current (and voltage) than for the case of spatially selective feedback.

Wavelength-scale changes of the feedback mirror's position were allowed for by using a piezoelectric mirror mount. With these position changes, no phase sensitivity was observed in this experiment, which is consistent with past works considering a large external cavity [62].

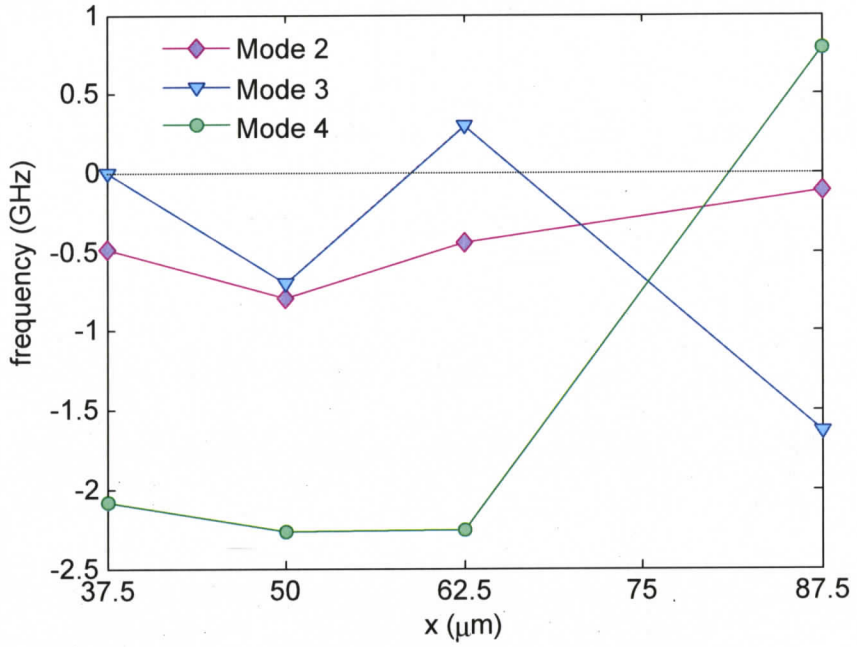

(a)

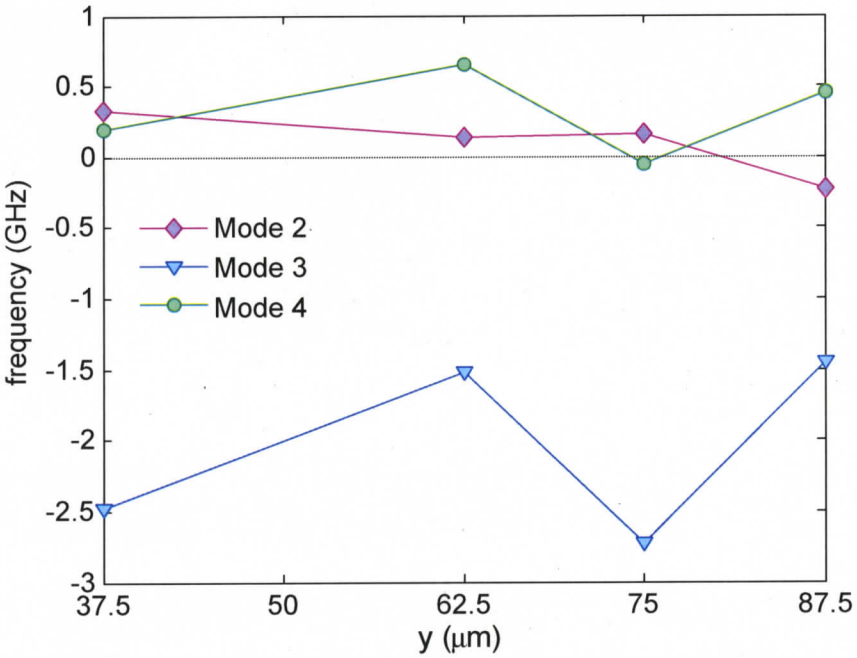

(b)

Figure 34 Frequency shifts of the mode 2, 3 and 4 as the pinhole was translated across (a) the x-axis from 37.5 to 87.5 μm while holding the y-axis fixed at 100 μm, and (b) the y-axis from 37.5 to 87.5 μm while holding the y-axis fixed at 50 μm. Dash line represents the frequency of all modes without feedback.

5.4 MIRROR ALIGNMENT

Changing the alignment of the mirror will change the phase and external cavity length of the VCSEL. To varying the alignment of the mirror, the piezo-mirror was adjusted by varying the applied voltage to the piezoelectric stack in the mirror mount via the three-axis (*x*-, *y*- and *z*-axes) piezo controller, denoted by X, Y and Z in Figure 35 to Figure 38. The mirror was moved 60nm/1Volt (Refer Section 4.1.5). The initial position of the mirror was X=100V, Y=100V and Z=100V. It was found that during translation mirror movement (Figure 35), *x*-angled alignment only (Figure 36), *y*-angled alignment only (Figure 37), and *z*-angled alignment only (Figure 38), there were not many changes on the spectra of the VCSEL with feedback. These results are in agreement with the conclusion from [62] that for long external cavities (>15 cm), the influence of light emission phase variation is insignificant.

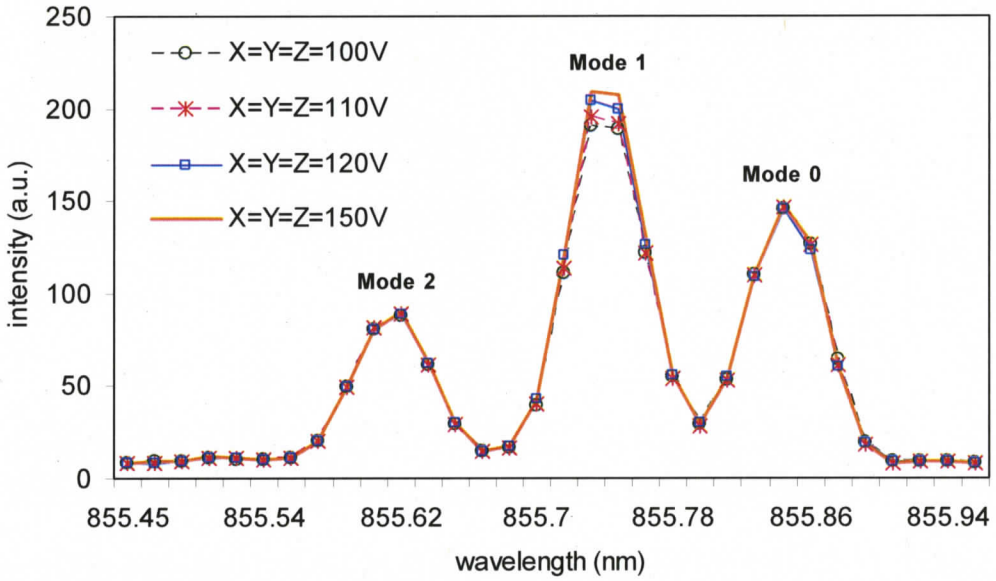

Figure 35 VCSEL with spatially filtered feedback operating at 8.5 mA when mirror was moved translationally (all axes adjusted).

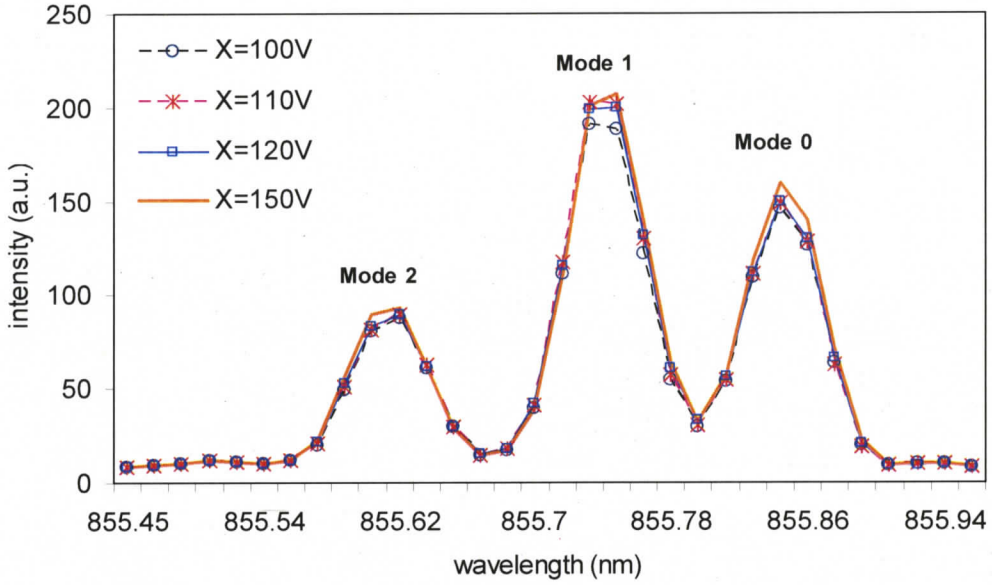

Figure 36 VCSEL with spatially filtered feedback operating at 8.5 mA when only *x*-axis (X) voltage of the piezo controller was varied. (Y=100V, Z=100V)

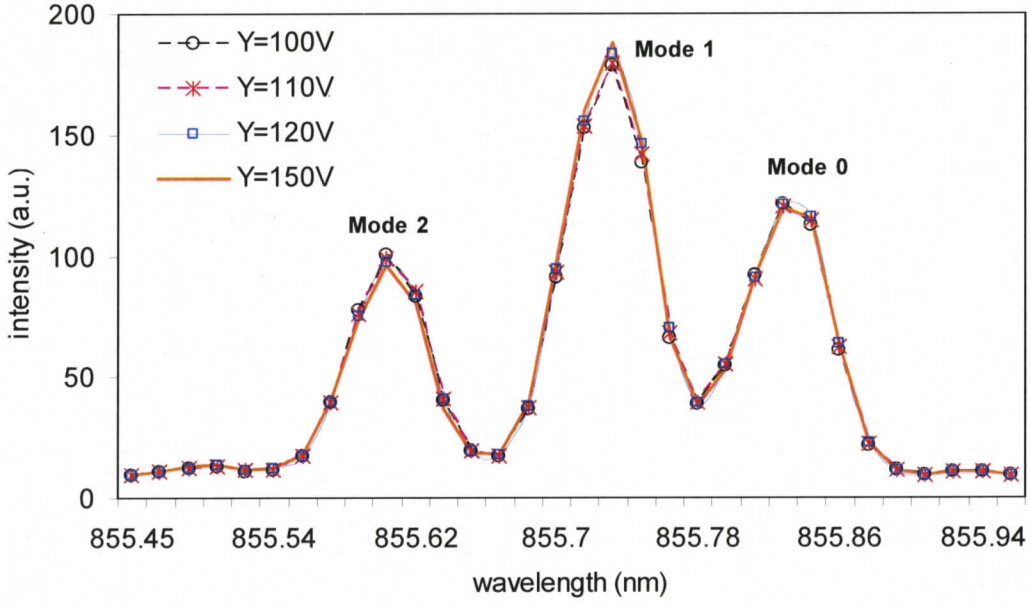

Figure 37 VCSEL with spatially filtered feedback operating at 8.5 mA when only *y*-axis (Y) voltage of the piezo controller was varied. (X=100V, Z=100V)

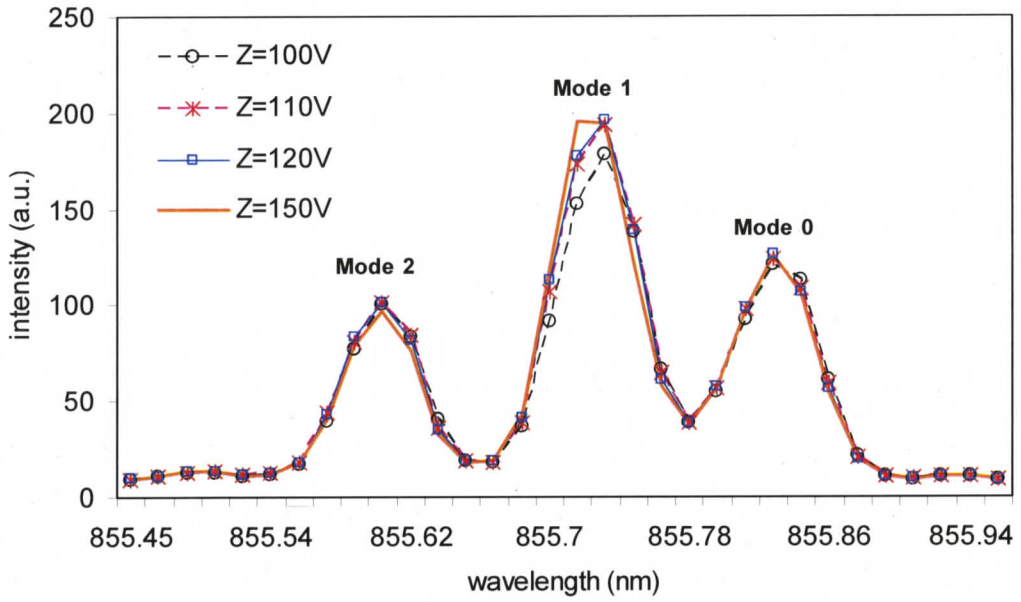

Figure 38 VCSEL with spatially filtered feedback operating at 8.5 mA when only *z*-axis (Z) voltage of the piezo controller was varied. (X=100V, Y=100V)

The next case study on the mirror alignment was done without a spatial filter, with all other components maintained in the setup. It was found that mode control can be achieved when the mirror is tilted to change the feedback strength to the laser. Figure 39 shows the spectrum of the VCSEL when it is free-running at 10 mA (solid line), when feedback was provided at a lower feedback strength (indicated by the lower voltage drop, V_f = 40 μV) and when feedback light was provided at a higher feedback strength (indicated by V_f= 50 μV).

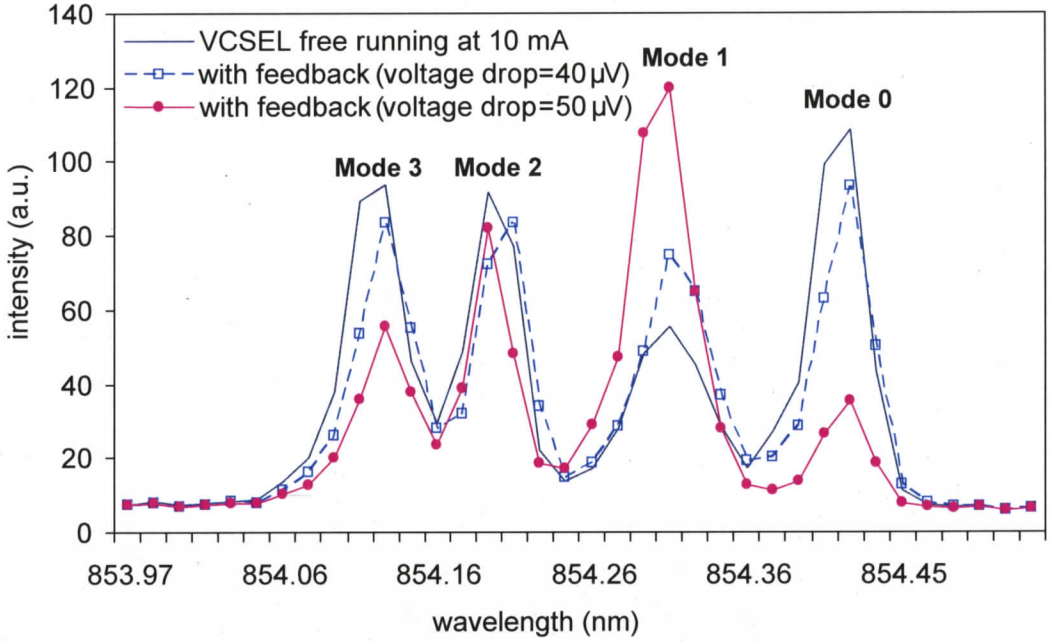

Figure 39 Spectra of VCSEL operating at 10 mA taken without feedback, with feedback at lower feedback strength (40 μV) and with higher feedback strength (50 μV).

At the lower feedback strength mirror alignment position, Mode 1 increased while all other modes decreased slightly were observed. When the feedback strength was increased further by adjusting one of the adjuster screws, the Mode 1 intensity increased further while decreasing Mode 0 and 3 even more. Mode 2 maintained about the same intensity. Therefore, with different alignment positions of the mirror, we are able to control the transverse modes of VCSEL. However, this has been reported in another paper [75] so this parameter was not studied thoroughly in this thesis.

5.5 Recovery Time

We have observed that the spectrum of the VCSEL did not instantly return to the initial pattern when the feedback was removed. The tests were carried out at two different locations on the feedback map shown in Figure 27(a) and in a two-mode regime (mode 0 and mode 1) at the injection current of 4.2 mA with 42 μm pinhole.

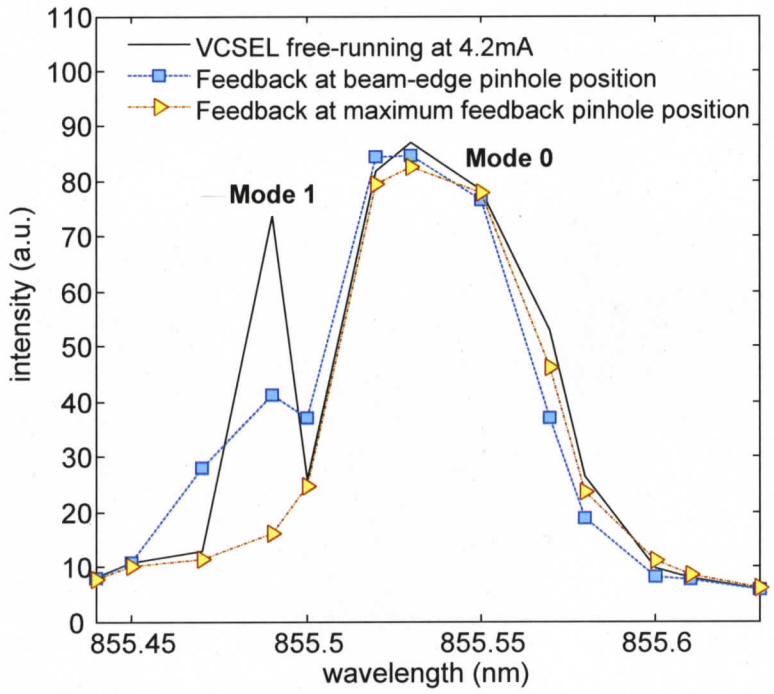

Figure 40 Spectra of VCSEL taken at 4.2 mA showed higher-order mode suppression when feedback was provided at the beam-edge and maximum pinhole positions. Mode 0 and mode 1 were 855.53 nm and 855.49 nm, respectively.

The pinhole was moved around the feedback map providing selective feedback to the VCSEL cavity gain region. When optical feedback was provided at the beam-edge and maximum feedback pinhole locations, mode 1 was suppressed as described previously in Section 5.2 and illustrated in Figure 40.

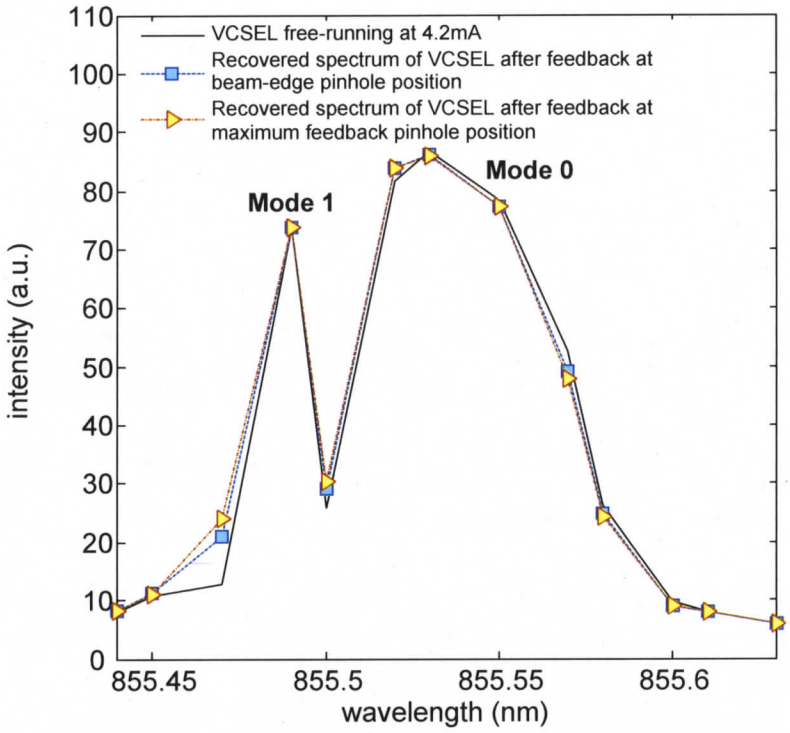

Figure 41 Recovered spectra of VCSEL after the feedback light was removed at beam-edge and maximum feedback positions. Mode 0 and mode 1 were 855.53 nm and 855.49 nm, respectively.

Figure 41 shows the recovered spectra of the VCSEL at both the beam-edge and maximum feedback positions, while Figure 42 shows the recovery time results for the VCSEL after blocking the optical feedback. The first test was performed on the beam-edge point marked by '■' in Figure 27(a). Pinhole was stopped at that position after translation around the *x-y* image plane. Then the mirror was blocked to remove the optical feedback. Spectra of the free-running VCSEL were recorded as a function of time to examine the intensity of mode 1 recovering to its free-running initial intensity (before the optical feedback was provided). The same test was done on the maximum feedback position marked by '▷' in Figure 27(a). It was found that at both the beam-edge and maximum feedback pinhole positions, the recovery time for mode 1 to return to its initial intensity was ~38 minutes.

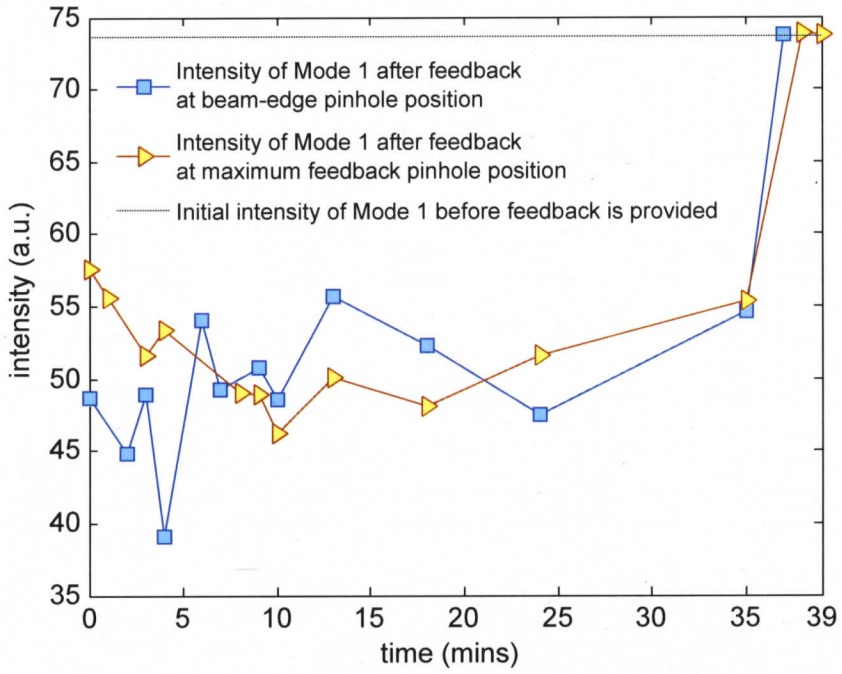

Figure 42 Time of recovery for mode 1 at beam-edge and maximum feedback points marked by '■' and '▷' in Figure 27(a) when feedback was removed from the laser

The delayed recovery of the VCSEL subject to spatially-selective feedback is attributed to the nonlinear interactions within the VCSEL cavity. In the past, long-term writing, erasing and manipulating optical spots have been shown for a VCSEL below threshold and with optical pumping [80]. In that case, the self-sustained behavior was enabled by the nonlinearity of the VCSEL cavity. Similar nonlinear effects are expected to be at play in the spatially-selective feedback system. Many research works have already studied and demonstrated the hysteresis phenomena of VCSELs due to the cavity spatial solitons properties of microcavity lasers [80-82].

We are unable to explain the wide variety of results seen for different operating conditions in the experiment. For example, at higher injection currents, the recovery time for the VCSEL was found to be up to several hours. In addition to the delayed recovery, we found that there were significant history-dependent effects, if the VCSEL was not allowed to recover before translating the pinhole, or if spatially selective feedback was maintained in the same position for an extended period. Further investigations are

required to fully understand these effects, which we believe are intimately related to the nonlinear response of the VCSEL.

5.6 SUMMARY

In this chapter, by varying the design parameters (i.e., the pinhole size, injection current, external cavity length), various experimental results were presented for the performance of the spatially filtered feedback system of a VCSEL. Discussion was also made on the various phenomena that were observed on the VCSEL. The next chapter will sum up the contributions and the future works of this thesis.

CHAPTER 6

CONCLUSION AND FUTURE WORK

This chapter gives conclusions of the research work. Major contributions are summarized and possible future research as well as applications are suggested.

6.1 CONTRIBUTIONS

In this thesis, a method of spatially-selective feedback using spatial filters that are smaller than the size of the VCSEL aperture image has been presented. The threshold reduction across the VCSEL as the result of feedback induced reduction in the carrier density was mapped out. This feedback-induced voltage profile mapping is a novel approach that provides an interesting measurement of electro-optical coupling inside the VCSEL.

Single-mode selection by spatially-selective feedback-induced higher-order mode suppression in a multimode VCSEL for low injection currents was demonstrated. With 20× microscope objective and maximum feedback voltage drop through the smaller 42 μm pinhole, single-mode operation of the VCSEL was maintained up to 4.55 mA of injection current, i.e., at 1.3× the threshold current.

In addition to single mode operation, it is desirable to control the multimode dynamics of VCSELs for a number of applications. For higher injection currents, mode control, in terms of amplitude and frequency changes, was demonstrated. Considering spatial resolution in the experiment, the diffraction limit of 1.6 μm and 2.6 μm at the object plane of the VCSEL (i.e. on the VCSEL's aperture) was obtained with 40× and 20× microscope objective respectively. Therefore, using the smaller pinhole size (42 μm) in combination with 40× microscope objective, greater side-mode suppression at high injection current of 8.5 mA was observed. Using the bigger pinhole size (81 μm), that is

double the previous 42 μm pinhole size, would increase the feedback strength by a factor of 4, thus the intensity increase and frequency shift of the modes were more significant.

Besides mode control, the memory or hysteresis (bistability) effect of VCSELs has initiated many studies for the optical information processing applications. VCSELs are proposed to be used as optical memory and all optical switching. The long-lived state of VCSELs was observed during the experiments and it was found that the VCSEL under study here required a recovery time after feedback was removed. This recovery time of around 38 minutes was observed at maximum and minimum voltage-change feedback pinhole positions when VCSEL was operating at low injection current of 4.2 mA.

Lastly, the objectives of this study are accomplished successfully. An idea of using pinhole on the image plane of a multi-mode VCSEL as a spatial filter between the laser and feedback mirror, in order to suppress or control higher transverse modes inside the VCSEL was demonstrated. The size and location of a pinhole were confirmed to be effective to control the feedback with varied intensity and spatial selection, and affected mode competition inside the laser cavity. Interesting phenomena of long-term recovery from feedback state to free-run state were also presented.

6.2 Future Work and Potential Applications

Future work should explore the polarization of the spatially-selective feedback system as the polarization properties of this system were not studied. Also, this system showed intriguing history-dependent effects with long recovery times, which are likely related to the nonlinear properties of the VCSEL. We have demonstrated that the state of the laser may be maintained for over 30 minutes, even after the feedback was removed. However, with different injection currents and feedback conditions, recovery time of up to hours was observed. Therefore, this behaviour warrants further investigation.

The mode control enabled by spatially filtered feedback may enable applications such as transverse mode-locking [129]. The scheme also provides opportunities for precise frequency tuning between modes, and consequently, it offers a novel approach for tuning of high-frequency mode-beating sources [130-132]. For example, it is possible to obtain

high frequency intensity oscillations from the mode-beating between transverse modes in a VCSEL. Selective frequency shifts between the modes may be used to tune the oscillation frequency, and selective power control of the modes may be used to obtain a greater modulation depth for the oscillation. As another example, transverse mode-locking requires the cooperative behaviour between multiple-transverse modes, and it is desirable to be able to selectively tune the different mode characteristics.

The long-term recovery effects demonstrated here will have an influence on the stabilization time for potential applications involving selective feedback. For example, when attempting to change the beat-frequency or amplitude of multimode operation, which is of interest for high-frequency sources, it will be required to wait over the time-scale of minutes to hours to obtain stable operation. In addition, there has been considerable interest in using the self-sustaining optics and nonlinear response of micro-cavity lasers for optical information processing, which would benefit from the ability to selectively address transverse modes. In some cases, the long-term recovery could be beneficial, specifically for applications in optical information processing, such as optical storage, or optical memories.

BIBLIOGRAPHY

[1] G. P. Agrawal, *Fiber-Optic Communication Systems*. New York: John Wiley & Sons, Inc., 2002.

[2] W. T. Silfvast, *Laser fundamentals*. 2nd ed. Cambridge, UK: Cambridge University Press, 2004.

[3] S. L. Chuang, *Physics of optoelectronic devices*. New York: Wiley, 1995.

[4] B. L. Anderson and R. L. Anderson, *Fundamentals of Semiconductor Devices*. New York, NY: The McGraw-Hill Companies, Inc., 2005.

[5] R. F. Pierret, *Semiconductor Device Fundamentals*. Addison-Wesley Publishing Company, Inc., 1996.

[6] D. Halliday, R. Resnick and J. Walker, *Fundamentals of Physics Extended*. 5th ed.: John Wiley and Sons, Inc., 1997.

[7] L. A. Coldren and Corzine S. W., *Diode Lasers and Photonic Integrated Circuits*. New York: John Wiley & Sons, Inc., 1995.

[8] S. Lakkarsu, "Correlation of electrical and optical derivatives in semiconductor lasers using a novel current modulation technique," M.Sc thesis, Department of Electrical Engineering, North Carolina State University, Raleigh, 2005.

[9] N. K. Dutta and G. P. Agrawal, *Long-wavelength Semiconductor Lasers*. New York: Van Nostrand Reinhold Company, Inc., 1986.

[10] G. H. M. van Tartwijk and D. Lenstra, "Semiconductor lasers with optical injection and feedback," *Quantum and Semiclassical Optics,* vol. 7, pp. 87-143, Aug 1995.

[11] R. Lang and K. Kobayashi, "External optical feedback effects on semiconductor injection laser properties," *IEEE Journal of Quantum Electronics,* vol. 16, pp. 347-355, 1980.

[12] C. H. Henry, "Theory of the linewidth of semiconductor lasers," *IEEE Journal of Quantum Electronics,* vol. 18, pp. 259-264, 1982.

[13] G. Keiser, *Optical fiber communications*. 3rd ed. Boston, MA: McGraw-Hill, 2000.

[14] H. Soda, K. Iga, C. Kitahara, and Y. Suematsu, "GaInAsP-InP surface-emitting injection-lasers," *Japanese Journal of Applied Physics,* vol. 18, pp. 2329-2330, 1979.

[15] J. L. Jewell, A. Scherer, S. L. McCall, Y. H. Lee, S. Walker, J. P. Harbison, and L. T. Florez, "Low-threshold electrically pumped vertical-cavity surface-emitting microlasers," *Electronics Letters,* vol. 25, pp. 1123-1124, Aug 1989.

[16] K. D. Choqutte and K. M. Geib, "Fabrication and performance of vertical-cavity surface-emitting lasers," in *Vertical-Cavity Surface-Emitting Lasers*, C. Wilmsen, H. Temkin, and L. A. Coldren, Eds. Cambridge: Cambridge University Press, 1999, pp. 193-232.

[17] S. F. Yu, *Analysis and Design of Vertical Cavity Surface Emitting Lasers*. New Jersey: John Wiley & Sons, Inc., September 2003.

[18] F. Koyama, "Recent advances of VCSEL photonics," *Journal of Lightwave Technology,* vol. 24, pp. 4502-4513, Dec 2006.

[19] C. J. Chang-Hasnain, "Vertical-cavity surface-emitting lasers," in *Semiconductor Lasers: Past, Present, and Future*, G. P. Agrawal, Ed. Woodbury, New York: American Institute of Physics, 1995, pp. 159-165.

[20] C. J. Chang-Hasnain, "Tunable VCSEL," *IEEE Journal of Selected Topics in Quantum Electronics,* vol. 6, pp. 978-987, Nov-Dec 2000.

[21] M. C. Y. Huang, K. B. Cheng, Y. Zhou, A. P. Pisano, and C. J. Chang-Hasnain, "Monolithic integrated piezoelectric MEMS-tunable VCSEL," *IEEE Journal of Selected Topics in Quantum Electronics,* vol. 13, pp. 374-380, Mar-Apr 2007.

[22] C. J. Chang-Hasnain, M. Orenstein, A. Von Lehmen, L. T. Florez, J. P. Harbison, and N. G. Stoffel, "Tranverse mode characteristics of vertical-cavity surface-emitting lasers," *Applied Physics Letters,* vol. 57, pp. 218-220, 1990.

[23] C. J. Chang-Hasnain, J. P. Harbison, G. Hasnain, A. C. Von Lehmen, L. T. Florez, and N. G. Stoffel, "Dynamic, polarization and transverse mode characteristics of vertical-cavity surface-emitting lasers," *IEEE Journal of Quantum Electronics,* vol. 27, pp. 1402-1409, Jun 1991.

[24] H. Li, T. L. Lucas, J. G. McInerney, and R. A. Morgan, "Transverse-modes and patterns of electrically pumped vertical-cavity surface-emitting lasers," *Chaos Solitons & Fractals,* vol. 4, pp. 1619-1636, Aug-Sep 1994.

[25] K. Panajotov, J. Danckaert, G. Verschaffelt, M. Peeters, B. Nagler, J. Albert, B. Ryvkin, H. Thienpont, and I. Veretennicoff, "Polarization behavior of vertical-cavity surface-emitting lasers: Experiments, models and applications," in *AIP Conference Proceedings*, 2001.

[26] K. Panajotov, B. Ryvkin, J. Danckaert, M. Peeters, H. Thienpont, and I. Veretennicoff, "Polarization switching in VCSEL's due to thermal lensing," *IEEE Photonics Technology Letters,* vol. 10, pp. 6-8, Jan 1998.

[27] K. D. Choquette, K. L. Lear, R. E. Leibenguth, and M. T. Asom, "Polarization modulation of cruciform vertical-cavity laser diodes," *Applied Physics Letters,* vol. 64, pp. 2767-2769, May 1994.

[28] D. Vakhshoori, J. D. Wynn, G. J. Zydzik, R. E. Leibenguth, M. T. Asom, K. Kojima, and R. A. Morgan, "Top-surface emitting lasers with 1.9 V threshold voltage and the effect of spatial hole-burning on their transverse mode operation and efficiencies," *Applied Physics Letters,* vol. 62, pp. 1448-1450, Mar 1993.

[29] G. C. Wilson, D. M. Kuchta, J. D. Walker, and J. S. Smith, "Spatial hole-burning and self-focusing in vertical-cavity surface-emitting laser diodes," *Applied Physics Letters,* vol. 64, pp. 542-544, Jan 1994.

[30] A. Valle, J. Sarma, and K. A. Shore, "Spatial holeburning effects on the dynamics of vertical-cavity surface-emitting laser-diodes," *IEEE Journal of Quantum Electronics,* vol. 31, pp. 1423-1431, 1995.

[31] G. Hasnain, K. Tai, L. Yang, Y. H. Wang, R. J. Fischer, J. D. Wynn, B. Weir, N. K. Dutta, and A. Y. Cho, "Performance of gain-guided surface emitting lasers with semiconductor distributed bragg reflectors," *IEEE Journal of Quantum Electronics,* vol. 27, pp. 1377-1385, Jun 1991.

[32] K. L. Lear, R. P. Schneider, K. D. Choquette, and S. P. Kilcoyne, "Index guiding dependent effects in implant and oxide confined vertical-cavity lasers," *IEEE Photonics Technology Letters,* vol. 8, pp. 740-742, Jun 1996.

[33] B. Tell, K. F. Browngoebeler, R. E. Leibenguth, F. M. Baez, and Y. H. Lee, "Temperature dependence of GaAs-AlGaAs vertical-cavity surface-emitting lasers," *Applied Physics Letters,* vol. 60, pp. 683-685, Feb 1992.

[34] K. D. Choquette, D. A. Richie, and R. E. Leibenguth, "Temperature dependence of gain-guided vertical-cavity surface-emitting laser polarization," *Applied Physics Letters,* vol. 64, pp. 2062-2064, Apr 1994.

[35] K. D. Choquette, R. P. Schneider, K. L. Lear, and R. E. Leibenguth, "Gain-dependent polarization properties of vertical-cavity lasers," *IEEE Journal of Selected Topics in Quantum Electronics,* vol. 1, pp. 661-666, Jun 1995.

[36] D. B. Young, J. W. Scott, F. H. Peters, M. G. Peters, M. L. Majewski, B. J. Thibeault, S. W. Corzine, and L. A. Coldren, "Enhanced performance of offset-gain high-barrier vertical-cavity surface-emitting lasers," *IEEE Journal of Quantum Electronics,* vol. 29, pp. 2013-2022, Jun 1993.

[37] K. D. Choquette, K. L. Lear, R. P. Schneider, and K. M. Geib, "Cavity characteristics of selectively oxidized vertical-cavity lasers," *Applied Physics Letters,* vol. 66, pp. 3413-3415, 1995.

[38] Y. Mitsuhashi, J. Shimada, and S. Mitsutsuka, "Voltage change across the self-coupled semiconductor laser," *IEEE Journal of Quantum Electronics,* vol. 17, pp. 1216-1225, 1981.

[39] L. Goldberg, H. F. Taylor, A. Dandridge, J. F. Weller, and R. O. Miles, "Spectral characteristics of semiconductor lasers with optical feedback," *IEEE Journal of Quantum Electronics,* vol. 18, pp. 555-564, 1982.

[40] P. B. Subrahmanyam, Y. Zhou, L. Chrostowski, and C. J. Chang-Hasnain, "VCSEL tolerance to optical feedback," *Electronics Letters,* vol. 41, pp. 1178-1179, Oct 2005.

[41] K. Petermann, "External optical feedback phenomena in semiconductor lasers," *IEEE Journal of Selected Topics in Quantum Electronics,* vol. 1, pp. 480-489, Jun 1995.

[42] N. Schunk and K. Petermann, "Numerical analysis of the feedback regimes for a single-mode semiconductor laser with external feedback," *IEEE Journal of Quantum Electronics,* vol. 24, pp. 1242-1247, 1988.

[43] S. W. Z. Mahmoud, M. F. Ahmed, and R. Michalzik, "Influence of optical feedback-induced phase on turn-on dynamics of vertical-cavity surface-emitting semiconductor lasers," in *Proceedings of the 46th IEEE International Midwest Symposium on Circuits and Systems (MWSCAS)*, Cairo, Egypt, Dec. 2003, pp. 1354-1358.

[44] A. Hsu, J. F. P. Seurin, S. L. Chuang, and K. D. Choquette, "Optical feedback in vertical-cavity surface-emitting lasers," *IEEE Journal of Quantum Electronics,* vol. 37, pp. 1643-1649, Dec 2001.

[45] J. Heinrich, E. Zeeb, and K. J. Ebeling, "Transverse modes under external feedback and fiber coupling efficiencies of VCSEL's," *IEEE Photonics Technology Letters,* vol. 10, pp. 1365-1367, Oct 1998.

[46] M. Y. A. Raja, A. Al-Dwayyan, Y. Cao, and C. X. Wang, "Polarization and spatial-mode behavior of short-wavelength VCSELs," *Optics and Laser Technology,* vol. 34, pp. 129-134, Mar 2002.

[47] D. Lenstra, B. H. Verbeek, and A. J. Denboef, "Coherence collapse in single-mode semiconductor lasers due to optical feedback," *IEEE Journal of Quantum Electronics,* vol. 21, pp. 674-679, 1985.

[48] S. J. Jiang, M. Dagenais, and R. A. Morgan, "Spectral characteristics of vertical-cavity surface-emitting lasers with strong external optical feedback," *IEEE Photonics Technology Letters,* vol. 7, pp. 739-741, Jul 1995.

[49] S. J. Jiang, Z. Pan, M. Dagenais, R. A. Morgan, and K. Kojima, "Influence of external optical feedback on threshold and spectral characteristics of vertical-cavity surface-emitting lasers," *IEEE Photonics Technology Letters,* vol. 6, pp. 34-36, Jan 1994.

[50] C. H. L. Quay, I. Z. Maxwell, and J. A. Hudgings, "Coherence collapse and redshifting in vertical-cavity surface-emitting lasers exposed to strong optical feedback," *Journal of Applied Physics,* vol. 90, pp. 5856-5858, Dec 2001.

[51] H. M. Hlaing, D. M. Thomazy, B. J. Viechnicki, and H. Lin, "Linewidth narrowing caused by optical feedback in a multi-mode vertical-cavity surface-emitting laser," *Optics Communications,* vol. 265, pp. 580-584, Sep 2006.

[52] Y. C. Chung and Y. H. Lee, "Spectral characteristics of vertical-cavity surface-emitting lasers with external optical feedback," *IEEE Photonics Technology Letters,* vol. 3, pp. 597-599, Jul 1991.

[53] K. P. Ho, J. D. Walker, and J. M. Kahn, "External optical feedback effects on intensity noise of vertical-cavity surface-emitting lasers," *IEEE Photonics Technology Letters,* vol. 5, pp. 892-895, Aug 1993.

[54] K. I. Kallimani and M. J. O'Mahony, "Relative intensity noise for laser diodes with arbitrary amounts of optical feedback," *IEEE Journal of Quantum Electronics,* vol. 34, pp. 1438-1446, Aug 1998.

[55] J. Y. Law and G. P. Agrawal, "Feedback-induced chaos and intensity-noise enhancement in vertical-cavity surface-emitting lasers," *Journal of the Optical Society of America B-Optical Physics,* vol. 15, pp. 562-569, Feb 1998.

[56] S. Sivaprakasam, S. Bandyopadhyay, Y. Hong, P. S. Spencer, and K. A. Shore, "Polarization-resolved relative intensity noise measurements of a vertical-cavity surface-emitting laser subjected to strong optical feedback," *IEEE Photonics Technology Letters,* vol. 16, pp. 9-11, Jan 2004.

[57] K. Panajotov, M. Arizaleta, M. Camarena, H. Thienpont, H. J. Unold, J. M. Ostermann, and R. Michalzik, "Polarization switching induced by phase change in extremely short external cavity vertical-cavity surface-emitting lasers," *Applied Physics Letters,* vol. 84, pp. 2763-2765, Apr 2004.

[58] P. Besnard, M. L. Chares, G. Stephan, and F. Robert, "Switching between polarized modes of a vertical-cavity surface-emitting laser by isotropic optical feedback," *Journal of the Optical Society of America B-Optical Physics,* vol. 16, pp. 1059-1063, Jul 1999.

[59] M. Sciamanna, K. Panajotov, H. Thienpont, I. Veretennicoff, P. Megret, and M. Blondel, "Optical feedback induces polarization mode hopping in vertical-cavity surface-emitting lasers," *Optics Letters,* vol. 28, pp. 1543-1545, Sep 2003.

[60] J. Y. Law and G. P. Agrawal, "Effects of optical feedback on static and dynamic characteristics of vertical-cavity surface-emitting lasers," *IEEE Journal of Selected Topics in Quantum Electronics,* vol. 3, pp. 353-358, Apr 1997.

[61] Y. H. Hong and K. A. Shore, "Influence of optical feedback time-delay on power-drops in vertical-cavity surface-emitting lasers," *IEEE Journal of Quantum Electronics,* vol. 41, pp. 1054-1057, Aug 2005.

[62] P. S. Spencer, C. R. Mirasso, and K. A. Shore, "Effect of strong optical feedback on vertical-cavity surface-emitting lasers," *IEEE Photonics Technology Letters,* vol. 10, pp. 191-193, Feb 1998.

[63] G. P. Agrawal, "Line narrowing in a single-mode injection laser due to external optical feedback," *IEEE Journal of Quantum Electronics,* vol. QE-20, pp. 468-471, 1984.

[64] H. Li, J. Ye, and J. G. McInerney, "Detailed analysis of coherence collapse in semiconductor lasers," *IEEE Journal of Quantum Electronics,* vol. 29, pp. 2421-2432, Sep 1993.

[65] R. W. Tkach and A. R. Chraplyvy, "Regimes of feedback effects in 1.5-μm distributed feedback lasers," *Journal of Lightwave Technology,* vol. 4, pp. 1655-1661, 1986.

[66] M. A. Arteaga, H. J. Unold, J. M. Ostermann, R. Michalzik, H. Thienpont, and K. Panajotov, "Investigation of polarization properties of VCSELs subject to optical feedback from an extremely short external cavity - Part II: Experiments," *IEEE Journal of Quantum Electronics,* vol. 42, pp. 102-107, Jan-Feb 2006.

[67] M. A. Arteaga, H. J. Unold, J. M. Ostermann, R. Michalzik, H. Thienpont, and K. Panajotov, "Investigation of polarization properties of VCSELs subject to optical feedback from an extremely short external cavity - Part I: Theoretical analysis," *IEEE Journal of Quantum Electronics,* vol. 42, pp. 89-101, Jan-Feb 2006.

[68] Y. H. Hong, R. Ju, P. S. Spencer, and K. A. Shore, "Investigation of polarization bistability in vertical-cavity surface-emitting lasers subjected to optical feedback," *IEEE Journal of Quantum Electronics,* vol. 41, pp. 619-624, 2005.

[69] M. C. Soriano, M. Yousefi, J. Danckaert, S. Barland, M. Romanelli, G. Giacornelli, and F. Marin, "Low-frequency fluctuations in vertical-cavity surface-emitting lasers with polarization selective feedback: Experiment and theory," *IEEE Journal of Selected Topics in Quantum Electronics,* vol. 10, pp. 998-1005, Sep-Oct 2004.

[70] M. W. Pan, B. P. Shi, and G. R. Gray, "Semiconductor laser dynamics subject to strong optical feedback," *Optics Letters,* vol. 22, pp. 166-168, 1997.

[71] J. Martín-Regalado, G. H. M. van Tartwijk, S. Balle, and M. San Miguel, "Mode control and pattern stabilization in broad-area lasers by optical feedback," *Physical Review A,* vol. 54, pp. 5386-5393, Dec 1996.

[72] S. Wolff, A. Rodionov, V. E. Sherstobitov, and H. Fouckhardt, "Fourier-optical transverse mode selection in external-cavity broad-area lasers: Experimental and numerical results," *IEEE Journal of Quantum Electronics,* vol. 39, pp. 448-458, Mar 2003.

[73] D. L. Cheng, E. C. Liu, and T. C. Yen, "Single transverse mode operation of a self-seeded commercial multimode VCSEL," *IEEE Photonics Technology Letters,* vol. 16, pp. 278-280, Jan 2004.

[74] H. X. Chen and G. W. Schinn, "Single polarization, single transverse mode, and widely tunable narrow-linewidth laser from a multimode vertical cavity surface-emitting laser by use of a coupled cavity," *Optics Letters,* vol. 30, pp. 1006-1008, May 2005.

[75] H. Lin and H. M. Hlaing, "Transverse mode selection in a vertical-cavity surface-emitting laser by using preferential alignment of optical feedback," *Optics Communications,* vol. 274, pp. 130-135, Jun 2007.

[76] F. Marino, S. Barland, and S. Balle, "Single-mode operation and transverse-mode control in VCSELs induced by frequency-selective feedback," *IEEE Photonics Technology Letters,* vol. 15, pp. 789-791, Jun 2003.

[77] M. Okada, "Wavelength tuning characteristics of a vertical cavity surface emitting laser diode with an external short cavity," *Optical Review,* vol. 11, pp. 193-198, May-Jun 2004.

[78] D. L. Cheng, T. C. Yen, W. Chang, W. C. Kuo, K. S. Kao, and C. P. Hsu, "Polarization mode-hopping suppression and performance enhancement by optical feedback in a current-driven polarization switching VCSEL," *IEEE Photonics Technology Letters,* vol. 19, pp. 1961-1963, Nov-Dec 2007.

[79] Y. H. Hong, P. S. Spencer, and K. A. Shore, "Suppression of polarization switching in vertical-cavity surface-emitting lasers by use of optical feedback," *Optics Letters,* vol. 29, pp. 2151-2153, Sep 2004.

[80] S. Barland, J. R. Tredicce, M. Brambilla, L. A. Lugiato, S. Balle, M. Giudici, T. Maggipinto, L. Spinelli, G. Tissoni, T. Knodl, M. Miller, and R. Jager, "Cavity solitons as pixels in semiconductor microcavities," *Nature,* vol. 419, pp. 699-702, Oct 2002.

[81] Y. Tanguy, T. Ackemann, W. J. Firth, and R. Jager, "Realization of a semiconductor-based cavity soliton laser," *Physical Review Letters,* vol. 1, Jan 2008.

[82] L. Spinelli, G. Tissoni, M. Brambilla, F. Prati, and L. A. Lugiato, "Spatial solitons in semiconductor microcavities," *Physical Review A,* vol. 58, pp. 2542-2559, Sep 1998.

[83] A. Naumenko, N. Loiko, M. Sondermann, K. Jentsch, and T. Ackemann, "Abrupt turn-on and hysteresis in a VCSEL with frequency-selective optical feedback," *Optics Communications,* vol. 259, pp. 823-833, Mar 2006.

[84] R. A. Morgan, M. K. Hibbsbrenner, J. A. Lehman, E. L. Kalweit, R. A. Walterson, T. M. Marta, and T. Akinwande, "Hybrid dielectric/AlGaAs mirror spatially filtered vertical cavity top-surface emitting laser," *Applied Physics Letters,* vol. 66, pp. 1157-1159, Mar 1995.

[85] G. E. Giudice, D. V. Kuksenkov, L. G. de Peralta, and H. Temkin, "Single-mode operation from an external cavity controlled vertical-cavity surface-emitting laser," *IEEE Photonics Technology Letters,* vol. 11, pp. 1545-1547, Dec 1999.

[86] Y. A. Wu, C. J. Changhasnain, and R. Nabiev, "Singlemode emission from a passive-antiguide-region vertical-cavity surface-emitting laser," *Electronics Letters,* vol. 29, pp. 1861-1863, Oct 1993.

[87] M. A. Arteaga, M. Lopez-Amo, H. Thienpont, and K. Panajotov, "Role of external cavity reflectivity for achieving polarization control and stabilization of vertical cavity surface emitting laser," *Applied Physics Letters,* vol. 90, Jan 2007.

[88] A. Gavrielides, T. Erneux, D. W. Sukow, G. Burner, T. McLachlan, J. Miller, and J. Amonette, "Square-wave self-modulation in diode lasers with polarization-rotated optical feedback," *Optics Letters,* vol. 31, pp. 2006-2008, 2006.

[89] C. Masoller and N. B. Abraham, "Polarization dynamics in vertical-cavity surface-emitting lasers with optical feedback through a quarter-wave plate," *Applied Physics Letters,* vol. 74, pp. 1078-1080, Feb 1999.

[90] H. Li, A. Hohl, A. Gavrielides, H. Hou, and K. D. Choquette, "Stable polarization self-modulation in vertical-cavity surface-emitting lasers," *Applied Physics Letters,* vol. 72, pp. 2355-2357, 1998.

[91] Q. S. Yang and A. Sasoh, "Frequency characteristics and dynamical behaviors of self-modulation in vertical-cavity surface-emitting lasers," *Optics Communications,* vol. 219, pp. 307-315, 2003.

[92] X. F. Li, W. Pan, B. Luo, D. Ma, and G. Deng, "Static and dynamic characteristics of VCSELs with polarisation-selective optical feedback," *IEE Proceedings-Optoelectronics,* vol. 153, pp. 67-74, 2006.

[93] C. Masoller and N. B. Abraham, "Low-frequency fluctuations in vertical-cavity surface-emitting semiconductor lasers with optical feedback," *Physical Review A,* vol. 59, pp. 3021-3031, 1999.

[94] J. Jewell, "Surface-emitting lasers reach R & D threshold," *Laser Focus World,* vol. 26, pp. 151-156, May 1990.

[95] J. Hashizume, S. Shinada, F. Koyama, and K. Iga, "Reflection induced voltage change of surface emitting laser for optical probing," *Optical Review,* vol. 9, pp. 186-188, Sep-Oct 2002.

[96] D. Heinis, Y. Poujet, and C. Gorecki, "A new concept of an integrated SNOM microscope using optical feedback within vertical cavity surface emitting lasers," *Journal of the Korean Physical Society,* vol. 47, pp. S182-S185, Aug 2005.

[97] D. Heinis, C. Gorecki, S. Bargiel, and B. Cretin, "Feedback-induced voltage change of a Vertical-Cavity Surface-Emitting Laser as an active detection system for miniature optical scanning probe microscopes," *Optics Express,* vol. 14, pp. 3396-3405, Apr 2006.

[98] K. H. Hahn, M. R. Tan, Y. M. Houng, and S. Y. Wang, "Large-area multitransverse-mode VCSELs for modal noise-reduction in multimode fiber systems," *Electronics Letters,* vol. 29, pp. 1482-1483, Aug 1993.

[99] K. Hahn and K. Giboney, "VCSEL-based Fiber-Optic Data Communications," in *Vertical-Cavity Surface-Emitting Lasers: Design, Fabrication, Characterization and Applications*, C. Wilmsen, H. Temkin, and L. A. Coldren, Eds.: Cambridge University Press, 1999, p. 373.

[100] P. Debernardi, G. P. Bava, C. Degen, I. Fischer, and W. Elsasser, "Influence of anisotropies on transverse modes in oxide-confined VCSELs," *IEEE Journal of Quantum Electronics,* vol. 38, pp. 73-84, Jan 2002.

[101] A. Sharma, J. M. Yarrison-Rice, H. E. Jackson, and K. D. Choquette, "Near-field spectroscopic characterization of a 10 mu m aperture selectively oxidized vertical cavity surface emitting laser," *Journal of Applied Physics,* vol. 92, pp. 6837-6844, Dec 2002.

[102] T. C. Lu, W. C. Hsu, Y. S. Chang, H. C. Kuo, and S. C. Wang, "Spectrally resolved spontaneous emission patterns of oxide-confined vertical-cavity surface-emitting lasers," *Journal of Applied Physics,* vol. 96, pp. 5992-5995, Dec 2004.

[103] K. J. Knopp, D. H. Christensen, G. Vander Rhodes, J. M. Pomeroy, B. B. Goldberg, and M. S. Unlu, "Spatio-spectral mapping of multimode vertical cavity surface emitting lasers," *Journal of Lightwave Technology,* vol. 17, pp. 1429-1435, Aug 1999.

[104] B. B. Goldberg, M. S. Unlu, W. D. Herzog, H. F. Ghaemi, and E. Towe, "Near-field optical studies of semiconductor heterostructures and laser diodes," *IEEE*

Journal of Selected Topics in Quantum Electronics, vol. 1, pp. 1073-1081, Dec 1995.

[105] E. Betzig and J. K. Trautman, "Near-field optics - microscopy, spectroscopy and surface modification beyond the diffraction limit," *Science,* vol. 257, pp. 189-195, Jul 1992.

[106] V. de Lange, K. Sun, and R. Gordon, "Inside vertical, cavity surface-emitting lasers: Extracting the refractive, index from spatial-spectral mode images," *IEEE Journal of Quantum Electronics,* vol. 43, pp. 225-229, Mar-Apr 2007.

[107] K. Y. Lau, C. Harder, and A. Yariv, "Interaction of a bistable injection laser with an external optical cavity," *Applied Physics Letters,* vol. 40, pp. 369-371, 1982.

[108] J. A. Hudgings, S. F. Lim, G. S. Li, W. P. Yuen, K. Y. Lau, and C. J. Chang-Hasnain, "Compact, integrated optical disk readout head using a novel bistable vertical-cavity surface-emitting laser," *IEEE Photonics Technology Letters,* vol. 11, pp. 245-247, 1999.

[109] D. G. Deppe, C. Lei, T. J. Rogers, and B. G. Streetman, "Bistability in an AlAs-GaAs-InGaAs vertical-cavity surface-emitting laser," *Applied Physics Letters,* vol. 58, pp. 2616-2618, 1991.

[110] D. L. Huffaker, W. D. Lee, D. G. Deppe, C. Lei, T. J. Rogers, J. C. Campbell, and B. G. Streetman, "Optical memory using a vertical-cavity surface-emitting laser," *IEEE Photonics Technology Letters,* vol. 3, pp. 1064-1066, Dec 1991.

[111] X. F. Tang, J. P. vanderZiel, B. Chang, R. Johnson, and J. A. Tatum, "Observation of bistability in GaAs quantum-well vertical-cavity surface-emitting lasers," *IEEE Journal of Quantum Electronics,* vol. 33, pp. 927-932, Jun 1997.

[112] Y. Tanguy, T. Ackemann, and R. Jager, "Characteristics of bistable localized emission states in broad-area vertical-cavity surface-emitting lasers with frequency-selective feedback," *Physical Review A,* vol. 74, 2006.

[113] L. A. Lugiato, "Introduction to the feature section on cavity solitons: An overview," *IEEE Journal of Quantum Electronics,* vol. 39, pp. 193-196, 2003.

[114] V. N. Morozov, J. A. Neff, and H. J. Zhou, "Analysis of vertical-cavity surface-emitting laser multimode behavior," *IEEE Journal of Quantum Electronics,* vol. 33, pp. 980-988, 1997.

[115] J. Y. Law and G. P. Agrawal, "Effects of spatial hole burning on gain switching in vertical-cavity surface-emitting lasers," *IEEE Journal of Quantum Electronics,* vol. 33, pp. 462-468, Mar 1997.

[116] H. B. Zhang, G. Mrozynski, A. Wallrabenstein, and J. Schrage, "Analysis of transverse mode competition of VCSELs based on a spatially independent model," *IEEE Journal of Quantum Electronics,* vol. 40, pp. 18-24, Jan 2004.

[117] X. F. Li, W. Pan, B. Luo, D. Ma, and G. Deng, "Theoretical analysis of multi-transverse-mode characteristics Of vertical-cavity surface-emitting lasers," *Semiconductor Science and Technology,* vol. 20, pp. 505-513, Jun 2005.

[118] J. Tatum, D. Smith, J. Guenter, and R. Johnson, "High Speed Characteristics of VCSELs," in *Fabrication, Testing, and Reliability of Semiconductor Lasers II.* vol. 3004, P. o. t. SPIE, Ed., 1997, pp. 151-159.

[119] Finisar Advanced Optical Components Division, "1.25GBps 850nm VCSEL TO-46 Package (HFE4080-321)," 2007, Specification sheet, (Accessed on: Jan. 2007). http://www.finisar.com/download_mUr5eEHFE4080-321.pdf.

[120] E. Hecht, *Optics*. 2nd ed. New York: Addison-Wesley Publishing Company, Inc., 1987.

[121] Spectral Products CVI Laser Corporation, "Spectral Products Catalog," 2003, Specification sheet, (Accessed on: Jan 2007). http://www.optronis.com/Datenblaetter/cvi/CVI%20Spectral%20Products.pdf

[122] Perkin Elmer Instruments, "What is a Lock-in Amplifier?," 2000, Technical note, www.cpm.uncc.edu/programs/tn1000.pdf (Accessed on: Aug 2007).

[123] Bentham Instruments Ltd, "What is a Lock-in?," Technical note, www.bentham.co.uk/pdf/Lock-in%20amplifier%20tutorial.pdf (Accessed on: Aug 2007).

[124] Thorlabs, "MDT693A/MDT694A Piezo Controllers," 2006, Specification sheet, http://www.thorlabs.com/Thorcat/12500/12534-D02.pdf (Accessed on: Aug 2007).

[125] Thorlabs, "AE0505D08F Piezoelectric material," 2006, Specification sheet, http://www.thorlabs.com/Thorcat/15600/15641-S01.pdf (Accessed on: Aug 2007).

[126] Thorlabs, *Piezoelectric Kinematic Mount*, 2007.

[127] M. S. Torre, C. Masoller and P. Mandel, "Transverse-mode dynamics in vertical-cavity surface-emitting lasers with optical feedback," *Physical Review A,* vol. 66, pp. (053817-1) - (053817-9), Nov. 2002.

[128] L. A. Coldren, E. R. Hegblom, "Fundamental issues in VCSEL design," in *Vertical-Cavity Surface-Emitting Lasers: Design, Fabrication and Characterization and Applications*, C. Wilmsen, H. Temkin, and L. A. Coldren, Ed. UK: Cambridge University Press, 1999.

[129] R. Gordon, A. P. Heberle, and J. R. A. Cleaver, "Transverse mode-locking in microcavity lasers," *Applied Physics Letters,* vol. 81, pp. 4523-4525, Dec 2002.

[130] C. Z. Ning and P. Goorjian, "Ultrafast directional beam switching in coupled vertical-cavity surface-emitting lasers," *Journal of Applied Physics,* vol. 90, pp. 497-499, Jul 2001.

[131] P. M. Goorjian and C. Z. Ning, "Ultrafast beam self-switching by using coupled vertical-cavity surface-emitting lasers," *Journal of Modern Optics,* vol. 49, pp. 707-718, Apr 2002.

[132] C. Z. Ning, "Self-sustained ultrafast pulsation in coupled vertical-cavity surface-emitting lasers," *Optics Letters,* vol. 27, pp. 912-914, Jun 2002.